
# Structure formation in binary dipolar monolayers

## PhD thesis

Imre Varga

University of Debrecen
Faculty of Sciences
Debrecen
2007

Ezen értekezést a Debreceni Egyetem TTK Fizika Doktori Iskola Szilárdtestfizika és anyagtudomány programja keretében készítettem a Debreceni Egyetem TTK doktori (PhD) fokozatának elnyerése céljából.

Debrecen, 2007. október 15. Varga Imre

Tanúsítom, hogy Varga Imre doktorjelölt 2002-2007 között
a fent megnevezett Doktori Iskola Szilárdtestfizika és anyagtudomány programjának keretében irányításommal végezte munkáját.
Az értekezésben foglalt eredményekhez a jelölt önálló alkotó tevékenységével meghatározóan hozzájárult.
Az értekezés elfogadását javaslom.

Debrecen, 2007. október 15. Dr. Kun Ferenc
témavezető

# Contents

# 1 Chapter

# Introduction

Structure formation by self-assembly in many particle systems has been the subject of intensive scientific research during the past decades. In a large variety of systems, due to their thermal motion and interaction the particles aggregate and build-up clusters with a large variety of structural properties. Diffusion driven aggregation of particles has been extensively studied in the 80's and 90's and by today this problem is well understood. However, structure formation when the interaction of the particles has a dominant role in the process has been much less investigated. A special type of attraction driven self-assembly occurs in electro- and magnetorheological fluids (also called smart fluids) which are composed of particles suspended in an electro-magnetically passive viscous liquid. The particles either have a permanent dipole moment or attain an induced moment due to polarization when subjected to an external electric or magnetic field. In rheological fluids the long range anisotropic interaction and the inherent frustration of the dipolar particle system result in a large variety of interesting phenomena from cluster-cluster aggregation to the formation of crystalline lattices with various types of symmetry. Since the presence of aggregates also changes the rheological and optical properties of the colloid, which can easily be controlled by external fields, rheological fluids have a large variety of technological applications. Dipolar monolayers are obtained when the motion of

particles is restricted to the two-dimensional plane. Such two-dimensional systems provide a deep insight into the dynamics of pattern formation and to the structure of aggregates, furthermore, open up possibilities to study the statistical physics of low dimensional systems such as the phenomena of two-dimensional melting and structural phase transitions.

Binary colloidal dispersions are obtained when two types of particles with different material properties, mass, size, charge, number, ... are suspended in a viscous liquid. Such colloids have recently been found to show interesting aggregation phenomena with novel structural and kinetic properties. The simplest realization of binary colloids is a 1:1 mixture of two components having positive and negative charges. Binary colloids are involved in a large variety of natural phenomena and have potential industrial applications from waste water treatment through mineral flotation to cell recovery, which calls for a thorough experimental and theoretical investigation.

During my Ph.D. studies I investigated the structural and dynamic properties of so-called binary dipolar monolayers (BDM). BDMs are planar colloidal systems containing two sorts of particles which have a permanent or induced dipole moment. The direction of the dipole moment of the particles is fixed to be perpendicular to the plane of motion and has opposite orientation for the two components. Because of these features, BDMs are also called Ising dipolar systems. The first experimental realization of BDMs was presented only very recently by sedimenting two types of particles in a liquid and subjecting the system to an AC electric field perpendicular to the bottom plate of the container. The particles attained an induced dipole moment which had opposite orientation (up and down) in a certain frequency range of the driving field. Depending on the composition of the system and on the driving frequency, a large variety of novel structure formation has been reported. However, due to technical limitations these experiments could not provide a quantitative insight into the structure and dynamics of binary dipolar monolayers but initiated an intensive research in this field.

The goal of my Ph.D. was to carry out a thorough experimental and

theoretical investigation in order to understand self-assembly processes in binary dipolar monolayers, to identify the most important parameters of the system governing the pattern selection, to explore all possible structures and to study the statistical physics of this special two-dimensional system. I constructed a simple and straightforward experimental technique which overcomes the former difficulties and provides an easy-to-control realization of binary dipolar monolayers. Based on this technique I wanted to explore the behavior of BDMs varying its parameters in a broad range. Parallel to the experiments I worked out a realistic model of BDMs which captures all the relevant features of binary dipolar colloids. Under simplifying assumption I could obtain analytic solution for certain particle configurations, but in its entire complexity the model can only be treated numerically by computer simulations. Confronting the experimental findings with the results of analytic calculations and computer simulations I could substantially improve the understanding of binary dipolar monolayers.

The structure of the thesis is the following: Chapter 2 gives an overview of the literature of structure formation in rheological systems by summarizing the most important experimental and theoretical results and basic notions of the field. The second main part of the thesis presents the results of my research. Chapter 3 summarizes the experimental technique demonstrating its capabilities. In Chapter 4 I present my model of BDMs and the computer simulation technique I applied to determine the time evolution of the particle system. The dynamics of BDMs strongly depend on the concentration of particles that's why first I present the results on the structural and kinetic aspects of heteroaggregation in Chapter 6, which is followed by the analyzes of crystal structures of dipoles in Chapter 7. As a peculiar behavior of BDMs, in Chapter 8 I demonstrate that so-called molecular crystalline structures can be formed by dipolar particles, *i.e.* structures with positional and orientational order.

# 2 Chapter

# Motivations

The goal of this chapter is to give an overview of the most important experimental and theoretical studies on the structure formation in two-dimensional dipolar systems. I introduce the basic notions of the field, furthermore, I review the results known in the literature, which motivated our research.

## 2.1 Rheological fluids - dipolar monolayers

Rheological fluids are usually composed of particles suspended in an electromagnetically passive liquid. The particles either have a permanent dipole moment or can attain an induced dipole moment when subjected to an external electric or magnetic field. The long-range anisotropic dipolar interaction and the inherent frustration of the system result in very interesting ordering phenomena and structure formation [31, 102, 40]. Starting from a random initial configuration, the particles usually aggregate and form growing clusters with a large variety of structural properties. The presence of growing aggregates changes also the rheological and optical properties of the colloid which can be controlled by the external field. Due to the possibility of external control, rheological fluids have a large number of applications in dampers, smart breaks, hydraulic controls, servo valves, shock absorbers, furthermore, in optical filters and structural composites [6, 81, 99, 75].

In rheological fluids, we are interested in, the particles typically have spherical shape with a radius ranging from a few $\mu m$ to 100 $\mu m$. Sophisticated techniques have been developed to fabricate glass spheres in the micrometer range on the surface of which a layer of material with high magnetic susceptibility is evaporated (typically a nickel layer). In these colloids, due to the relatively large particle size (mass) the thermal noise does not have a relevant effect on the motion of particles so that under normal conditions the particle system has a deterministic time evolution. In order to get a deeper insight into the structure and dynamics of rheological fluids, in the experiments the motion of particles is often restricted to two dimensions resulting in a particle monolayer. Dipolar monolayers can be realized by confining the particles to the air-liquid or liquid-liquid interface, or by sedimenting the particles to the bottom of a liquid container. When the particles are in contact with the hard ground, additional techniques such as putting the system on a vibrating table are applied to reduce the friction force [6, 45, 38, 7, 79, 80]. The experimental setups used to study structure formation of dipolar particles are realizations of classical many-body systems with a long range anisotropic interaction. In the following the presentation is restricted to quasi two-dimensional systems, for the three-dimensional systems we refer to the literature. One of the main advantages of the systems we consider is that they make possible to study a broad range of physical phenomena from aggregation through crystallization to the complex dynamics of many-body systems.

## 2.2 Structure formation by self-assembly

As early as the 1970's, de Gennes and Pincus predicted [14] that without a magnetic field the magnetic particles suspended in a liquid form randomly oriented chains competing with closed rings and extended clusters. Under an external field $H$ the aggregates change to chains along the field direction, which then merge and form columns of particles. In order to study the dynamics of magnetic particle systems in two dimensions magnetization-

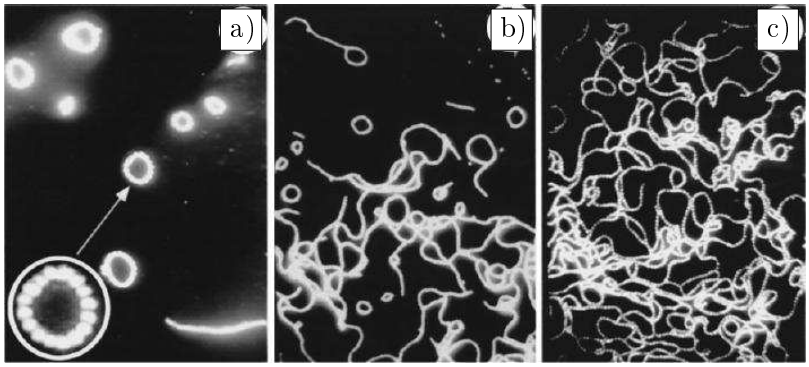


2.1. Figure: Clusters formed by dipolar particles in the absence of an external field varying the concentration. $(a)$ At low concentrations the particles form chains and rings, $(b, c)$ increasing the concentration more complex aggregates occur [100].

controllable microspheres were fabricated by coating uniform-sized glass beads with a nickel layer of a given thickness [100, 23, 77]. Using such microspheres they found that the features of pattern formation in two dimensions are in good agreement with the theoretical predictions [14]: At low concentrations, most microspheres form chains and clusters. Simultaneously, some chains or clusters close themselves to form rings. When the concentration is increased, connected rings and larger clusters appear. However, when the concentration was increased above a certain value, all rings and chains merged to form closed clusters or net-like structures. Examples of two dimensional dipolar systems are presented in Fig. 2.1 varying the particle concentration in the absence of an external magnetic field. Here the particles were sedimented in silicon oil to the bottom of the container. To facilitate the motion of particles, the container was slightly vibrated vertically. One can observe the formation of rings (Fig. 2.1$(a)$) then the transition to the labirinthin structure as the concentration is increased in Figs. 2.1$(b, c)$.

Subjecting the system to a homogeneous external magnetic field, the aggregation process drastically changes. The dipole moments of the particles get aligned with the field, hence, the aggregation process favors the formation

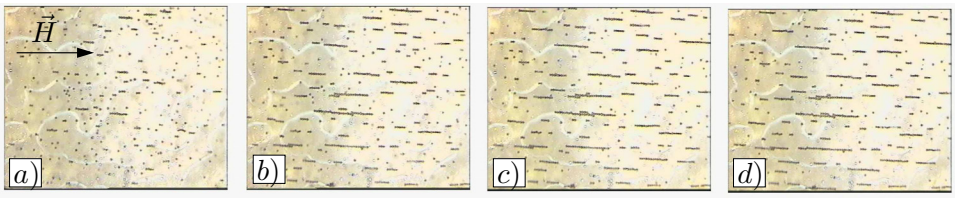


2.2. Figure: Experimental examples for the aggregation of permanent dipoles in a homogeneous external magnetic field. Initially the particles were randomly dispersed on the liquid surface. Then the particles aggregate ($a$) and form short chains which join into longer and longer chains ($b, c, d$) aligned with the field $\vec{H}$.

of chains along the field direction. In the example presented in Fig. 2.2, the micrometer sized particles were floating on the surface of silicon oil so that they could move without the disturbing effect of friction.[1]

### 2.2.1 Theoretical approaches to aggregation

The kinetics of irreversible aggregation is usually described by Smoluchowski's mean field theory where coagulation processes can be written in terms of the following reaction scheme

$$A_i + A_j \xrightarrow{K_{ij}} A_{i+j}, \tag{2.1}$$

where $A_i$ denotes a cluster of mass $i$ [98]. When two clusters of mass $i$ and $j$ meet, they join irreversibly to form a cluster of mass $i + j$ at a rate governed by the constant $K_{ij}$. Smoluchowski's kinetic theory well describes systems characterized by a low concentration of particles with only binary collisions among clusters; spatial correlations of the condensed phase are not considered, *i.e.* the interactions are of short ranged.

Meakin, Kolb, Botet, and Julien developed a computer aggregation model of Brownian particles, which undergo diffusive motion and stick together to

[1] Pictures made by Weijia Wen at the Hong Kong University of Science and Technology. Private communication.

form rigid clusters [50, 36, 37]. They generalized the diffusion limited aggregation (DLA) process [103], where only single particles can diffuse, allowing diffusion of all clusters. This model is denoted as the cluster-cluster aggregation (CCA) model, where the newly formed clusters diffuse along with the single particles and continue to grow by aggregation when they meet other clusters or particles. When the particles join together on a first contact, it is referred to as the diffusion limited cluster aggregation (DLCA) model. Later on several improvements of this model have been proposed, which take into account also the long range anisotropic interaction of particles [23, 52, 84, 86]. These models remove some limitations of the Smoluchowski mean field theory and enable studies of higher concentrations of particles taking into account the spatial and long range correlations between them.

Vicsek and Family pointed out that the time evolution of such aggregating systems obeys some general scaling laws [51, 96, 95]. They analyzed the behavior of the size distribution of clusters $n_S(t)$ as a function of the cluster size $S$ and the time $t$ in order to describe the temporal evolution of the aggregation process [96]. The cluster size distribution $n_S(t)$ is defined as the number of clusters containing $S$ particles at time $t$. It was shown that $n_S(t)$ can be well represented by the following scaling form

$$n_S(t) \sim t^{-w} S^{-\tau} f(S/t^Z), \tag{2.2}$$

where the cutoff function has the properties $f(x) \approx 1$ for $x \ll 1$, and $f(x) \ll 1$ for $x \gg 1$. The novel feature of Eq. (2.2) is the presence of two new dynamic exponents $w$ and $Z$ in addition to the usual static exponent $\tau$. This representation explicitly shows the algebraic decay of $n_S(t)$ with time and cluster size, which is a specific feature of the cluster-cluster aggregation process, because for large $t$, small clusters die out by forming larger ones. The scaling function Eq. (2.2) is expected to be valid in the dilute limit ($\rho \to 0$) at large $S$ and $t$. The characteristic cluster size is determined by the denominator $t^Z$, which shows that the average cluster size $S_{av}(t) \sim t^Z$ diverges as $t \to \infty$. The scaling expression Eq. (2.2) can be written in an

alternative form

$$n_S(t) \sim S^{-\Theta} g(S/t^Z), \tag{2.3}$$

with a scaling function $g(x) \ll 1$ for $x \gg 1$, and $g(x) \sim x^{\Delta}$ for $x \ll 1$. Vicsek and Family [96] determined the scaling relation between the exponents

$$w = (2 - \tau)Z, \tag{2.4}$$

$$Z\Delta = w, \tag{2.5}$$

$$\Theta - \Delta = \tau. \tag{2.6}$$

Using these scaling relations one can obtain $\Theta = 2$, so for $x \gg 1$, the size distribution of clusters $n_S(t)$ decays as $1/S^2$, independent of the dimension, modified by a function which decreases faster than any power of $S$. Plotting $n_S(t)S^2$ as a function of $S/S_{av}$ the curves obtained at different times $t$ fall on the same bell-shaped curve. Another important characteristic quantity of the aggregation process is the total number of cluster $n_c$ as a function of time. Using expression Eq. (2.2) it was shown [95] that $n_c(t)$ has the time dependence

$$n_c(t) = \sum_S n_S(t) \sim t^{-Z'} \equiv \begin{cases} t^{-Z} & for \quad \tau < 1, \\ t^{-w} & for \quad \tau > 1. \end{cases} \tag{2.7}$$

It was found that this general scaling structure provides a good description of the temporal evolution of a large variety of aggregation processes from diffusion limited aggregation through reaction limited processes to aggregation where the interaction of particles has a dominant role [11, 17, 27, 59, 86, 84]. An example of the time evolution of the cluster number $n_c(t)$ and average cluster size $S_{av}(t)$ obtained by experiments on the cluster-cluster aggregation process of dipoles in a homogeneous external field is presented in Fig. 2.3.

The structure of growing aggregates can be characterized by the radius of gyration $R_g$ of the clusters, which scales with the number of particles $S$

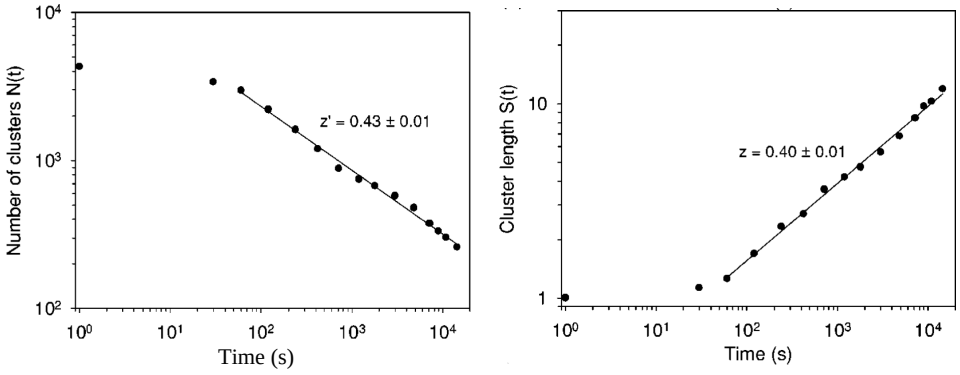


2.3. Figure: Example for the time evolution of the average number of clusters ($a$) and average cluster size ($b$) in an ensemble of particles with permanent dipole moment subject to a homogeneous external magnetic field [11]. The power law behavior can clearly be observed. The dynamic exponents $Z$ and $Z'$ are nearly equal.

(for large $S$) as

$$R_g(S) = \frac{1}{S(S-1)} \sum_{i \neq j=1}^{S} (\vec{r}_i - \vec{r}_j)^2 = bS^{1/D}, \tag{2.8}$$

where $b$ is a characteristic length and $D$ is an universal exponent that depends on the dimension of the space $d$ and on the type of interaction. The fractal dimension $D$ characterizes the structure of aggregates, if its value is equal to the embedding dimension the structure is compact, while the structure has fractal properties when $D$ is a fractional number. Tavares *et al.* [84] studied the aggregation of quasi-two-dimensional dipolar fluids at low concentrations without external field by Monte Carlo simulations, and found that the value of the exponent $D$ is equal to 1.33 for large clusters and $D = 1$ for small ones [84].

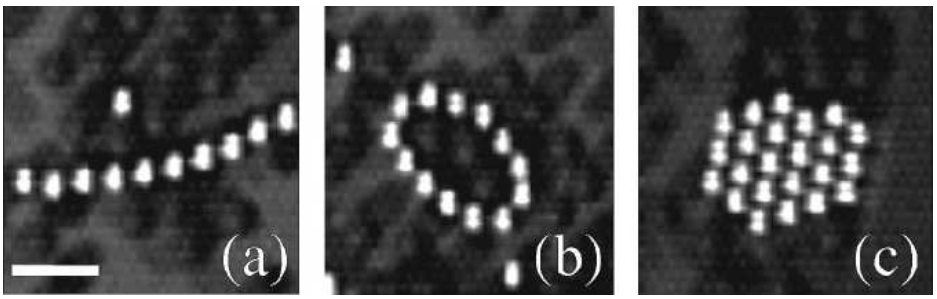


2.4. Figure: Examples of ($a$) chains, ($b$) rings, and ($c$) crystallites observed in an experiment where magnetized steel beads were vibrated in a container. The scale bar denotes 1 cm, the particle diameter was $d = 3$ mm [7].

### 2.2.2 Vibro-fluidized magnetic granular matter

The experimental technique of using a vibrating table to reduce the effect of friction on the particle system, makes also possible to control the temperature of the system up to some extent [7, 79]. Based on this technique, recently, several experimental studies were performed where interesting phase transitions were reported [7, 79]. Besides the direct interest in the physics of granular media, these studies provide insight into the fundamental problem of dipolar hard sphere fluids where the nature of solid-liquid transitions is still debated. Vibro-fluidized magnetic particles can be considered as a simplified model of a ferro-fluid, where similar experiments are technically difficult to perform. Vibro-fluidized inelastic spherical particles are an important model system which captures the essence of dissipative interactions on the statistical properties of dry non-cohesive granular materials [29]. This system has emerged as an important test to investigate the applicability of dissipative kinetic theory [30, 97]. Experiments measuring the position and velocity of individual particles show the formation of clusters, non-Gaussian velocity distributions, and the violation of equipartition [45]. In a number of applications, additional cohesive interactions often exist due to the presence of moisture, electrostatic screening, and magnetization.

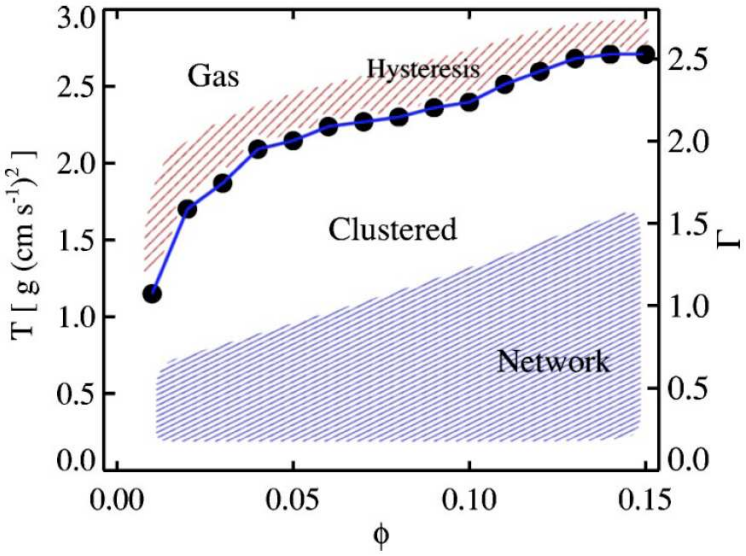


2.5. Figure: Phase diagram of a system of magnetized spheres which suffer dissipative collisions. The temperature of the system is controlled by externally imposed vibration. Typical structures of the "Clustered" phase are presented in Fig. 2.4.

Studying the effects of long-range interactions on the phases observed in cohesive granular materials, at high vibration amplitudes a gas of magnetized particles is observed with velocity distributions similar to non-magnetized particles [7]. The temperature of the system was defined as the kinetic temperature of the particle ensemble based on the velocity distribution of particles. Below a transition temperature compact clusters are observed to form and coexist with single particles. The cluster growth rate is consistent with a classical nucleation process. However, the temperature of the particles in the clusters is significantly lower than the surrounding gas, indicating a break-down of equipartition. If the system is quenched to low temperatures, a meta-stable network of connected chains self-assembles due to the anisotropic nature of magnetic interactions between particles. It was found that in vertically vibrated 2D mixtures of magnetic and non-magnetic

granular spheres, the magnetic spheres can self organize, depending on the volume fraction of magnetic particles and on the relative strength of magnetic dipole-dipole interaction to the external vibration amplitude. Some examples of the observed structures are shown in Fig. 2.4. Based on the experiments, a phase diagram of magnetic granular materials was proposed in Ref. [7] in terms of the density $\phi$ and temperature $T$ of the system, see Fig. 2.5.

The effect of the "shape" of the particles' dipole field was studied in a similar manner using a vertically vibrated monolayer of magnetic spheres [79]. In these experiments the spheres of diameter $D$ encase cylindrical magnetic cores of length $l$. For large $D/l$, it was found that in the ground state of the system the particles form a hexagonal-close-packed pattern in which the dipole vectors of particles assume a macroscopic circulating vortical pattern. For smaller $D/l$, the particles form concentric rings. These experiments together with computer simulations showed that the static configurational magnetic energy (which depends on $D/l$) is a determining factor in pattern selection even though the system is driven and dissipative.

## 2.3 Crystalline structures

Since its discovery more than two decades ago, colloidal crystals have blossomed into a rich area of research encompassing diverse approaches for controlled fabrication of three-dimensional mesocrystals, *i.e.*, crystals with lattice constants ranging from submicrons to ten of microns. Two-dimensional, or planar colloidal crystals have been observed through a number of self-assembly techniques, such as magnetic hole formed with non-magnetic particles in ferro-fluid [77], field induced assembly of floating magnetic particles [101], electric-field-induced planar crystals, and surfactant mediated colloid crystals. In particular, two-dimensional magnetic colloidal crystals have afforded fundamental studies on 2D melting and crystallization, mediated with the hexatic phase [13, 19, 24, 31, 40, 53, 77, 87, 88, 102, 108].

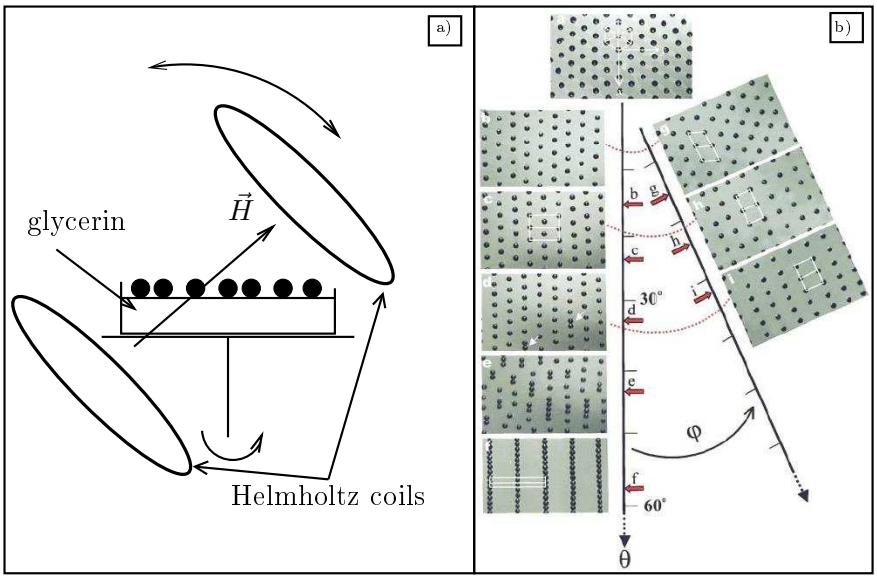


2.6. Figure: (*a*) Experimental setup of Ref. [101]. Particles are placed onto a liquid surface in a container which can be rotated about the vertical axis. The system is in a magnetic field generated by Helmholtz-coils. The direction of the field can be controlled by the setup. (*b*) The formation of different planar structures starting from the simple triangular lattice along the polar angle $\theta$, shown increasing downward, and along the azimuthal angle $\phi$ of the magnetic field. Here the $z$ axis is the surface normal at the center of the liquid meniscus, and the $x$ axis is defined in the uppermost picture as the horizontal direction.

### 2.3.1 Dipolar planar crystals

It was shown in Ref. [101] that in a certain parameter range of systems of mono-dispersed magnetic particles, two-dimensional crystals can be formed on a fluid surface with not just the triangular lattice, but also with all the other planar crystal symmetries such as the oblique, centered-rectangular, rectangular, and square lattices. These lattice structures, some of which are meta-stable, can be reversible tuned by adjusting the polar and azimuthal angles of the external magnetic field relative to the surface normal and the symmetry direction of the 2D lattices.

The experiment of Ref. [101] starts with placing a set of particles on the surface of a liquid. In the absence of magnetic field, the coated microspheres aggregate in the center region of the slightly curved liquid surface. When a perpendicular magnetic field is applied, the spheres move radially outward and form a stable hexagonal lattice. This behavior clearly indicates a competition between the repulsive magnetic interaction and the "attractive" interaction due to the weight of the particle projected along the surface tangent. Such a competition is possible because the attractive and repulsive interactions are on the same order of magnitude.

Structural transitions were realized by tilting the magnetic field at an angle $\theta$ away from the $z$ direction and rotating an angle $\phi$ relative to the $x$ axis defined as a symmetry axis of the system. A pictorial summary of all the different structures observed, and their occurrence in the $\theta$, $\phi$ coordinates is shown in Fig. 2.6. With increasing $\theta$ and fixed $\phi = 0$, the lattice constant along $x$ axis decreases while that along the $y$ direction increases to form short chains. Further increase in $\theta$ leads to perfectly equally spaced, straight chains aligned along the field direction.

To obtain the planar crystal structures, one can start from the case shown in the Fig. 2.6($b$) and rotate the center stage holder along the $\phi$ direction. If the rotation was very slow then the whole pattern would just rotate in step with the magnetic field, so that no change would occur in the lattice structure. However, a faster rotation rate would result in structure changes. These facts indicate a long relaxation time for the observed structures. The square and rectangular planar structures are obtained by starting either from ($c$) and ($d$) then rotating along the $\phi$ direction to ($h$) and ($i$), respectively, or by starting from ($g$) and further rotating along the $\theta$ direction. These structures are meta-stable, in the sense that if strongly perturbed, they would go back to the $\phi = 0$ state. Nevertheless, all planar structures can be obtained uniquely and repeatably as a function of $\theta$ and $\phi$.

The elastic constants of similar two dimensional colloidal crystals have been determined by measuring strain fluctuations induced by Brownian mo-

tion of particles [108]. Using video microscopy and digital image processing, random fluctuations of the displacement of particles could be measured from which one can obtain system size dependent elastic constants. Finite size scaling analysis makes possible to determine the value of elastic constants in the thermodynamic limit [108].

Recently, it has been demonstrated how the formation of planar dipolar crystals and the transition between them can be understood starting from the anisotropic dipole-dipole interaction of the particles. Based on analytic calculations and computer simulations it was possible to construct a simplified phase diagram of the planar dipolar system [19].

### 2.3.2 Molecular crystals on substrates

The theoretical scenario put forward by Kosterlitz, Thouless, Halperin, Nelson and Young for 2D melting has fostered many experimental investigations [56]. Most of these studies focused on 2D ordering on homogeneous substrates. It was only very recently that colloidal crystallization on 2D (triangular or square) periodic substrates has been investigated both experimentally [9] and numerically [66]. A rich variety of novel colloidal states were reported mainly based on computer simulations. In the experiments the substrates with periodic structure of potential minima are generated by interference patterns of laser beams [46, 4, 104]. When the number of colloids $N_c$ is larger than the number $N$ of substrate minima, the $N_c/N$colloids trapped in each well can be considered as a single bound entity with only rotational degrees of freedom. These colloidal molecules (dimers for $N_c = 2N$, trimers for $N_c = 3N$,...) were found experimentally and numerically to display long range orientational order. The corresponding state has been coined colloidal molecular crystal (CMC) in the literature [4, 53, 66, 82, 88, 104].

Figure 2.7 presents the colloidal positions for a system with a square substrate $(a, b, c, d)$ and a triangular substrate $(e, f, g, h)$ obtained by computer simulations [66]. For example, in Fig. 2.7$(b)$, for twice as many colloids as substrate minima $N_c = 2N_m$, each minimum captures two colloids. Neither

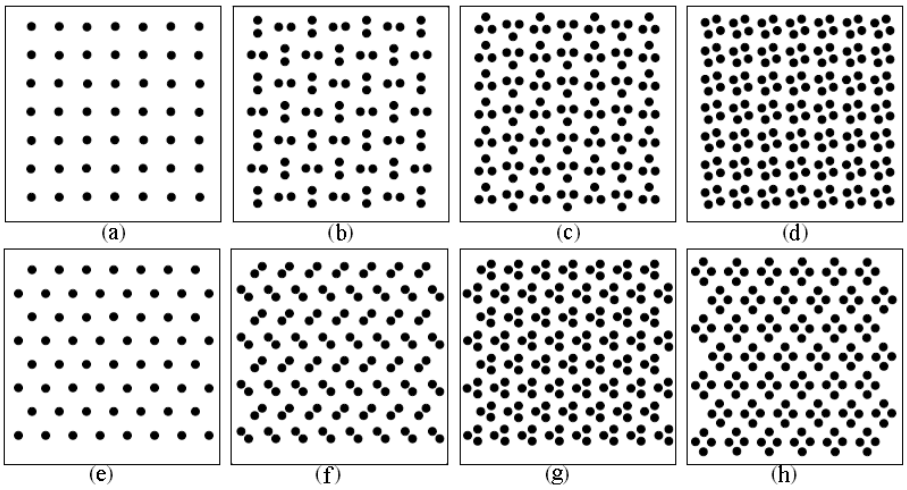


2.7. Figure: The colloid configurations (black dots) at $T = 0.0$ for a square 2D periodic substrate $(a)$ $N_c = N_m$, $(b)$ $N_c = 2N_m$, $(c)$ $N_c = 3N_m$, $(d)$ $N_c = 4N_m$ and for a triangle substrate $(e)$ $N_c = N_m$, $(f)$ $N_c = 2N_m$, $(g)$ $N_c = 3N_m$ $(h)$ $N_c = 4N_m$ [66].

colloid is located at the exact minima; instead, they are offset from it due to the colloid-colloid repulsion. The states inside the minima can be regarded as a colloidal dimer with a rotational degree of freedom. Figure 2.7$(b)$ also shows that there are two types of ordering in the system: one arising from the square substrate, and the other one due to the specific rotational orientation of the colloidal dimers, with neighboring dimers perpendicular to one another. The orientational ordering of the dimers is due to the colloidal repulsion, and allows the distance between the colloids to be maximized under the constraint of the square substrate.

Once an $n$-mer is formed in a trap, how does it interact with a neighboring $n$-mer? Summing the screened contributions from each particle forming dimers $i$ and $j$, one obtains the leading order large distance expression

$$\phi_{ij}(r, \Theta_{ij}, \Theta_{ji}) \sim \cosh[\kappa d \cos(\Theta_{ij})] \cosh[\kappa d \cos(\Theta_{ji})] \frac{e^{-\kappa r}}{r}, \qquad (2.9)$$

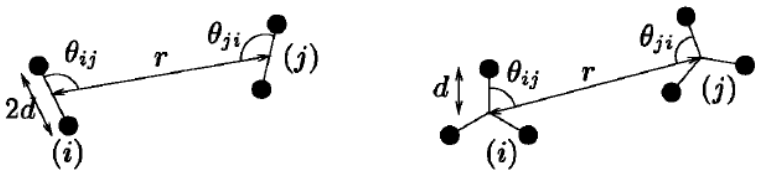


2.8. Figure: Definition of the notations adopted to compute dimer (*left*) and trimer (*right*) interaction. The black dots show the colloids and the line between them is a guide to the eye [1].

where $\kappa^{-1}$ is the Debye screening length of the interaction and $d$ is the distance between the mass center of $n$-mer and one of its particles. For the definition of variables see Fig. 2.8. The key point here is that the radial and angular dependence of the interaction potential are factorized.

It has been shown numerically that dimers on a square 2D substrate (hereafter referred to as the underlying lattice of traps) adopt the ground state represented in Fig. 2.9($a$) [66]. Such an ordering should follow from minimizing the total electrostatic energy $\varepsilon$ where each pair of dimers interacts through the potential Eq. (2.9). Given the exponential screening with distance and $\kappa^{-1}$ is smaller than the lattice spacing, one can further restrict to nearest neighbors of dimers and write the relevant angular dependent part of the energy as

$$\varepsilon = \sum_{<i,j>} \cosh[\kappa d \cos(\Theta_{ij})] \cosh[\kappa d \cos(\Theta_{ji})], \tag{2.10}$$

where the angular brackets denote nearest neighbors. A given pair minimizes its repulsion by setting $\Theta_{ij} = \Theta_{ji} = \pi/2$ (parallel dimers, perpendicular to the center-to-center vector, see Fig. 2.8). It is instructive to approximate the cosh function in Eq. (2.10) by a parabola. Introducing next a new set of variables, where $\Theta_i \in [-\pi/2, \pi/2]$ is defined as the angle between the dimer axis and one of the principal lattice directions, one gets

$$\varepsilon = const + (\kappa d)^4 \sum_{<i,j>} (\cos\Theta_i)^2 (cos\Theta_j)^2. \tag{2.11}$$

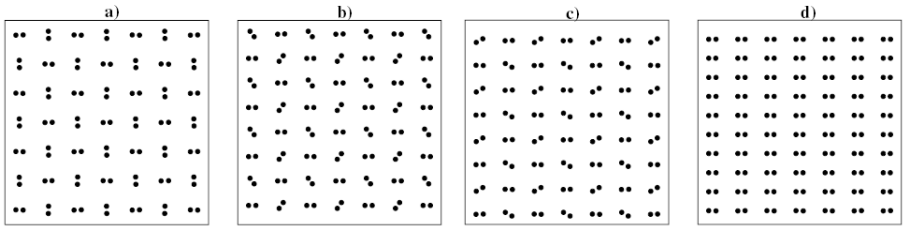


2.9. Figure: Configuration of colloids at $T = 0$ on a rectangular lattice of traps at different values of the aspect ratio $\alpha$ [1].

At high temperature, the system has to be in a disordered state, a paramagnetic phase in spin language, and on purely dimensional grounds Eq. (2.11) indicates that the critical temperature of the anti-ferromagnetic/paramagnetic transition scales like $T_c \sim (\kappa d)^4$. At a fixed temperature $T$, increasing the substrate pinning strength $V_0$ (*i.e.* the deepness of potential minima on the substrate), the $n$-mers constituting a colloidal molecule become of smaller spatial extent: $d$ decreases, so that $T_c$ eventually becomes smaller than $T$. Orientational order is correspondingly lost. More specifically, one finds $T_c \sim V_0^{-4/3}$ for the relation of the critical temperature and of the pinning strength.

When the substrate is varied new states emerge. As an example we consider dimers on a rectangular lattice with a unit cell of length $\alpha l$ and $l$. By definition $\alpha < 1$, and the direction along the long axis is called "horizontal" for convenience. When the aspect ratio $\alpha$ is one, the checkerboard order is that of Fig. 2.9($a$) (anti-ferromagnetic-like phase (AF)). On the other hand, when $\alpha \ll 1$, there are only two nearest neighbors per particle, and from expression Eq. (2.9) the preferred configuration is $\Theta_{ij} = \Theta_{ji} = \pi/2$: all dimers are parallel to the horizontal direction (ferromagnetic phase (FM)). The transition between the FM and AF phases has been studied theoretically by Agra et al. [1].

The substrate is an essential ingredient of CMCs, *i.e.* it creates the underlying periodic structure and ensures the confinement of colloids giving

rise to single bounded entities. Confining substrates have experimentally been realized by interference patterns of laser beams [4, 46].

CMCs exhibit interesting two-step melting transitions. The first stage of melting occurs when the $n$-mers begin to rotate and lose orientational ordering, while in the second stage, the $n$-mers dissolve and individual colloids begin to diffuse throughout the sample [66, 53]. The orientational melting was shown to fall in the Ising universality class [1, 72]. A reentrant disordering can also occur when the $n$-mers are compressed by the increasing substrate force, decreasing both the distance between the colloids and the multipole moment, until the multipole interaction energy drops below the thermal energy. Surprisingly, increasing the substrate strength $V_0$ at fixed $T$ also leads to reentrant melting: the colloidal molecular crystal is destabilized into the partially ordered solid, and orientational order is lost.

## 2.4 Binary colloids

All the colloidal systems presented until now have a single component, *i.e.* the particles had identical properties. During my Ph.D. I studied the behavior of so-called binary colloidal systems which have two components with different material, size, shape, ... . Similarly to colloids of a single component, binary colloids show also aggregation and crystallization phenomena but the larger number of degrees of freedom and the more complicated interaction of particles give rise to a higher complexity. The analysis of mono-colloids is a good starting point to describe the behavior of binary system, however, the emergent novel features require additional experimental and theoretical techniques and careful treatments. In the following I briefly present the most important recent results of binary colloidal systems and highlight the main problems these investigations addressed.

### 2.4.1 Colloidal heteroaggregation

Aggregation of binary colloids with varying compositions, charge or size has been shown to be important in applications such as mineral flotation [16, 3], composite materials manufacturing [43, 85, 54, 20, 78, 105, 57, 83, 15], waste water treatment [10, 18], new molecular materials [26, 42] and cell recovery [55, 28, 49], among others. Heteroaggregation is the process of aggregation between particles of different types. The simpler case of homo-aggregation, where only one type of particle is present, is well studied and documented in the literature [25]. In the latter case, two limiting regimes have been observed: (I) diffusion-limited cluster aggregation (DLCA), in which every collision between particles results in the formation of a bond, and (II) reaction-limited cluster aggregation (RLCA), in which a large number of particle collisions are necessary before a stable bond is established. However, when systems are composed of several species, the reaction kinetics are much more complex and no general kinetic theory is so far available [25, 27]. The most simple experimental realization of binary colloids is a 1:1 mixture of two components of identical material properties having positive and negative charges. Particles of the two components aggregate under the action of screened Coulomb forces and form aggregates which can even change the rheological properties of the colloid [41, 44, 60, 61, 62, 78].

A complete description of the heteroaggregation kinetics is a hard task since the aggregates must be characterized not only by the number of particles but also their composition. Moreover, heteroaggregation between oppositely charged particles can be affected by polymeric adlayers [34] or by polymer bridging [89]. Although some studies of heteroaggregation kinetics appear in the literature [5, 21, 47, 48, 70, 107], relatively little attention has been paid to the heteroaggregation structure [33, 35, 60].

A very interesting unique feature of heteroaggregation has recently been revealed by computer simulations of colloids composed of oppositely charged but otherwise identical particles [44, 61, 62]. It was found that clusters of an even and an odd number of particles (*i.e.* neutral and charged, respectively)

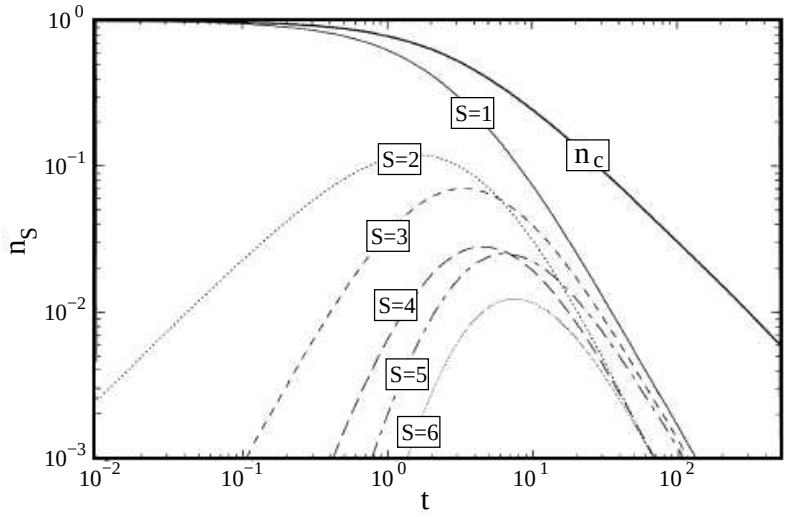


2.10. Figure: Evolution of the concentration of clusters of different number of particles up to hexamers, and the total number of aggregates [61].

have a different behavior: even clusters disappear faster than the odd ones, furthermore, at a given time the concentration of clusters shows even-odd oscillations. They plotted the number of clusters formed containing $n$ particles as a function of time, and found that these curves show the usual bell-shaped form, except for the monomer one, which decays continuously (see Fig. 2.10). The most important difference between the hetero- and homoaggregation is that in the former the curves intersect in case of large Debye screening length. As a result, at long times, some aggregates are absent, while others are still present. This feature is the so-called cluster discrimination. When the interaction forces are screened, this segregation disappears, and all of the curves decay in a similar way. At high screening length, the concentration of aggregates oscillates with the number of particles in the aggregate for small clusters, the period of this oscillation is two particles. Charged cluster, with an odd number of particles, are observed to become dominant, while neutral ones, with an even number disappear faster as one can see in Fig. 2.10. On

the other hand, the total number of clusters decrease according to a power-law at long times with an exponent lower than one. It was shown that cluster discrimination is the consequence of long-range interactions and disappears when the range of interaction gets reduced due to screening [44, 61, 62]. It is difficult to observe cluster discrimination experimentally, because in colloids electrostatic interactions are strongly screened, furthermore, experimental techniques such as light scattering have difficulties to identify single clusters larger than trimers [41, 60, 78].

### 2.4.2 Binary dipolar monolayers

The idea of binary dipolar monolayers (BDM) was first introduced only very recently by Ristenpart *et al.* who performed experiments on the behavior of suspensions with two sorts of particles with similar radii subjected to an $AC$ electric field [68, 69]. It was demonstrated that the $AC$ driving field leads to the formation of novel types of morphologies. They explained the behavior in terms of electro-hydrodynamic flow and induced-dipole interaction. The suspension was a mixture of silica and polystyrene particles suspended in de-ionized water as it is illustrated in Fig. 2.11. After sedimentation the particles formed a disordered monolayer on the bottom of the container. It was observed in the experiments that the application of a high frequency field induces particles to separate laterally into a disordered arrangement due to repulsion transverse to the applied field. Lowering the frequency causes particles to come together, forming planar aggregates. The aggregate morphology depends on the local relative particle concentrations. With a sizeable excess of polystyrene, "flower-like" aggregates form with individual silica particles surrounded by six polystyrene particles. In regions with either a $1:1$ or $2:1$ ratio of particles, a binary super-lattice crystallizes when the frequency is lowered gradually. With a $2:1$ ratio of polystyrene to silica, a triangular super-lattice forms, similar to the (001) plane of an $AB_2$ crystal. If the concentration of polystyrene and silica are approximately equal, then either square-packed super-lattices or stripes of alternating par-

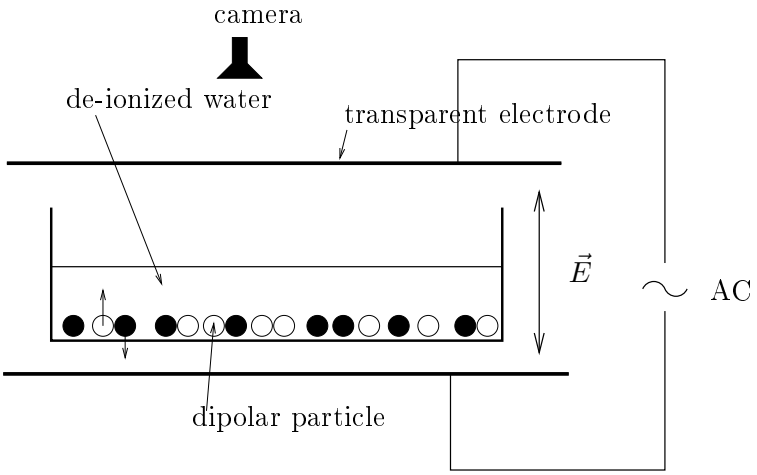


2.11. Figure: The experimental setup of Ref. [68] to study binary dipolar monolayers. The two sorts of particles sedimented to the bottom of the container. When a high frequency electric field was applied, the particles moved laterally and built up complex structures.

ticle types form. Figure 2.12 provides a summary of structures observed in the experiments of Ref. [68].

The crystallization process is largely independent of field strength above a threshold. Changing the field strength at constant frequency results in little or no discernible change in whether they are closely aggregated or widely separated. The absence of field strength dependence suggests that repulsive and attractive interaction forces scale with field strength in the same fashion. Various super-lattice structures form, reproducibly, in independent experiments and various cluster morphologies are observed: ringed clusters, striped clusters, disordered clusters, and regions where the two types of particles are completely segregated.

Although repulsive lateral interactions keep identical particles apart at "high" frequencies, binary suspensions aggregate. At a low total particle concentration chains of alternating particle types form. At higher concentrations square and triangular super-lattices form depending on the relative

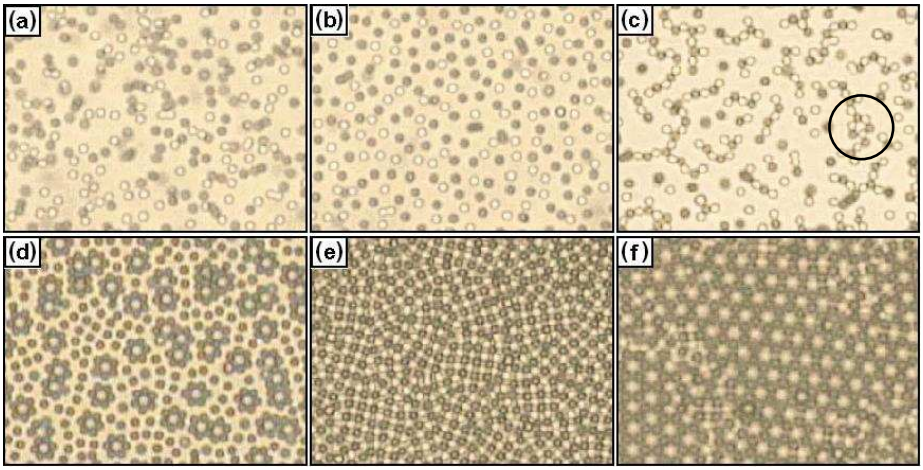


2.12. Figure: Images of planar structures formed in binary suspensions [68]. ($a$) Random arrangement before application of a field. ($b$) Lateral separation when an $AC$ electric field is applied. ($c$) At low concentration chains of alternating particles are observed together with branched aggregates. One particle ring is highlighted by the circle. ($d$) Individual silica particles are typically surrounded by six polystyrene particles forming "flower-like" islands. ($e$) Square-packed lattice obtained in a 1:1 mixture. ($f$) Hexagonal structure formed with a 2:1 ratio of polystyrene to silica at high concentration.

concentrations. Clustering at high frequencies is sensitive to the field amplitude. At large amplitude most of particles arrange themselves in highly ordered binary super-lattices.

This stimulating experiment left many open questions behind and initiated an intensive research on the behavior of colloidal monolayers under $AC$ external driving and especially on the behavior of binary dipolar monolayers [57, 71, 76].

## 2.5 Goals of the investigations

The experiments of Refs. [68, 69] had several technical problems which resulted in serious limitations: the frictional barrier between the particles and

the bottom of the container had a disturbing effect. In order to overcome the frictional barrier in certain cases a vibrating table had to be applied which can also affect the structures formed. The high frequency external driving gives rise to electro-hydrodynamic flow of the carrier liquid which changes the effective interaction of the particles and makes very difficult to understand the relevant aspects of processes. The magnitude of the induced dipole moment of the particles could be controlled only within a very narrow range. Due to these reasons the experiments of Refs. [68, 69] provided only a qualitative insight into the structure and kinetics of binary dipolar monolayers. No quantitative results could be obtained, furthermore, it was not clear up to which extent the friction force and the induced flow of the carrier liquid could affect the structure formation. Binary dipolar monolayers could also allow for a unique possibility to study heteroaggregation phenomena in two dimensions making observations from the third dimension where the history of all the clusters could be tracked. However, with the experimental setups used in the literature such studies are not possible.

In recent years a large amount of experimental observations has been accumulated but the theoretical explanation is still lacking. Hence, it is also a great challenge to carry out a detailed theoretical study of structure formation in binary dipolar monolayers.

The goals of my research can be summarized as follows:

- I wanted to work out an experimental technique which overcomes the difficulties of former experiments allowing for a detailed quantitative study of binary dipolar monolayers. Varying the parameters of the system I wanted to explore both aggregation and crystallization phenomena of the monolayer.

- It was my aim to carry out a thorough theoretical investigation of BDMs to obtain a clear explanation of the experimental results, to identify the relevant parameters of BDMs governing the structure formation processes, and to explore all structures that can emerge in

the system. For the theoretical investigations I wanted to work out a realistic model of BDMs which captures the relevant interactions of the particles and of the embedding liquid, and analyze the model by analytic calculations and computer simulations.

- Comparing the theoretical results to my experimental findings and to the ones presented in the literature I wanted to get a deeper insight into the behavior of BDMs.

# 3 Chapter

# Experimental technique

In order to get a deeper insight into the dynamics of dipolar systems we proposed a novel experimental realization of BDMs without the application of an external driving field. This chapter provides a detailed presentation of our experimental techniques together with tests of the setup and the method of data evaluation [93, 90].

## 3.1 Dipolar particles on a liquid surface

Our experimental setup provides a simple way to study the structure formation in a binary dipolar monolayer. In the experiments, macroscopic metal particles of cylinder shape are magnetized along their axis. In order to facilitate the particle motion, the magnetic particles are attached to cork discs of regular shape so that the composite particle can float on the surface of a liquid. Figure 3.1 illustrates that the two particles are adjusted on the top of each other to have a common axis, which ensures stability when floating. In all experiments, water was used as a carrier liquid to which a surfactant was added to reduce the effect of surface tension on the motion of the particles. The particles are placed onto the water surface with the heavier part pointing downward, *i.e.* the magnets are always under the water, see Fig. 3.1. In the experiments, magnetic particles of three different strength were

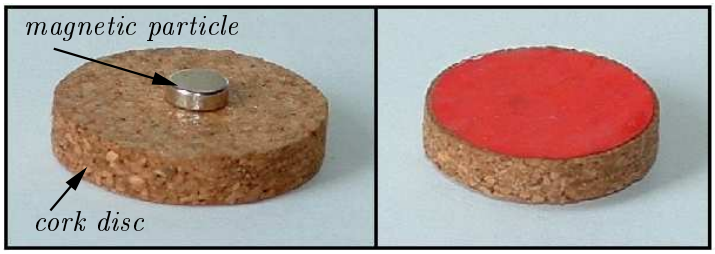


3.1. Figure: Magnetized particle attached to a cork disc of larger diameter (*left*). The composite particle can float upside down on the surface of water (*right*). The diameter $d$ and height $h$ values are $d = 4$ mm and $h = 1.5$ mm, and $d = 26$ mm and $h = 5$ mm, for the magnetic particle and cork disc, respectively.

used with slightly different geometrical extensions attached to cork discs of two different sizes. The cork discs have radius $R_1 = 13$ mm and $R_2 = 8.7$ mm and height $h_1 = 5$ mm and $h_2 = 4$ mm respectively, which proved to be sufficient to prevent the flipping of magnets of identical orientation in the vicinity of each other even for the largest magnetization used in the present study. In the experiments two plastic containers of different sized are used. The smaller one with dimensions 500mm $\times$ 500mm $\times$ 50mm and the larger one with dimensions 1000mm $\times$ 1000mm $\times$ 50mm. The larger container made possible to use a larger number of particles which is especially important at low concentration. The two components of the binary dipolar monolayer are realized by the two opposite orientations of the dipole moments of the particles perpendicular to the water surface. Initially the particles are placed onto a hard plastic net fixed on a wooden frame. The net can float on the surface, which keeps the particles fixed in their initial positions which had been generated beforehand by a computer program and the particles were positioned by hand accordingly, making use of a centimeter grid under the transparent container. A representative example of initial states is presented in Fig. 3.2 where 198 particles were placed on the plastic net. By immersing the net into the water the particles start to float on the surface at the same time. The free side of the cork discs is colored according to the orientation

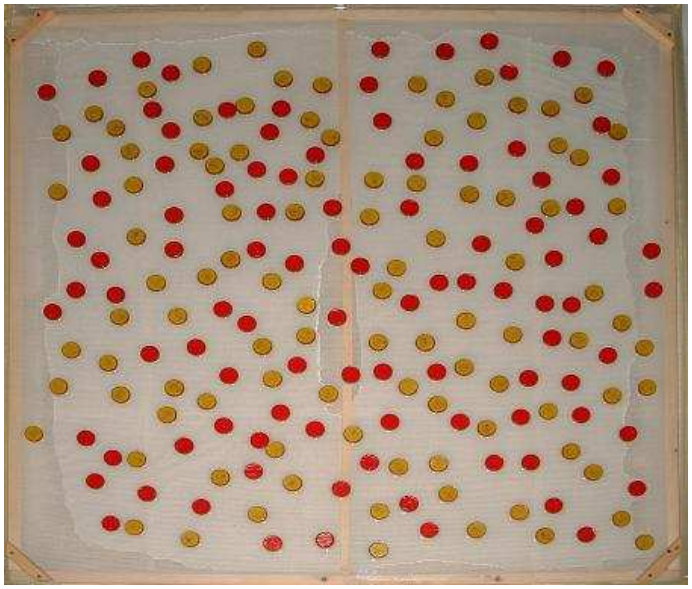

3.2. Figure: Initial configuration of 198 particles in a square box of side length $L = 1000$ mm resulting in a concentration $\phi \approx 0.1$. The same amount of particles of opposite magnetic moment/different colors is used so that $\phi_r = 1$.

of the dipole moments of the magnetic particles, *i.e.* the red color in Fig. 3.2 indicates dipole moment pointing upward perpendicular to the water surface, while yellow stands for downward dipoles. The floating particles move under the action of their mutual dipole-dipole interaction and form various structures.

We place into the experimental box $N_+$ particles with dipole moment $\mu_+$ pointing upward (+) and $N_-$ particles with dipole moment $\mu_-$ pointing downward (−). The total concentration $\phi$ of the particles in our experimental box is defined as the coverage

$$\phi = \frac{N_+ R_+^2 \pi + N_- R_-^2 \pi}{L^2}, \tag{3.1}$$

where $R_+$ and $R_-$ denote the radius of cork discs carrying the magnetic particles of the two components. (Note that $R_+$ and $R_-$ assume one of the

values $R_1$ and $R_2$.) The partial concentrations of the two components $\phi_+$ and $\phi_-$ can be defined analogously and their relative concentration $\phi_r$ follows as $\phi_r = \phi_-/\phi_+$. Experiments were performed by varying the concentration $\phi$ and the relative concentration $\phi_r$ in a broad range by controlling the number of particles $N_+$ and $N_-$ while the container size $L$ was fixed. Studying aggregation and crystallization phenomena we also carried out experiments varying the relative dipole moment $\mu_r = \mu_-/\mu_+$ and the polydispersity $\sigma = R_-/R_+$ of the two components. More explanation of the parameters characterizing the system will be provided in Chapter 4.

The cork discs have two roles in the experimental setup: they ensure floating of the magnets reducing the friction force and they prevent flipping of particles making the dipole orientation fixed perpendicular to the plane of motion. One of the main advantages of our experimental techniques, in contrast to previous experiments of Ristenpart et al. [68], is that no external field is necessary to fix the dipole moments. In our setup the magnitude of the dipole moment of the composite particles is controlled by the placement of particles with the appropriate parameter values.

## 3.2 Motion of particles

The experimental setup ensures that the motion of particles is deterministic since the thermal motion is suppressed by the relatively large particle mass. Assuming that the magnetic properties of the particles can be represented by assigning point-like dipole moments to their center, the force between two particles $i$ and $j$ floating on the water surface at relative position $\vec{r}_{ij}$ with parallel dipole moments of magnitudes $\mu_i$, $\mu_j$ can be cast in the form

$$\vec{F}_{ij}^{dd} = 3\frac{\vec{\mu}_i\vec{\mu}_j}{r_{ij}^4}\frac{\vec{r}_{ij}}{r_{ij}}. \tag{3.2}$$

The force in Eq. (3.2) is central, it falls always in the line connecting the two particles, and it is attractive (repulsive) for particles with opposite (parallel) dipole moments. The effect of the fluid on the particles is characterized by

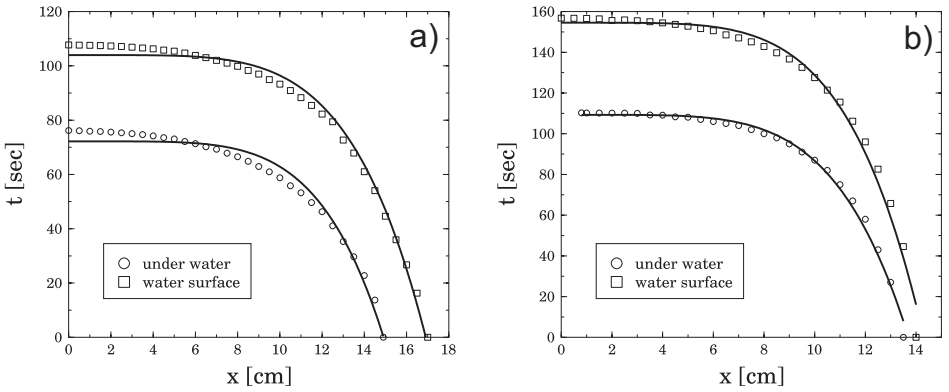


3.3. Figure: The time $t$ as a function of distance $x$ measured during the motion of a magnetic particle: ($a$) prolate particle with extensions $d = 2$ mm and $h = 6$ mm, and ($b$) oblate magnetic particle of diameter $d = 4.0$ mm and height $h = 1.5$ mm attached to a cork disc. The solid lines show the best fits obtained with Eq. (3.6) for both moving on and under the water surface.

the Stokes drag, *i.e.* the force exerted by the fluid $\vec{F}_i^s$ on particle $i$ is assumed to have the form

$$\vec{F}_i^s = -\alpha \vec{v}_i, \tag{3.3}$$

where $\vec{v}_i$ denotes the velocity of the particle relative to the fluid and $\alpha$ is the drag coefficient.

As a first step of the experiments, the motion of a particle in the dipole field of another particle of the same shape but opposite dipole orientation has been measured and compared to analytic calculations based on the interactions defined above. In these tests one particle was fixed while another particle with opposite dipole orientation was released from a distance $x_o$ with zero initial speed $v_0 = 0$. Both particles were initially placed far from the container walls and surfactants had been added to the water to minimize the effect of surface tension.

The equation of motion of the released particle is obtained as

$$m\frac{d^2x}{dt^2} = F_{ij}^{dd} - \alpha\frac{dx}{dt}, \tag{3.4}$$

where $m$ denotes the entire mass of the moving particle. Assuming that the system is fully dissipative and non-inertial, Eq. (3.4) can be reduced to a first order differential equation for the particle position $x$ with the solution

$$t = \frac{\alpha}{3\mu_i\mu_j}\left(x_0^5 - x^5\right). \tag{3.5}$$

The time needed for the moving particle to reach the stationary particle can be determined by setting $x = d$ in the above equation, where $d$ is the diameter of the cork disc. In the experiment, the particle motion was recorded by a digital camera with a distance scale in the foreground, from which kinematic quantities could easily be determined. The time $t$ as a function of distance $x$ was measured for magnetic particles of two different extensions $d = 2$ mm, $h = 6$ mm (more bar-like), and $d = 4.0$ mm, $h = 1.5$ mm (more disc-like), with the same arrangement of swimmers. For the two particle arrangements two sets of measurements were performed: in the first experiment the particles were floating on the water surface, while in the second one, the particles were placed inside a closed container and the external pressure was adjusted to keep the moving particle floating under the liquid surface.

In order to compare the experimental results to the theoretical prediction of Eq. (3.5), the measured data were fitted to the curve

$$t = -a(x^{-b} + c), \tag{3.6}$$

where $a, b$, and $c$ are fitting parameters. The experimental results together with the best fits obtained are presented in Figs. 3.3$(a, b)$. Error bars are not shown in the figures since they are of the same size as the symbols.

It can be observed in the figures that although the motion of particles on the surface and inside the liquid sets in approximately at the same initial distance $x_0$, the time values $t$ obtained are significantly higher for surface motion. This effect is caused by the surface waves generated by the moving particle which results in an additional energy loss and slower motion. However, for both types of motion the experimental results can be well fitted by the functional form of Eq. (3.6). The best fits were obtained with

the parameter values $b = 5.05$ and $b = 4.96$ in Fig. 3.3($a$), and $b = 5.18$ and $b = 5.14$ in Fig. 3.3($b$) for surface and bulk motion, respectively. Comparing the two figures, it can be noted that the fit has a somewhat better quality for particles with more elongated (bar) shape than for the one with disc-shaped dipoles since in this case the point-like dipole approximation provides a more accurate description of the magnetic field. The satisfying values of $b$ obtained by the fitting near the predicted value of 5 imply that the point-dipole approximation and the Stokes drag provide a reasonable description of the dynamics of the system for both particle shapes. Induced mass effects for the acceleration, as well as corrections to the dipole potentials, could be neglected. These experimental findings are important for the understanding of measurements on more complex particle systems and help to construct realistic models of BDMs which capture all relevant interactions of the system (see Chapter 4).

## 3.3 Experiments on self-assembly

After testing the motion of single particles we carried out a large set of experiments in order to study the dynamics of pattern formation in BDMs and to characterize the structure of aggregates obtained. In these experiments the large container of side length $L = 1000$ mm was used. The particles were placed randomly on the rigid plastic net which was then immersed into the carrier water to start the motion of particles. The time evolution of the system was recorded by a digital video camera from which individual snapshots could be extracted. A representative example of the time evolution of the binary dipolar monolayer obtained with our experimental techniques is demonstrated in Fig. 3.4. The experiment was carried out at a concentration $\phi = 10.5\%$ in such a way that the two components had the same magnitude of dipole moment $\mu_r = 1$, the same size $\sigma = 1$, and the same particle number $\phi_r = 1$. To prepare the disordered initial configuration, random particle positions were generated by a computer program then the particles were placed by hand on the top of the plastic net. The particles

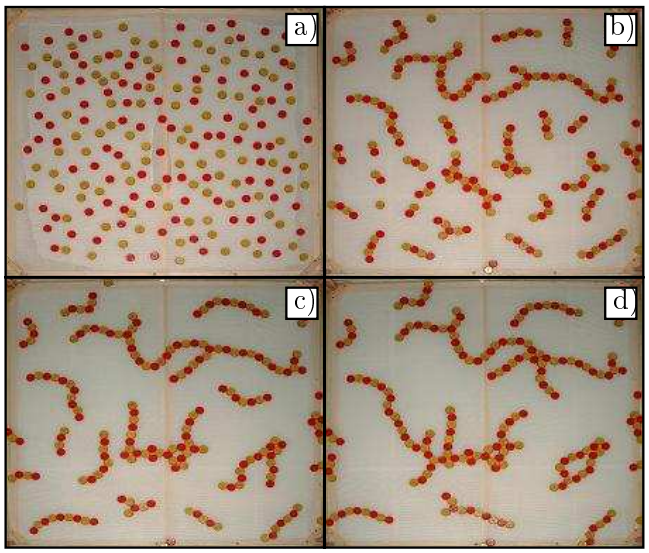


3.4. Figure: Representative example of the time evolution of the experimental system at a concentration $\phi = 0.105$. The relative dipole moment, polydispersity, and relative concentration of the components were set to $\mu_r = 1$, $\sigma = 1$, and $\phi_r = 1$, respectively. The total duration of the experiment was 60 s, snapshots were taken at time values *a*) $t = 0s$, *b*) $t = 10s$, *c*) $t = 30s$, *d*) $t = 60s$.

started to move at the same time when the net was immersed into the water. The time evolution of the system was followed until a frozen state was attained where no further changes occurred. In such a configuration either a single cluster is formed which spans the entire system (high concentration) or the distance of clusters becomes so large that the dipolar interaction is not sufficient to move them. The snapshots of Fig. 3.4 were taken from the digital video film.

In order to give a quantitative characterization of the dynamics of structure formation, and of the geometrical structure of growing aggregates, the coordinates of single particles have to be determined from the digital images. The analysis of the movies were carried out on a computer using public licence computer programs such as GIMP. Since the camera was not exactly

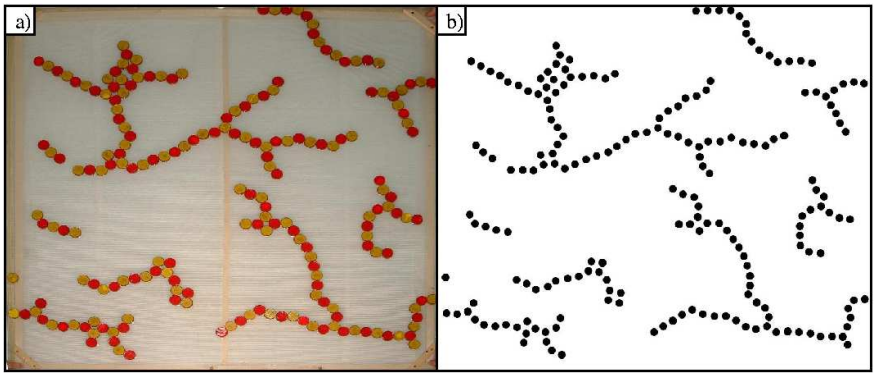


3.5. Figure: For the digital image processing GIMP was used throughout the experiments. In the original snapshot ($a$) black dots were placed on the particles from which a black-and-white image was generated ($b$). We worked out a cluster searching computer program which identifies connected sets of particles.

placed above the center of the square-shaped experimental box, the snapshots were first slightly transformed to avoid the trapezoid perspective of the square box. In order to extract the coordinates of particles in the digital images, we generated black-and-white pictures, where black dots indicate particles on the white background (see Fig. 3.5). This was achieved by defining an additional black-and-white layer above the image in GIMP then the original picture was removed. Finally, we worked out a computer program which determines the coordinates of the center of black discs. Based on the coordinates the program identifies particle clusters and determines all the characteristic quantities of their mass, size, and structure. The black-and-white images were stored as arrays containing ones and zeros such that the identification of aggregates was performed as searching for clusters of ones on the background of zeros. For cluster searching we implemented an efficient algorithm which accelerated the data evaluation.

# 4 Chapter

# Theoretical investigations

Parallel to the experiments we carried out a thorough theoretical investigation of the dynamics of structure formation in binary dipolar monolayers and of the structure of aggregates obtained. We analyzed the formation and stability of simple structures like chains, rings and polygons of particles by analytic means, however, the capabilities of analytical methods is rather limited in this field that is why a large part of our work is based on computer simulations. We worked out a realistic model of binary dipolar monolayers which captures the relevant interaction in the particle system and accounts for the initial and boundary conditions of the experimental setup presented in Chapter 3. In the experimental realizations of BDMs the particle mass is large enough to hinder thermal motion. Hence, molecular dynamics simulations generating deterministic particle trajectories provide an adequate description of the system when studying aggregation and crystallization processes. Our calculations showed that in BDMs molecular crystalline states can be formed which are purely based on the repulsive interaction of particle clusters. Such structures are very sensitive to perturbations that's why we complemented our molecular dynamics studies with thermal noise and carried out Brownian dynamics simulations of BDMs.

The simulation codes were written in Fortran which have been used on the Linux cluster of the Department of Theoretical Physics of the University

of Debrecen. On a Pentium 4 processor of 2GHz frequency and 2 Mbyte cache we could increase the particle number $N$ up to a few thousand with a reasonable CPU time. A large amount of simulations have been carried out varying the parameters of the system, namely, the total concentration $\phi$ of the particles, the relative concentration $\phi_r$, the relative dipole moment $\mu_r$ and the dispersity (relative particle size) $\sigma$ of the components in a broad range [90, 92, 106, 91].

## 4.1 Model construction

In our theoretical model of binary dipolar monolayers an ensemble of $N$ particles is considered in a square shaped box of side length $L$ on the two-dimensional plane. Point-like magnetic dipole moments are assumed to be placed in the middle of particles. For simplicity, the dipole moments of the particles are fixed during the time evolution of the system to be perpendicular to the plane of motion. Particles of the two components have oppositely oriented dipoles with magnitude $\mu_+$ (dipoles pointing upward (+)) and $\mu_-$ (dipoles pointing downward (−)). The two components of the system have $N_+$ particles with dipole moment $\mu_+$ and radius $R_+$, and $N_-$ particles with dipole moment $\mu_-$ and radius $R_-$. The total number of particles in the monolayer is $N = N_+ + N_-$.

The particles are considered to be suspended in an electromagnetically passive liquid so that electrohydrodynamic effects are completely excluded in the model. The liquid only exerts a friction force on the particles which move under the action of the dipole-dipole force. In order to take into account the finite size of the particles, we introduce a repulsive force between the particles when they touch each other [100, 39]. After generating an initial configuration with random particle positions in the simulation box, and fixing the dipole moments according to the different material's properties, the time evolution of the system is followed by solving numerically the equation of motion of particles for the two translational degrees of freedom with periodic boundary conditions (molecular dynamics simulation [2]).

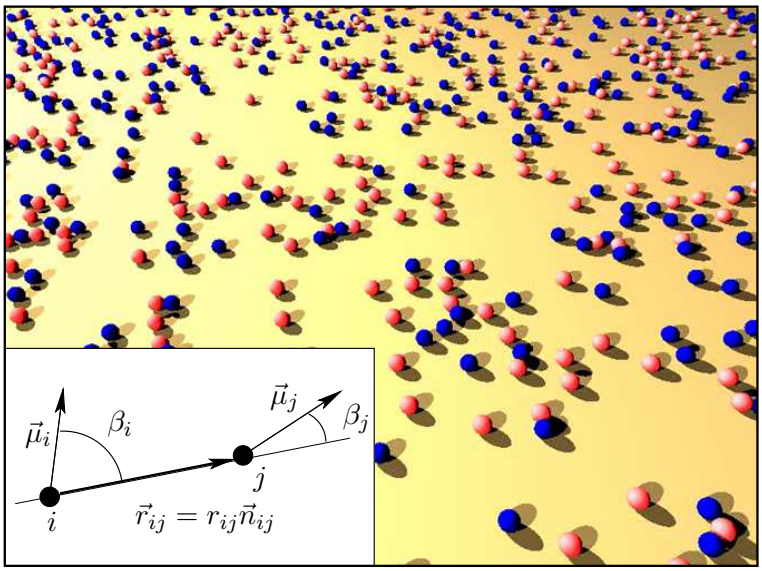


4.1. Figure: An initial configuration of the simulation with $N = 1000$ particles at the concentration $\phi = 0.075$ and relative concentration $\phi_r = 1$. The two components are indicated by different colors. The inset explains the notation used in the model description.

Generally, the interaction between two particles of dipole moments $\vec{\mu}_i$ and $\vec{\mu}_j$ with positions $\vec{r}_i$ and $\vec{r}_j$ can be cast in the form

$$\vec{F}_{ij}^{dd} = \frac{3}{r_{ij}^5}\left[\left(\frac{5(\vec{\mu}_i\vec{r}_{ij})(\vec{\mu}_j\vec{r}_{ij})}{r_{ij}^2} - (\vec{\mu}_i\vec{\mu}_j)\right)\vec{r}_{ij} - (\vec{\mu}_i\vec{r}_{ij})\vec{\mu}_j - (\vec{\mu}_j\vec{r}_{ij})\vec{\mu}_i\right], \quad (4.1)$$

where $\vec{r}_{ij} = \vec{r}_j - \vec{r}_i$ denotes the relative position of the particles. When the dipole moments are perpendicular to the plane of motion this equation simplifies to the form

$$\vec{F}_{ij}^{dd} = \frac{3\mu_i\mu_j}{r_{ij}^4}\vec{n}_{ij}. \quad (4.2)$$

Under such conditions the dipole-dipole force Eq. (4.2) is isotropic (central), it always falls in the plane of motion parallel to the line $\vec{n}_{ij}$ connecting the

two particles. (For an explanation of the notation see Fig. 4.1.) The force is repulsive for particles of the same type and attractive for different ones. It is interesting to note that the binary dipolar monolayer is rather similar to an ensemble of charges where the interaction force decreases faster than the Coulomb force.

Our measurements presented in Chapter 3 have shown that the action of the embedding liquid on the particles can be characterized by the Stokes drag

$$\vec{F}_i^{hyd} = -\alpha_i \frac{d\vec{r}_i}{dt}, \tag{4.3}$$

where $d\vec{r}_i/dt$ denotes the velocity of particle $i$. The drag coefficient $\alpha_i$ depends on the radius $R_i$ of the particles and on the viscosity $\eta$ of the liquid $\alpha_i = 6R_i\pi\eta$.

The particles are assumed to be deformable bodies which can overlap each other during their motion. To capture the finite size of the particles an elastic force is included between overlapping particles $r_{ij} < d$ according to Hertz's contact law

$$\vec{F}_{ij}^{pp} = -k_{pp}((R_i + R_j) - r_{ij})^{\frac{3}{2}}\vec{n}_{ij} = -k_{pp}\vec{f}_{ij}^{dd}, \tag{4.4}$$

where $k_{pp}$ is a material dependent constant and the superscript $'pp'$ refers to the particle-particle contact. This equation shows that the force is proportional to the 3/2 power of the overlap distance, which can be obtained from the Lamé equations of elastic bodies. The value of $k$ is set such that the overlap $\delta = d - r_{ij}$ (for $r_{ij} < d$) remains always small $\delta \ll d$. Stochastic forces are not included in the model, so trajectories of particles are deterministic. The particle system is supposed to be fully dissipative, hence, the equation of motion simplifies to a first order differential equation system

$$\frac{d\vec{r}_i}{dt} = \frac{1}{\alpha_i}\sum_j \vec{F}_{ij}^{dd} - \frac{k_{pp}}{\alpha_i}\sum_{r_{ij}<R_i+R_j} \vec{f}_{ij}^{pp}, \qquad i = 1, ..., N. \tag{4.5}$$

which is solved numerically to obtain the trajectories $\vec{r}_i(t)$, $i = 1, \ldots, N$ of the particles [2]. Since no stochastic forces are introduced in the equa-

tion of motion Eq. (4.5), the trajectories of the particles are completely deterministic, disorder is solely introduced by the randomness of the initial configuration.

A model system of $N$ particles consists of $N_+$ and $N_-$ particles of dipole moment $\mu_+$ pointing upward (+), and dipole moment $\mu_-$ pointing downward (−), respectively. The partial concentrations of the components $\phi_+$ and $\phi_-$ are defined as the coverage $\phi_\pm = NR_\pm^2\pi/L^2$, whose ratio provides the relative concentration $\phi_r = \phi_-/\phi_+ = N_-/N_+$. The total particle concentration $\phi$ is defined analogously $\phi = \phi_+ + \phi_- = (N_+R_+^2\pi + N_-R_-^2\pi)/L^2$. The particle size dispersity $\sigma$ in the system is characterized by the ratio of the two radii $\sigma = R_-/R_+$. In the model the magnitudes $\mu_+$, $\mu_-$ of dipole moments can be freely varied which captures up to some extent the effect of frequency tuning in the experiment of Ref. [68]. For simplicity, in the computer simulations we fix $\mu_+$ and vary the ratio $\mu_r = \mu_-/\mu_+$, *i.e.* the relative dipole moment. Similarly, the radius $R_+$ is set to unity and the ratio $\sigma$ is varied in the calculations.

## 4.2 Initial configuration and boundary conditions

The simulations always start from a random initial configuration. In order to ensure the disordered spatial structure of finite size particles in the initial state, first point-like particles are placed in a two dimensional square box of side length $L$ randomly and independently with a uniform distribution. Then the particles are gradually blown-up, *i.e.*, the particle radius is gradually increased such that after each increment molecular dynamics simulation is performed taking into account only the repulsive force arising between the overlapping particles and the Stokes drag. To solve the equation of motion of the particles when generating the initial conditions, we use a fifth order predictor-corrector method [2]. As a result of the simulation all the particle can find an equilibrium, overlap-free position. This procedure is repeated until the particle radius $R$ reaches the desired value. Disorder is solely introduced by the randomness of the initial configuration, no random forces

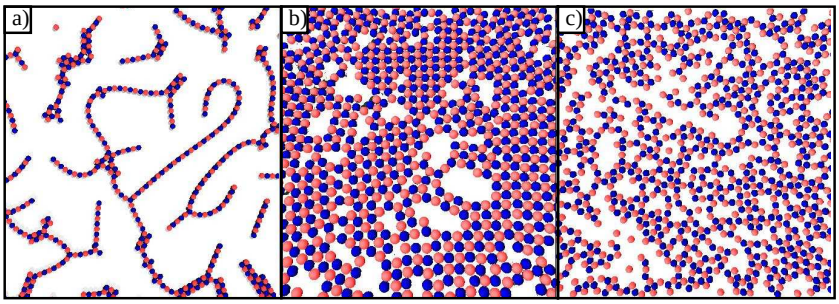


4.2. Figure: Examples of simulation results obtained with $N = 1000$ particles for $\sigma = 1.0$, $\phi_r = 1$, $\mu_r = 1.0$ at different concentrations $(a)$ $\phi = 0.1$, $(b)$ $\phi = 0.7$, $(c)$ $\phi = 0.5$.

are taken into account during the time evolution of the system (quenched disorder). An example of the initial configuration obtained by the simulation technique is presented in Fig. 4.2.

To simulate processes of binary dipolar monolayers the dipole moments of the particles are fixed perpendicular to the plane of motion. according to the different material's properties. It implies that we could model the frequency range of the experiments of Ref. [68] where different particles attract each other. In most of the simulations the number of particles $N$ was fixed and the concentration $\phi$ was controlled by setting appropriate value for the system size $L = \sqrt{\frac{N_+ R_+^2 \pi + N_- R_-^2 \pi}{\phi}}$. In order to reduce the surface effects in the simulation, we used periodic boundary conditions, assuming that the simulation box is part of a larger system. For simplicity, the minimum image convention was used such that the system was surrounded by its eight identical copies, which also implies that the dipole-dipole interaction was truncated at the cutoff distance $r_c = L/2$ [2].

## 4.3 Computer simulations

In order to obtain the time evolution of the system, molecular dynamics simulations were performed, *i.e.* we solved numerically the equation of motion

of the particle system Eq. (4.5). For this purpose we implemented a 5th order adaptive Runge-Kutta method which provides an efficient and accurate treatment of the problem. For details of the method see Ref. [58]. For the preparation of the initial condition also molecular dynamics simulations were carried where a 5th order Gear Predictor-Corrector Method was applied due to technical reasons [2]. Representative snapshots of computer simulations are presented in Fig. 4.2 which were obtained by varying the concentration of the particles $\phi$ when the other parameters were fixed $\phi_r = 1$, $\mu_r = 1$, $\sigma = 1$. Further details of the simulations will be presented in subsequent Chapters when discussing the research results.

The numerical results are stored in such a way that snapshots are made about the system by saving all the relevant information of the particles (position, velocity, ...) at certain times. The data evaluation and analysis of the simulation results were performed independently of the simulations. For this purpose we worked out a computer program which analyzes the series of snapshots (a few Gigabytes for a single simulation) and determines all the quantities of interest such as cluster structure, interaction energy, correlations function, order parameter as it will be presented later. This separation of the simulation and evaluation programs made possible an efficient use of computer resources.

# 5 Chapter

# Simple structures in binary dipolar monolayers

It was observed in experiments [68] that at low concentrations in binary dipolar monolayers the particles undergo a kinetic aggregation process giving rise to chains and closed loops (rings, polygons) of alternating particles. The occurrence of particle rings has also been observed in magnetorheological fluids [100, 39, 32] containing particles of permanent magnetic moments and in vibrofluidized dry granular materials of dipolar particles [79, 7] in the absence of external magnetic field. In these systems however, the dipole moment of the particles lies in the plain of the ring and the anisotropic nature of the dipole-dipole interaction makes possible the ring formation: compared to a straight chain of aligned dipoles the ring is energetically favorable because the closing of the two ends of the chain overweights the energy loss due to the misalignment of dipoles [100, 39, 32]. Since closed loops of dipoles become rather inactive in the system, they can have a substantial effect on the long time evolution of structure formation processes of BDMs.

In the following we analyze the energetics of chain and ring formation varying the number of particles and the relative dipole moment of the two components [90]. The energy of chains and rings can be derived from the

interaction energy of two dipoles $\vec{\mu}_i$ and $\vec{\mu}_j$ with positions $\vec{r}_i$ and $\vec{r}_j$

$$E = \frac{1}{r_{ij}^3}\left[(\vec{\mu}_i\vec{\mu}_j) - 3\,(\vec{\mu}_i\vec{n}_{ij})\,(\vec{\mu}_j\vec{n}_{ij})\right]. \tag{5.1}$$

Here $r_{ij} = |\vec{r}_i - \vec{r}_j|$ denotes the distance of the two particles, and $\vec{n}_{ij}$ is the unit vector pointing from particle $j$ to $i$, *i.e.* $\vec{r}_i - \vec{r}_j = \vec{n}_{ij} r_{ij}$. In our binary dipolar monolayer the particles of the two components are constrained to move in a plane and their dipole moments are fixed to be perpendicular to the plane of motion. In this case Eq. (5.1) can be reduced to the simple form

$$E = \frac{\mu_i \mu_j}{r_{ij}^3}, \tag{5.2}$$

where the magnitude of dipole moments $\mu_i$ can take two different values $\mu_+$ and $\mu_-$ corresponding to the two components. Details of the calculations have been presented in Ref. [90].

## 5.1 Chains of dipoles

In BDMs anisotropic chain-like clusters occur in spite of the isotropic inter-particle forces which can be explained such that at low concentrations cluster structures are determined by the tendency that particles with parallel (oppositely) directed dipole moments try to maximize (minimize) their distance. The energy of a chain composed of an even number $N$ of alternating particles can be written as a function of the relative dipole moment $\mu_r$ in the form

$$E_{ch} = \underbrace{-\mu_r \frac{\mu_+^2}{d^3} \sum_{k=1}^{N-1} \frac{N-k}{k^3}}_{E_{+-}} + \underbrace{\frac{1+\mu_r^2}{2} \frac{\mu_+^2}{d^3} \sum_{k=2}^{N-2} \frac{N-k}{k^3}}_{E_{--}+E_{++}}, \tag{5.3}$$

where the dipole moment $\mu_+$ is assumed to be fixed, furthermore, in the first and the second term the summation is restricted to odd, and even values of $k$, respectively.

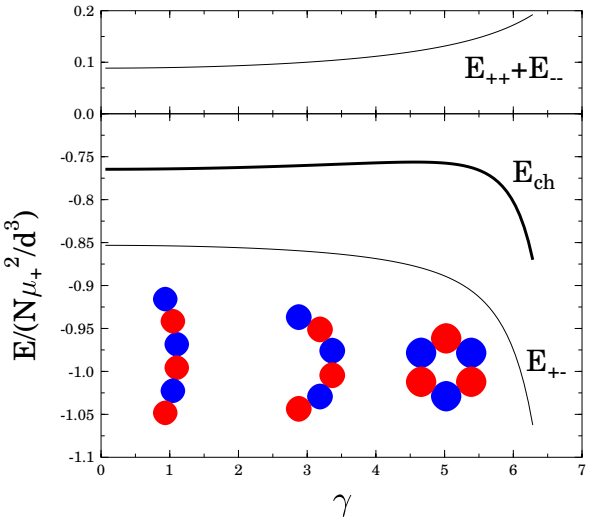


5.1. Figure: Energy of a bent chain divided by the number of particles as a function of the bending angle $\gamma$ obtained from Eq. (5.5) for $N = 6$. For clarity, the particle configurations are also shown for $\gamma = 1, \pi, 2\pi$.

In Eq. (5.3) the first term $E_{+-}$ denotes the interaction energy of different types of particles, while the second one is the sum of the interaction energies of the same type of particles $E_{++} + E_{--}$. In the special case of $\mu_r = 1$, when oppositely oriented dipoles have the same magnitude Eq. (5.3) simplifies to the form

$$\begin{aligned} E_{ch} &= \underbrace{-\frac{\mu_+^2}{d^3}\sum_{k=1}^{N-1}\frac{N-k}{k^3}}_{E_{+-}} + \underbrace{\frac{\mu_+^2}{d^3}\sum_{k=2}^{N-2}\frac{N-k}{k^3}}_{E_{--}+E_{++}} \\ &= \frac{\mu_+^2}{d^3}\sum_{k=1}^{N-1}(-1)^k\frac{N-k}{k^3}. \end{aligned} \tag{5.4}$$

Since thermal motion is hindered by the relatively large particle mass, when a chain is formed in the colloid, it cannot reorganize itself to further decrease its energy. We remark that the role of the Brownian motion of particles in

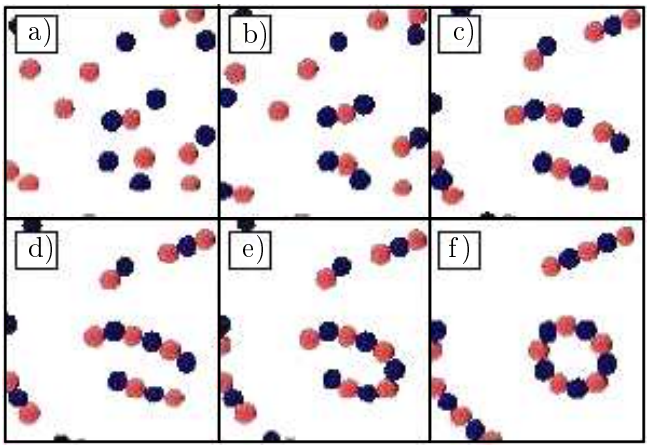


5.2. Figure: Formation of a ring of alternating particles starting from a random configuration at $\mu_r = 1$, $\phi_r = 1$, and $\phi = 0.125$. Two nearby chains join and create a ring.

the restructuring of colloidal aggregates has recently been demonstrated in Ref. [12] for a single component system. It was found that thermal motion facilitates the occurrence of loops and rings of particles. When longer chains are formed by the aggregation of shorter ones, usually they undergo a straightening process until they reach the deepest energy given by Eqs. (5.3) and (5.4).

## 5.2 Rings

In order to understand the appearance of closed loops of alternating particles observed in experiments we calculated how the energy of a chain changes when it is gradually bent and finally closed to form a ring. Due to symmetry reasons a perfect regular ring can only be an equilibrium configuration when both types of particles have the same magnitude of dipole moment $\mu_r = 1$ that's why the following calculations are restricted to this case. Under the bending process the particles are assumed to lie always on a circular arc

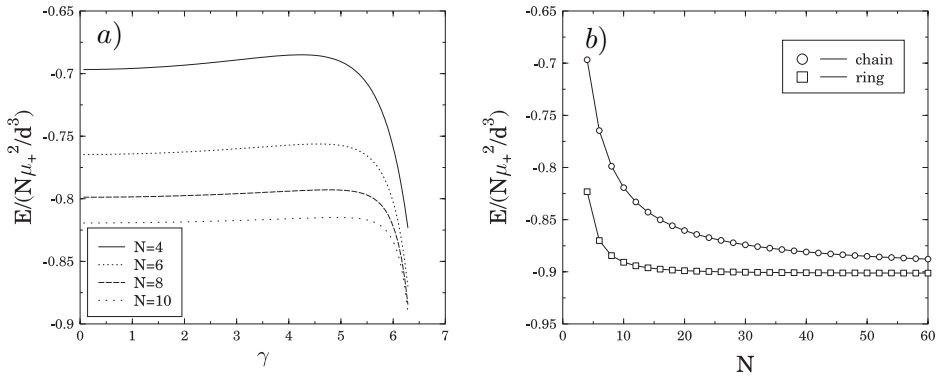


5.3. Figure: ($a$) Energy divided by the number of particles of a bent chain for $N = 4, 6, 8, 10$. $E_{ch}(\gamma = 0)$ and $E_{ch}(\gamma = 2\pi)$ provide the energy of a straight chain and a perfect ring, respectively. ($b$) Comparison of chain and ring energies as a function of the number of particles $N$. The energy difference of the two configurations disappears as $N$ increases.

parameterized by the bending angle $\gamma$ which ranges from 0 (straight chain) to $2\pi$ (closed ring). Starting from Eq. (5.4) the energy $E_{ch}$ of a bent chain as a function of $\gamma$ can be cast in the form for an even number $N$ of particles

$$E_{ch}(\gamma) = \frac{\mu_+^2 \sin^3\left(\frac{\gamma}{2N}\right)}{d^3} \left[\sum_{k=1}^{N-1} (-1)^k \frac{N-k}{\sin^3\left(k\frac{\gamma}{2N}\right)}\right]. \tag{5.5}$$

The form of $E_{ch}(\gamma)$ is illustrated in Fig. 5.1 for $N = 6$ where the interaction energy of identical $E_{++}(\gamma) + E_{--}(\gamma)$ and different particles $E_{+-}(\gamma)$ are also shown separately. Since during the gradual bending process the particles of the chain get closer to each other, the sum of the energies $E_{++} + E_{--}$ monotonically increases, which results in an increase of the total energy $E_{ch}$. However, the interaction energy $E_{+-}$ of different particles is a monotonically decreasing function of $\gamma$ which can overweight the repulsion of identical particles when surpassing a certain bending angle making the closed ring to be energetically favorable for the particle system. It follows from the above argument that a chain of an even number of particles cannot spontaneously

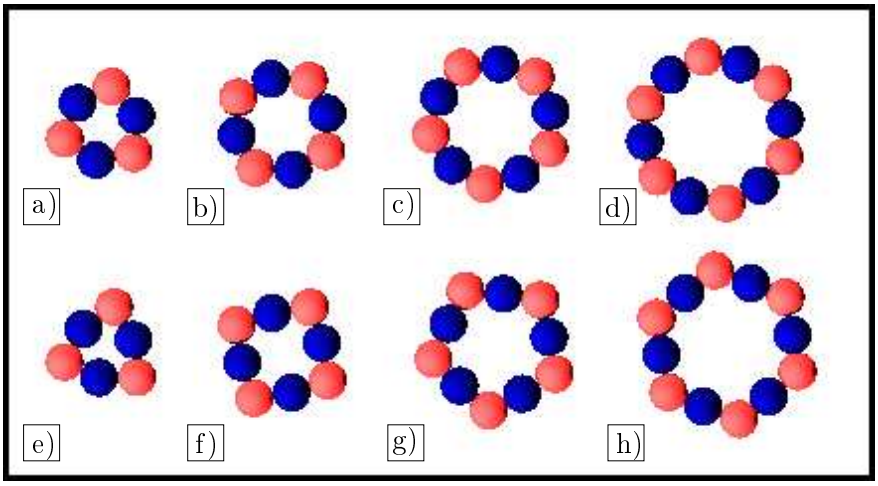


5.4. Figure: Transformation of regular rings (upper row) of alternating particles into regular polygons (lower row) when increasing the relative dipole moment starting from $\mu_r = 1$ for $N = 6$ $(a, e)$, $N = 8$ $(b, f)$, $N = 10$ $(c, g)$, and $N = 12$ $(d, h)$.

close to form a ring due to the energy barrier. Instead, rings emerge starting from a random configuration by the aggregation of nearby chains formed with appropriate orientation as it is demonstrated by Fig. 5.2. In the figure a magnified view of a region of a simulation box is presented where a ring occurred. The gradual aggregation of particles into chains can nicely be observed, which then merge and close into a ring. Fig. 5.3$(a)$ illustrates the energy of bent chains as a function of $\gamma$ for various number of particles $N$. It can be observed in the figure that the energy barrier for bending and the difference of the chain and ring energies, *i.e.*, the difference of $E_{ch}(\gamma = 0)$ and $E_{ch}(\gamma = 2\pi)$, decrease with increasing $N$. Comparing chain and ring energies in Fig. 5.3$(b)$ in a broad range of $N$, it can be seen that the difference decreases with increasing $N$ and it disappears in the limit of large $N$. So from energetic point of view there is no difference between a large ring and a chain.

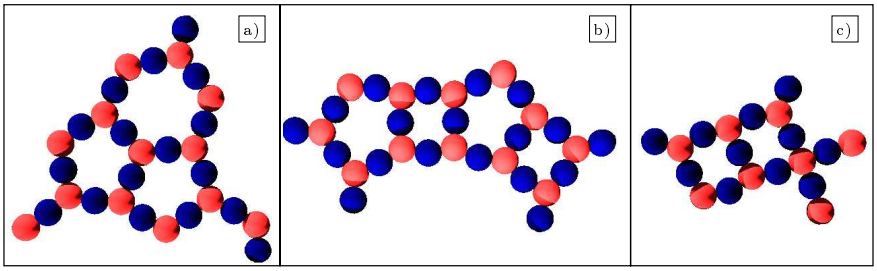


5.5. Figure: Net-like structures of polygons obtained by computer simulations with parameter values $\mu_r = 2.0$, $\phi_r = 1$, and $\phi = 0.125$.

## 5.3 Polygons

When increasing $\mu_r$ in the model starting from a regular ring at $\mu_r = 1$, the ring structure gets distorted because particles of the larger dipole moment tend to increase their distance. At any value of $\mu_r$ both types of particles lie always on a circle, however, the radius is larger for particles of the larger dipole moment. Finally, the structure ends up in a regular polygon of corner number $N/2$, where particles of the larger moment are located in the corners, and the smaller ones are in the middle of the sides of the polygon. The transformation of regular rings into regular polygons of alternating particles with increasing $\mu_r$ is demonstrated by Fig. 5.4.

Increasing the relative dipole moment $\mu_r$ further, the polygon structure suddenly opens up into a straight chain or breaks up into short chains. It follows from our calculations that the closed loops of particles observed in the experiments of Ref. [69] must attain a spatial structure between the perfect ring and polygon conformations. Since closed loops (distorted rings) emerge by the aggregation of appropriately oriented nearby chains and only in the case of even number of particles, it is a rather rare event depending also on the concentration. Simulations showed that they most frequently occur at concentrations $\phi \approx 0.125$ with $\phi_r = 1$, and $\mu_r = 1$. It also follows from the above arguments that polygonal structures can occur in extended

systems when $\mu_r > 1$ and the concentration is high enough to have merging chains. Computer simulations showed that polygons can also form a net-like structure and even an extended lattice which will be partly discussed in Chapter 8 in the context of molecular crystalline states. Figure 5.5 presents representative examples of nets of polygons obtained at $\mu_r = 2.0$ $\phi_r = 1$, and $\phi = 0.125$. Figure 5.5($c$) should be compared to the lattice structure of Fig. 8.4($a$).

# 6 Chapter

# Heteroaggregation phenomena

Binary dipolar monolayers provide a two-dimensional binary colloidal layer where heteroaggregation can be studied under well controlled conditions. It has been presented in Chapter 3 that our experimental technique overcomes the difficulties of heteroaggregation experiments by allowing for direct optical observation of single clusters [93]. In this Chapter we present a quantitative analysis of heteroaggregation in the two-component dipolar system focusing on the kinetics of aggregation and on the structure of growing aggregates. The direct optical observation makes possible the precise tracking of all clusters and a detailed investigation of cluster discrimination. We give experimental evidence that growing dipolar aggregates have a crossover from chain-like to branched structures whose fractal dimension is equal with that of self-avoiding random walks and reaction limited cluster-cluster aggregation. The average cluster size and average number of particles have a power law time dependence where the dynamic exponents increase with the concentration of particles. One of the most important outcome of our experiments is the clear evidence for cluster discrimination, *i.e.* experiments revealed a different behavior for clusters containing an even and odd number of particles up to the crossover cluster size. We determine the optimal conditions to observe cluster discrimination in BDMs [93, 94]. In the second part of the Chapter we present computer simulations of aggregation phenomena

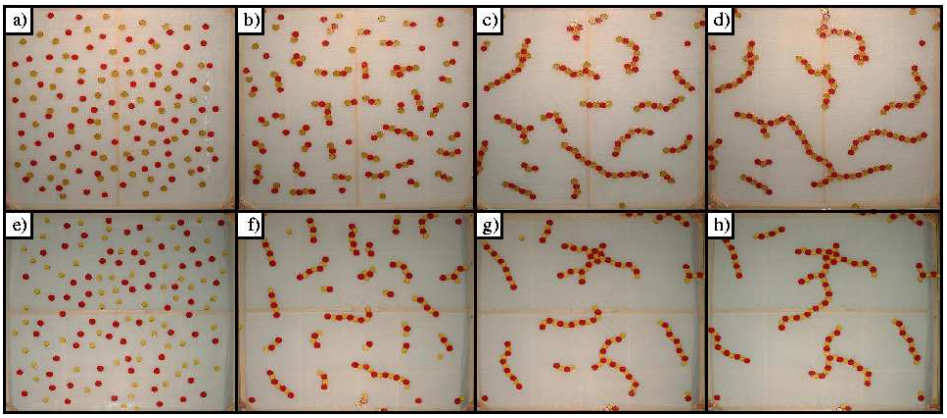


6.1. Figure: The time evolution of cluster-cluster aggregation for setup $(A)$ $(a, b, c, d)$ at the concentration $\phi = 7.5\%$ and for setup $(C)$ $(e, f, g, h)$ at $\phi = 6.0\%$. Starting from the random initial configuration $(a, e)$ first single particles aggregate and form short chains $(b, f)$, which then merge resulting in large branching structures $(c, d, g, h)$.

of BDMs. Under simplifying assumptions we also analyze the dynamics of aggregation by analytic means [90, 92, 106].

## 6.1 Process of aggregation

Our experimental setup provides a simple realization of BDMs where heteroaggregation can easily be studied under well controlled conditions. We considered three experimental setups with the parameter sets $(A)$ $\mu_r = 1$, $\sigma = 1$; $(B)$ $\mu_r = 2$, $\sigma = 1$; and $(C)$ $\mu_r = 1$, $\sigma = 1.5$. The two components had always the same particle number $\phi_r = 1$, while the concentration was varied: in the first two cases $(A)$ and $(B)$ three concentrations were considered $\phi = 5, 7.5\%$, and $10.5\%$, however, due to technical limitations in the third case only two different concentrations could be realized $\phi = 4, 6\%$. At each concentration the experiments were repeated 10 times starting from different random configurations. The process of aggregation was recorded by a digital video camera until a frozen state was attained where no fur-

ther changes occurred. In such a configuration either a single cluster was formed which spaned the entire system (typically at higher concentrations) or the distance of clusters became so large that the dipolar interaction was not sufficient to move them on the water surface (at low concentrations). The typical duration of the experiments was 1-3 minutes depending on the concentration.

Representative examples of the time evolution of the aggregating particle system can be seen in Fig. 6.1 for setups $(A)$ and $(C)$. It can be observed in the figure that starting from the random initial configuration (Fig. 6.1$(a, e)$), first single particles move and aggregate forming short chains (Fig. 6.1$(b, f)$). The single particle interaction Eq. (3.2) is isotropic, however, a chain behaves as an extended planar dipole resulting in an anisotropic chain-chain interaction. As a consequence, chains rotate on the water surface and try to merge at their ending points giving rise to longer chains. Comparing Figs. 6.1$(c, g)$ and 6.1$(d, h)$ it can be seen, however, that as chains get longer merging occurs not only at chain ends but also at internal particles which gives rise to branched planar structures. Note that closed loops rarely occur at this relatively low concentration, even branched clusters have always open structures.

## 6.2 Structure of growing aggregates

In the snapshots extracted from the movies, the cluster size $S$ was determined as the number of particles in the clusters. In order to characterize the structure of growing aggregates we calculated the radius of gyration $R_g$ for each cluster in the snapshots and averaged over clusters of the same size $S$. The radius of gyration characterizing the linear extension of a cluster of $S$ particles can be calculated as

$$R_g^2(S) = \frac{1}{S(S-1)} \sum_{i \neq j=1}^{S} (\vec{r}_i - \vec{r}_j)^2, \tag{6.1}$$

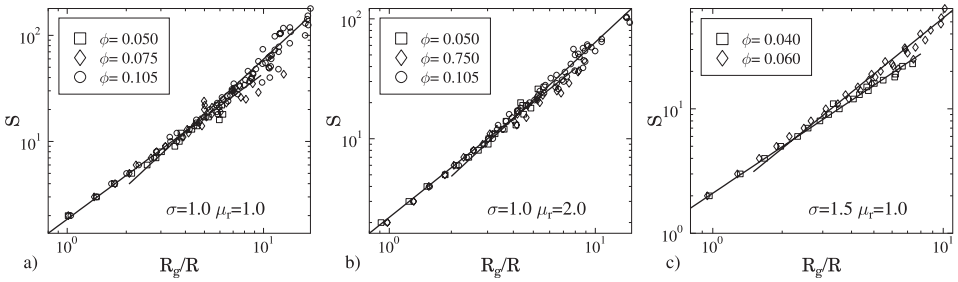


6.2. Figure: $S(R_g)$ obtained in experiments for the three experimental setups. The slopes of the fitted straight lines $D_1$ and $D_2$ are summarized in Table 6.1.

where $\vec{r}_i$ denotes the position vector of particle $i$ in the cluster. The cluster size $S$ is plotted as a function of the radius of gyration $R_g$ in Fig. 6.2 for the three sets of experiments. It can be observed that in all cases $S(R_g)$ shows a power law behavior

$$S(R_g) \sim R_g^D, \tag{6.2}$$

where the exponent $D$ is different for small $D_1$ and large $D_2$ cluster sizes. Since small clusters have chain-like morphology while the large ones are branched, the fractal dimension of large clusters have a significantly higher value $D_1 < D_2$. (The measured values of $D_1$ and $D_2$ are summarized in Table 6.1 for the three experimental setups.) Data analysis revealed that in spite of the chain-like morphologies, the value of the fractal dimension $D_1$ is considerably larger than 1. The reason is that the surface friction at the contact of particles and the absence of thermal motion prevent bent chains to relax to the energetically most favorable perfectly straight configurations.

When nearby straight chains merge with a large relative angle, typically

a highly bent chain occurs which has a low radius of gyration compared to the perfectly straight shape. In Chapter 5 we have shown by analytic calculations that the closed loop conformation has a deeper energy than

| | Setup (A):$\mu_r = 1, \sigma = 1$ | | | |
|---|---|---|---|---|
| $\phi$ [%] | $D_1(\Delta D_1)$ | $D_2(\Delta D_2)$ | $Z(\Delta Z)$ | $Z'(\Delta Z')$ |
| 5 | 1.36(0.05) | 1.61(0.07) | 0.46(0.04) | 0.40(0.04) |
| 7.5 | 1.36(0.05) | 1.59(0.07) | 0.58(0.05) | 0.49(0.04) |
| 10.5 | 1.36(0.05) | 1.61(0.07) | 0.98(0.09) | 0.71(0.07) |

| | Setup (B):$\mu_r = 2, \sigma = 1$ | | | |
|---|---|---|---|---|
| $\phi$ [%] | $D_1(\Delta D_1)$ | $D_2(\Delta D_2)$ | $Z(\Delta Z)$ | $Z'(\Delta Z')$ |
| 5 | 1.37(0.06) | 1.62(0.07) | 0.45(0.04) | 0.34(0.03) |
| 7.5 | 1.37(0.06) | 1.63(0.07) | 0.56(0.04) | 0.47(0.04) |
| 10.5 | 1.37(0.06) | 1.63(0.07) | 0.73(0.05) | 0.54(0.04) |

| | Setup (C):$\mu_r = 1, \sigma = 1.5$ | | | |
|---|---|---|---|---|
| $\phi$ [%] | $D_1(\Delta D_1)$ | $D_2(\Delta D_2)$ | $Z(\Delta Z)$ | $Z'(\Delta Z')$ |
| 4 | 1.28(0.06) | 1.55(0.07) | 0.58(0.04) | 0.49(0.04) |
| 6 | 1.28(0.06) | 1.55(0.07) | 0.59(0.04) | 0.55(0.04) |

6.1. Table: Summary of the measured values of the fractal dimensions $D_1$ and $D_2$, and of the dynamic exponents $Z$ and $Z'$ for the three experimental setups. All the quantities were averaged over 10 experiments. The errors are given in brackets for all the values.

straight chains, however, an energy barrier prevents bent chains from closing [90]. The interplay of contact friction and bending rigidity results in stable chains with high local bending angles (see Fig. 6.1). As a consequence, the fractal dimension of dipolar chains becomes larger than 1 indicating a more compact morphology. It has to be emphasized that the value of $D_1$ agrees very well with the fractal dimension of self avoiding random walks $D_{SAW} = 4/3$ in the two-dimensional embedding space $d = 2$, as it can be expected from the above argument [96, 95].

Our experiments revealed that the measured values of the fractal dimensions $D_1$ and $D_2$ of binary dipolar clusters are independent of the concentra-

tion $\phi$, relative dipole moment $\mu_r$, and polidispersity $\sigma$ of the particles (see Table 6.1), however, the location of the crossover point $S_c$ between the two regimes of different fractal dimensions $D_1$ and $D_2$ has a strong concentration dependence. At low concentrations the crossover cannot even be observed, all the clusters lie along the same power law of exponent $D_1$. Increasing the concentration the crossover point shifts downwards, *i.e.* $S_c$ is a decreasing function of $\phi$. Due to technical reasons, we could not vary the concentration $\phi$ in a broad range (at low concentrations the small particle number gives rise to poor statistics, while at high concentrations $\phi > 15\%$ crystallites can locally occur, see also Ref. [93]), thus from the experiments we could not deduce the functional form of $S_c(\phi)$. Above the crossover point $S_c$ when branching dominates, the measured fractal dimension $D_2 = 1.6 \pm 0.07$ falls close to the fractal dimension of reaction limited cluster-cluster aggregation (RLCCA) where merging of clusters of different sizes is also allowed $D_{RLCCA} = 1.59 \pm 0.01$ [95].

## 6.3 Dynamics of aggregation

The snapshots presented in Fig. 6.1 have shown that as time elapses the clusters get larger while their number decreases. The dynamics of the aggregation process can be characterized by studying the cluster size distribution $n_S(t)$ which is the average number of clusters of size $S$ at time $t$. The average cluster size $S_{av}$ and the average number of clusters $n_c$ in a given system can be obtained from $n_S(t)$ as

$$S_{av}(t) = \frac{\sum_S n_S(t) S^2}{\sum_S n_S(t) S}, \qquad \text{and} \qquad n_c(t) = \sum_S n_S(t), \tag{6.3}$$

which are then averaged over samples of different random initial conditions. Figure 6.3 presents $S_{av}$ and $n_c$ as a function of time for the three experimental setups. It can be observed that in all cases the curves can be well fitted by power law functional forms

$$S_{av} \sim t^Z, \qquad \text{and} \qquad n_c \sim t^{-Z'}, \tag{6.4}$$

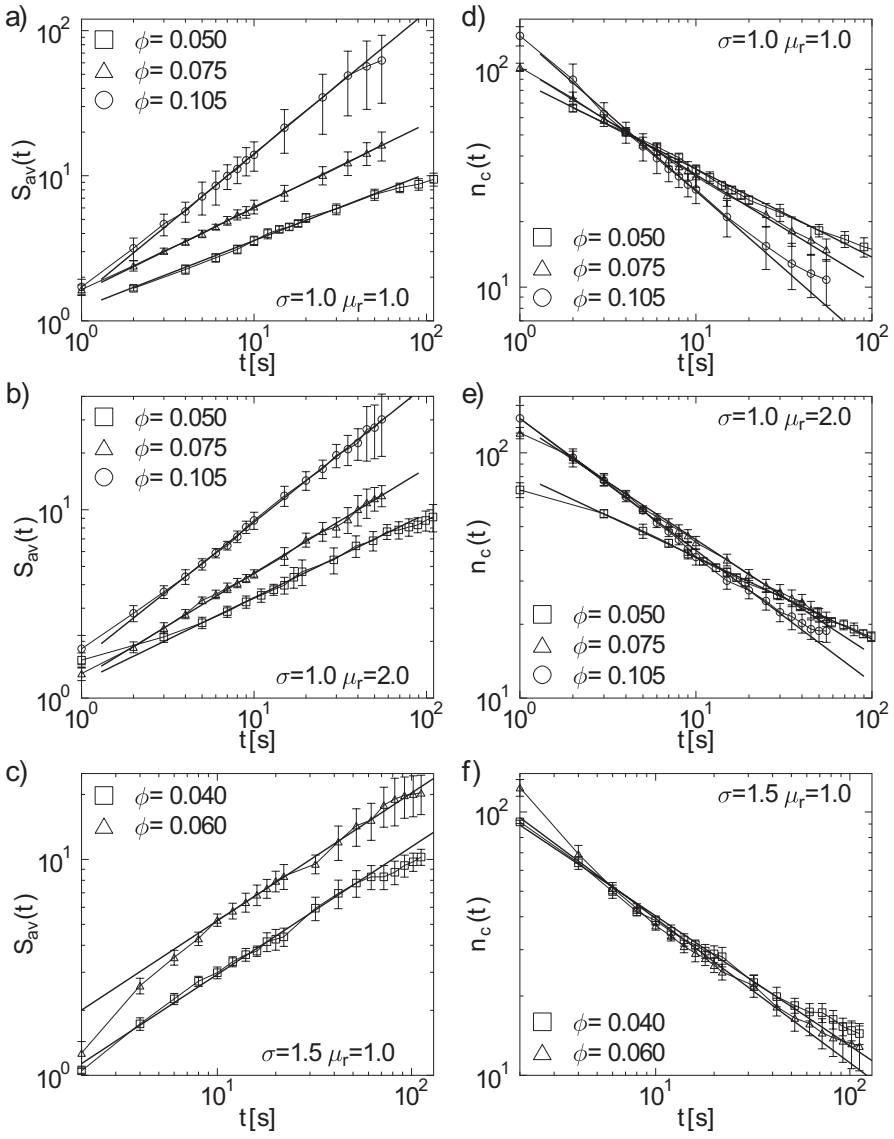


6.3. Figure: Average cluster size $S_{av}$ (*left column*) and average number of clusters $n_c$ (*right column*) as a function of time for the three experimental setups: $(a), (d)$ $\mu_r = 1$ and $\sigma = 1$, $(b), (e)$ $\mu_r = 2$ and $\sigma = 1$ $(c), (f)$ $\mu_r = 1$ and $\sigma = 1.5$.

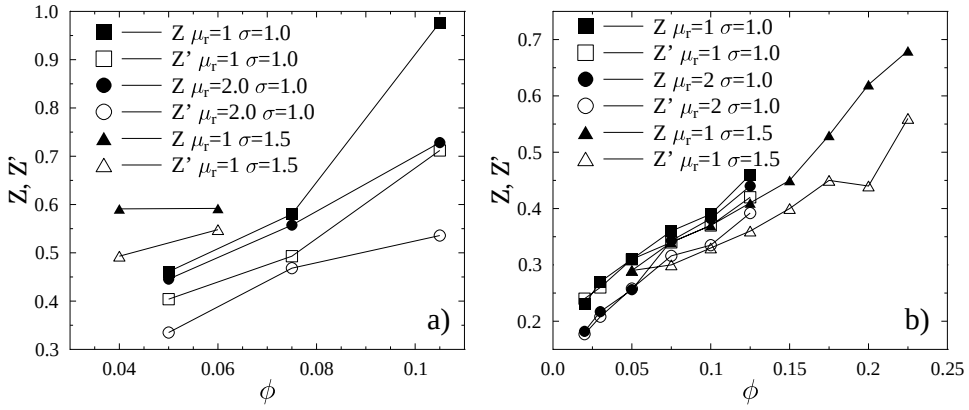


6.4. Figure: Dynamic exponents $Z$ and $Z'$ as a function of concentration $\phi$ $(a)$ obtained by experiments and $(b)$ by computer simulations for the three experimental setups. It can be observed that $Z(\phi) > Z'(\phi)$ in all cases but in the dilute limit the difference decreases.

where the exponents $Z$ and $Z'$ characterize the dynamics of aggregation. In each experiment 20 snapshots were extracted from the movies which made possible an accurate determination of $Z$ and $Z'$. In each setup the experiments were repeated 10 times with different initial positions of the particles. The values of the dynamic exponents $Z$ and $Z'$ are presented in Table 6.1. Fig. 6.4$(a)$ presents that the dynamic exponents have a strong concentration dependence, *i.e.* both $Z$ and $Z'$ increase with increasing $\phi$, furthermore, $Z(\phi) > Z'(\phi)$ holds in all the three experimental setups. The Vicsek-Family scaling theory of kinetic aggregation (see also Sec. 2.2.1) predicts for $n_S(t)$ the functional form

$$n_S(t) \sim s^{-2} f\left(\frac{s}{s^*(t)}\right) \sim t^{-w} s^{-\tau} g\left(\frac{s}{s^*(t)}\right), \tag{6.5}$$

where $s^*(t)$ is the typical cluster size, furthermore, $f$ and $g$ are scaling functions [95]. According to the theory, if $\tau < 1$ then $S_{av}(t) \sim s^*(t)$ and $n_c(t) \sim [s^*(t)]^{-1}$, and hence, the equality $Z = Z'$ follows. The scaling form Eq. (6.5) provides a good description for diffusion limited cluster-cluster ag-

gregation phenomena [95]. In our case $\tau < 1$ can be verified so that the observed inequality of $Z$ and $Z'$ implies that in the concentration range we considered in the experiments the Vicsek-Family scaling theory does not apply in its entire form for binary colloids. The values of $\mu_r$ and $\sigma$ influence the interaction of clusters and $\sigma$ has an additional effect on the mobility of the particles (see also Chapter 3 and Ref. [93]). It is interesting to note that increasing $\mu_r$ results in a reduction of the dynamic exponents, while the increasing mobility of the particles increases the value of $Z$ and $Z'$ (see Fig. 6.4($a$)).

## 6.4 Cluster discrimination

Figure 6.5($a$) shows representative examples of $n_S(t)$ for cluster sizes up to $S = 6$ in the experimental setup ($B$). It can be observed that in spite of the power law decrease of the total number of clusters $n_c$, the number of clusters of a given size has a complex time dependent behavior: $n_1(t)$ monotonically decreases, while the number of clusters, which are created by merging of small ones, has a bell shape with a maximum. It is important to note that for large time values there is a clear difference between the behavior of even and odd clusters: $n_S(t)$ has a slower decrease for odd $S$ values than for the even ones. The difference is more pronounced for small clusters, while for the large ones it slowly disappears. This cluster discrimination effect becomes even more transparent when comparing the number of clusters of different sizes $n_S$ at a given time $t$. In Fig. 6.5($b$) even-odd oscillation of $n_S$ can be observed which slowly disappears with increasing cluster size $S$. We obtained cluster discrimination in all the three experimental setups but the most pronounced effect occurs in setup ($B$) with $\mu_r = 2$ and $\sigma = 1$.

A similar cluster discrimination effect of heteroaggregation has been observed in binary colloids of oppositely charged particles [44, 61, 62]. It was also shown that discrimination occurs due to the long range interaction in the system and it is also related to the charge-neutral state of odd-even clusters [44, 61, 62]. In our system small clusters have chain-like morphol-

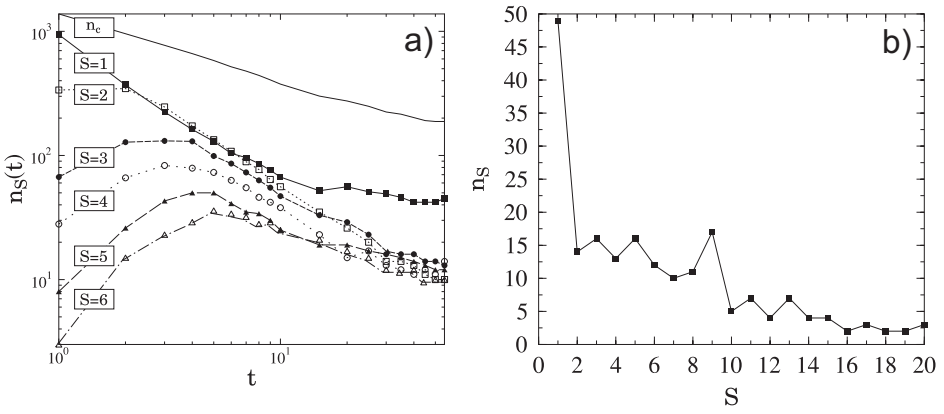


6.5. Figure: Cluster discrimination in BDMs obtained in setup $(B)$. $(a)$ $n_S(t)$ for different cluster sizes $S$ together with the total number of clusters $n_c$. $(b)$ Number of clusters $n_S$ of size $S$ in the system at a given time $t$.

ogy which tend to merge at chain ends due to the long-range anisotropic chain-chain interaction. Note that in setup $(B)$ where the cluster discrimination is more pronounced, both even and odd clusters are "charged" which shows that the morphology of clusters is crucial to understand the cluster discrimination in our system. Chains of an even number of particles have different type of particles at the two ends, while odd chains have identical ones. This implies a higher reactivity (a larger number of possibilities to merge other chains) for even clusters resulting in a faster decay than for the odd ones. When clusters develop branches the situation drastically changes. Screening of the dipolar interaction becomes stronger and the number of the geometrical degrees of freedom for the merging of clusters gets larger. It follows from the above argument that cluster discrimination could be obtained for cluster sizes below the crossover size $S_c$ defined in Sec. 6.2. Hence, the optimal conditions to observe cluster discrimination are low concentration (high $S_c$ value) and high charge asymmetry (large $\mu_r$ value).

## 6.5 Computer simulations

Computer simulations can provide a more detailed insight into the aggregation processes of BDMs. Realistic simulations can complement the experimental studies especially in those parameter regimes where measurements are limited by technical difficulties. We carried out computer simulations for all the three experimental setups varying the total concentration $\phi$ in a broad range. In the calculations the total number of particles was fixed to $N = 750$ which provided a reasonable CPU time even at the lowest concentration $\phi = 0.02$ considered. At each parameter set the simulations were repeated 30 times, which resulted in a good statistics and a higher accuracy of the numerically determined quantities compared to the measured ones [92, 106].

Figure 6.6($a$) presents the number of particles $S$ of clusters as a function of the radius of gyration $R_g$ for several concentration values in the case of setup *(A)*. It can be seen that similarly to the experimental results, the $S(R_g)$ curves are composed of two distinct parts of power law functional form Eq. (6.2). Note that in our model of two dimensional dipolar monolayers presented in Chapter 4 we did not introduce friction force for contacting particles. It has the consequence that particle chains formed by merging shorter chains can relax nearly to the straight configuration so that the fractal dimension $D_1$ of dipolar chains falls close to 1. Large dipolar clusters have a branching morphology which is characterized by a higher value of the fractal dimension $D_2 = 1.45 \pm 0.05$. The fractal dimensions $D_1$ and $D_2$ obtained by computer simulations have a significantly lower value than the measured ones, which indicates a less compact structure of clusters in the absence of contacts friction. It can be seen in Fig. 6.6($a$) that the values of the two fractal dimensions are independent of the concentration $\phi$, however, the crossover cluster size $S_c$ where the transition occurs from the straight chain to the more compact branched morphology, decreases with the concentration. The numerical value of $S_c$ was determined by fitting power laws (straight lines) to the two regimes of $S(R_g)$ where the intersection point

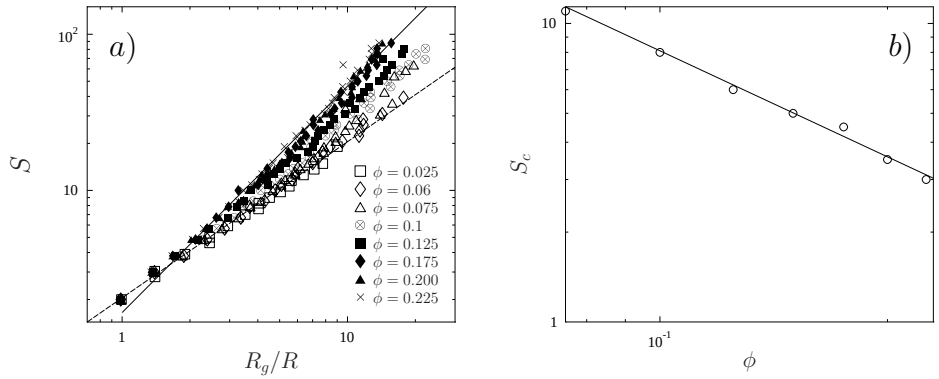


6.6. Figure: ($a$) The number of particles $S$ of clusters is presented as a function of the radius of gyration $R_g$. Simulations were carried out for Setup (A). The dashed and continuous straight lines have slope 1 and 1.45, respectively. The crossover mass $S_c$ was obtained as the crossing point of the straight lines fitted to the two regimes of different slopes. ($b$) The crossover cluster size $S_c$ as a function of the concentration $\phi$ where a straight line of slope $1.18 \pm 0.05$ was fitted to the data.

of the two curves defines $S_c$. The crossover cluster size $S_c$ is presented in Fig. 6.6($b$) as a function of $\phi$. Experiments and computer simulations showed that clusters develop branches when chains can merge not only at chain ends but also at internal locations. This internal merging can first occur when the length of growing chains become comparable to the inter-chain distance. It follows that the crossover chain length $S_c$ has a power law dependence on the concentration

$$S_c \sim \phi^{-\beta}, \tag{6.6}$$

where the value of the exponents is $\beta = 1.0$. The value of the exponent obtained numerically $\beta = 1.18 \pm 0.05$ is in a reasonable agreement with the analytic solution (see Fig. 6.6($b$)).

The average cluster size $S_{av}$ and the average cluster number $n_c$ are presented in Fig. 6.7 obtained by computer simulations for the three experimental setups. It can be observed that the numerical results have a good

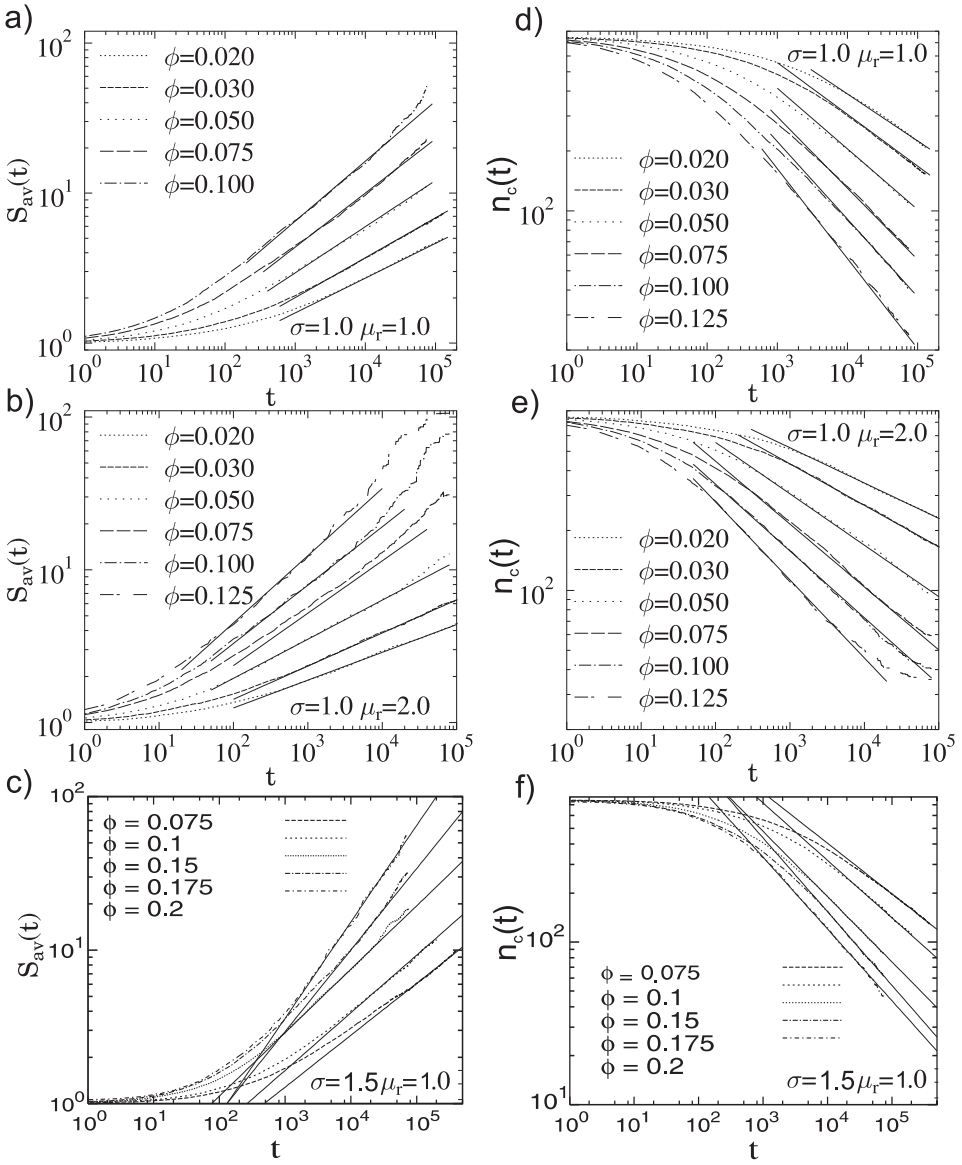


6.7. Figure: Average cluster size $S_{av}$ *(left column)* and average number of clusters $n_c$ *(right column)* as a function of time obtained by computer simulations of the three experimental setups.

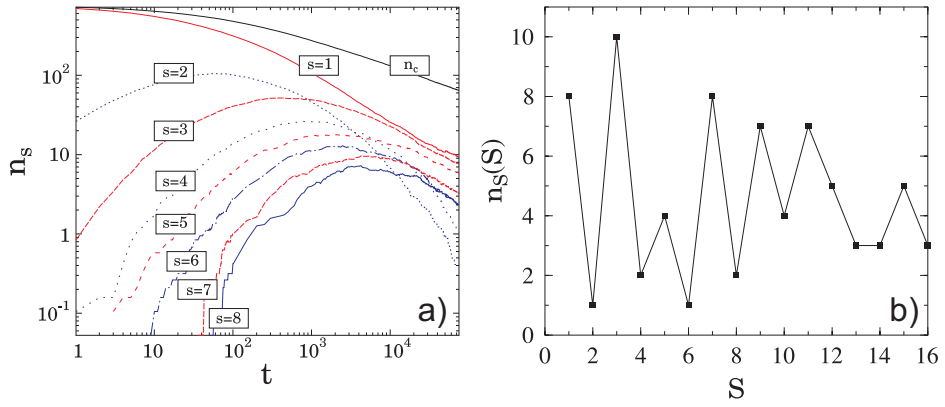


6.8. Figure: Cluster discrimination obtained by computer simulations. ($a$) The evolution of the concentration of clusters of a given size as a function of time. Even clusters decay faster than the odd ones. ($b$) The concentration of clusters at a given time shows even-odd oscillations.

agreement with the experimental findings, *i.e.* both quantities $S_{av}$ and $n_c$ have a power law behavior described by Eq. (6.4). The deviations from the power laws at large $t$ values arise due to the finite size of the system (as the system evolves the cluster number becomes very small and finally a single cluster is formed). We emphasize that computer simulations make possible to vary concentration of particles over a broad range and provide a very good statistics which facilitates the determination of the dynamic exponents $Z$ and $Z'$. Figure 6.4($b$) shows the dynamic exponents $Z$ and $Z'$ obtained from the analysis of Fig. 6.7 over the concentration range $\phi = 0.02 - 0.225$. It can be seen that for high concentrations the two exponents have different values and the inequality $Z(\phi) > Z'(\phi)$ holds, however, the calculations revealed that as the concentration decreases the two exponents become equal $Z(\phi) = Z'(\phi)$. It follows that in the dilute limit the Vicsek-Family scaling Eq. (6.5) is also valid for binary dipolar monolayers and the value of the dynamic exponents falls close to $0.2 - 0.25$.

Analyzing the concentration of clusters of different sizes, computer sim-

ulations revealed a strong cluster discrimination effect supporting the experimental results. In Fig. 6.8($a$) a clear difference can be observed in the long time behavior of the concentration $n_S$ of even and odd clusters. At a fixed time value $t$ the concentration of clusters has strong even-odd oscillations showing that even clusters have a higher reaction rate and decay faster than the odd ones. Simulations also showed that the cluster discrimination effect is strongly related to the morphology of aggregates, *i.e.* it occurs only for chain-like clusters and disappears above the crossover cluster size $S_c$ when the clusters become fractal objects, in agreement with the experiments.

## 6.6 Analytic considerations

In Fig. 6.4, it appears that the dynamic exponents become close to $0.2-0.25$ in the dilute limit. This value is much smaller than that of other cluster-cluster aggregations, particularly that of attraction-limited cluster-cluster aggregation of electrorheological suspensions in a strong electric field [74]. This means that the dynamics of binary dipolar particles cannot be described using a *hierarchical model* [8] approach similar to that carried out by See and Doi [74], in which only the two-body collision between nearest neighbor $2^k-$clusters is considered at the $k$th step of aggregation. In fact, because the typical cluster size is of the same order as $\phi^{-1}$ when the cluster-cluster aggregation of chains crosses that of fractal aggregates [92], we can consider that all clusters are straight chains if $\phi < 1/N$. The potential energy between two straight binary dipolar particle chains of the same size $S = 2^k$ and of the center-of-mass distance $r$ is expressed as

$$U(r) = \mu^2 \sum_{n=1}^{S} \sum_{m=1}^{S} \frac{(-1)^{n+m}}{[d_{nm}(r)]^3}, \tag{6.7}$$

where $d_{nm}(r)$ is the distance between the $n$th binary dipolar particle of one chain and the $m$th particle of the other. If $r \gg S(R_+ + R_-)$ then

$$U(r) \sim \frac{[\mu S(R_+ + R_-)]^2}{r^5}, \tag{6.8}$$

and thus $Z = 2/5$ is derived using the theory of See and Doi [74]. This value deviates from what we obtain, $Z(\phi \to 0) = 0.2 - 0.25$. This clearly demonstrates that in the case of the cluster-cluster aggregation of binary dipolar particles, the surrounding clusters and their screening effect are not negligible.

Studying aggregation phenomena in BDMs helps to achieve a comprehensive understanding of heteroaggregation phenomena in colloids. Experiments and computer simulations showed that at higher concentrations the behavior of the system drastically changes. When the concentration exceeds about 25 %, in the initial configuration there can be local regions with a relatively high particle density. When the particles set in motion, in these regions densely packed compact structures occur very rapidly with crystalline order. Further increasing the concentration the entire system can crystallize, where the symmetry of the crystalline lattice strongly depends on the parameters of BDMs. In the next Chapter I present experimental and theoretical results on crystallization processes in binary dipolar monolayers.

# 7 Chapter

# Crystallization

The first experimental investigations on binary dipolar monolayers of Ref. [68] showed that at high enough concentrations the particle system rapidly attains a frozen structure, which is typically composed of islands having crystalline order. Due to the limitations of the experimental techniques, Ref. [68] could only provide qualitative information on crystal structures of BDMs. In order to obtain a deeper insight into this crystallization process, I carried out experiments and computer simulations exploring a broad regime of the concentration of particles $\phi$, the relative concentration $\phi_r$ and relative dipole moment of the two components $\mu_r$. The goal of my work was to reveal all lattice types which can emerge in BDMs and to determine the parameter regimes where they are formed [90, 92, 93].

## 7.1 Basic configurations

In order to understand the formation of crystal structures in binary colloids and explore possible lattice morphologies beyond the square-packed one reported in Ref. [68], we calculated the energy of basic particle configurations from which lattices can be built up. The Basic Configurations (BC) are composed of one particle of type I (with dipole moment $\mu_+$) surrounded by 2 ($BCI$), 3 ($BCII$), 4 ($BCIII$), 5 ($BCIV$), or 6 ($BCV$) particles of type

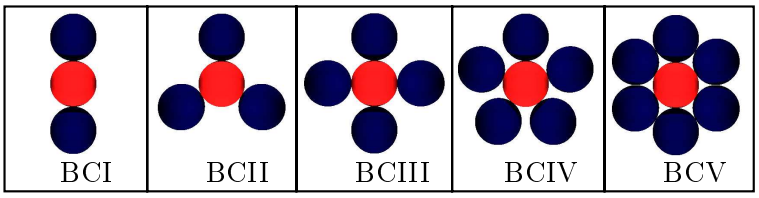


7.1. Figure: Basic configurations of BDMs. Particles are placed at the energetically most favorable location around an oppositely oriented dipole.

II (with dipole moment $\mu_-$) placed at the energetically most favorable locations. The basic particle configurations of BDMs are presented in Fig. 7.1. In order to simply cover also cases where the different types of particles are interchanged, the energy of BCs was calculated as a function of $\mu_r = \mu_-/\mu_+$ fixing the value of $\mu_+ = 1$

$$E_N(\mu_r) = \frac{\mu_+^2}{d^3}\left[\frac{\mu_r^2}{8}\sum_{k=1}^{N-2}\frac{N-k-1}{\sin^3(k\beta)} - \mu_r(N-1)\right], \tag{7.1}$$

where $\beta = \pi/(N-1)$ and the particle number takes the values $N = 3,4,5,6,7$.

The energy divided by the particle number $E_N(\mu_r)/N$ is presented in Fig. 7.2 as a function of $\mu_r$ for the possible values of $N$. It can be seen in the figure that all the BCs are stable (have a negative energy) only in certain $\mu_r$ ranges between 0 and a $\mu_r^{max}(N)$ since with increasing $\mu_r$ the attraction exerted by the central particle is not enough to compensate the mutual repulsion of the surrounding ones. Such configurations where the central particle is surrounded by particles of smaller dipole moment, *i.e.* $\mu_r < 1$ in Fig. 7.2, are always stable except for $BCV$ because $\mu_r^{max}(7) \approx 0.8$ falls below 1. The upper bounds of stability can be determined exactly from Eq. (7.1) such as $\mu_r^{max}(N) \approx 16, 5.2, 2.4, 1.3, 0.8$ were obtained for $N = 3,4,5,6,7$, respectively. Repeating the above basic structures with alternating particles various structures can be built up: $BCI$ forms the basis of chains and rings as it has been presented in Chapters 5 and 6. $BCII$ gives rise to a Honeycomb

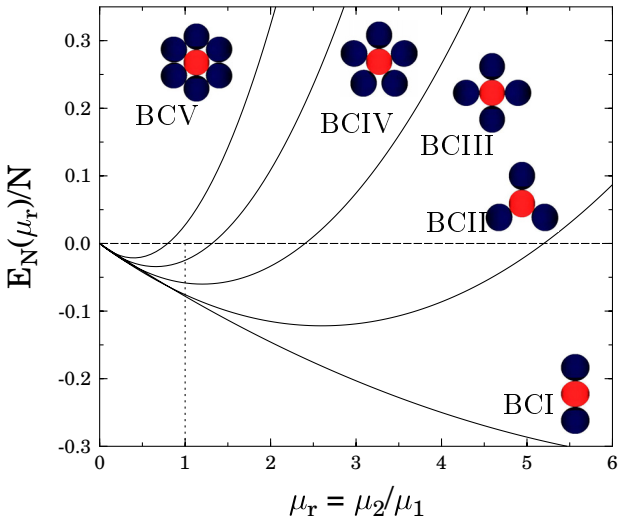


7.2. Figure: The energy Eq. (7.1) divided by the number of particles of basic configurations as a function of $\mu_r$ for $N = 3, 4, 5, 6, 7$. For clarity, the corresponding particle configurations are also presented.

lattice in which both types of particles have three neighbors of the other type, while *BCIII* leads to the square lattice. *BCIV* results only in flower-like structures, no lattice can be constructed in this case since the plane cannot be covered by regular pentagons. Moreover, *BCV* forms the basis of a special type of Honeycomb lattice, in which particles of the larger dipole moment have 6 neighbors of the smaller one but particles of the smaller moment have 3 neighbors of both types. The overall morphology attained by the entire particle system at a given value of $\mu_r$ is not necessarily based on the energetically most favorable basic configuration presented above, since the particles can freeze in local energy minima in the configuration space. To have a comprehensive understanding of crystallization in BDMs, after the analytic calculations I carried out computer simulations and experiments.

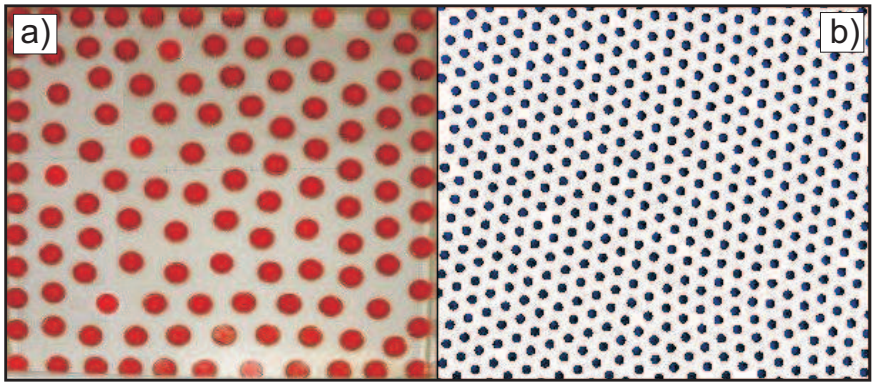


7.3. Figure: Triangular lattice of particles obtained for $\phi_+ = 1$, $\phi_- = 0$. ($a$) In the experiments $N = 100$ particles were used in a square-shaped container of side length $L = 500$ mm. ($b$) Simulations were carried out with $N = 500$ particles using periodic boundary conditions.

## 7.2 Crystal structures

Starting from a random initial configuration of the monolayer, the particles aggregate forming small clusters which then rapidly merge into a macroscopic cluster spanning over the entire system. In spite of the isotropic particle-particle interaction the cluster-cluster interaction is highly anisotropic which can result in trapping the particles into local energy minima in configuration space, especially when thermal motion is hindered by the relatively large particle mass. Hence, the relative dipole moment $\mu_r$, the total concentration $\phi$ and the relative concentration $\phi_r$ of components together determine the final structure. Based on the energy of basic configurations Eq. (7.1) and Fig. 7.2, it is possible to determine analytically regions of $\phi, \phi_r$, and $\mu_r$ which are needed to obtain a certain lattice structure or aggregate morphology.

In the experiments and computer simulations we observed that the structure of clusters is not frozen, *i.e.* due to the isotropic inter-particle forces, the cluster structure is quite flexible, in contrast to particle monolayers with

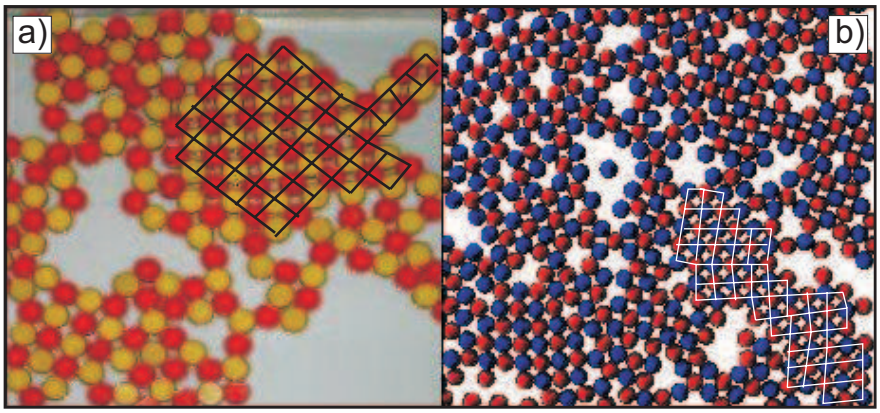


7.4. Figure: For the parameter values $\mu_r = 1$, $\phi_r = 1$ starting from a random initial configuration at high enough concentrations $\phi$ the particles rapidly form an extended structure with square packed crystallites. For clarity, both in the experimental ($a$) and simulation results ($b$) we highlighted some plaquettes of the square lattice structure.

in-plane dipoles where the anisotropic dipolar interaction makes the clusters more rigid [100]. In our case the flexibility has the consequence that when two clusters approach each other, they deform, facilitating the aggregation. Furthermore, the subsequent aggregation steps can result in rearrangements of particles reaching deeper energy minima. Typically, the perturbation of an aggregate by a particle, joining the cluster with a non-zero velocity, may give rise to an avalanche of restructuring events. This mechanism helps the compaction of clusters and the formation of crystalline lattices. Thermal noise can also have a similar effect, *i.e.* it prevents the system to freeze in local energy minima in the configuration space increasing the degree of crystallization when the temperature is not too high.

If one of the components has a much higher concentration than the other one (for instance, $\phi_+ \gg \phi_-$) at any concentration, due to the repulsive interaction of the identical particles a triangular lattice is formed with some binary islands. The limiting case when only one of the components is present

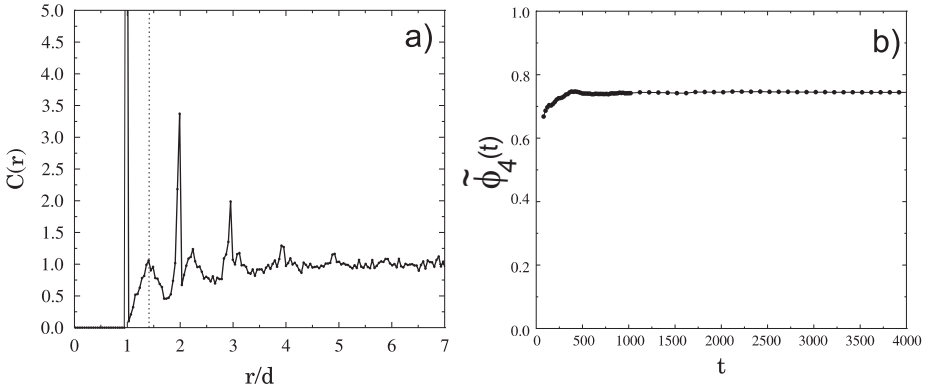


7.5. Figure: ($a$) The two-point correlation function presents well-defined peaks corresponding to the square lattice structure. ($b$) The bond orientational order parameter $\widetilde{\phi}_n$ calculated with $n = 4$ takes a value close to 1, which indicates that a large fraction of the system has a square packed structure.

$\phi_+ = 1$, $\phi_- = 0$ is shown in Fig. 7.3, where a regular triangular lattice is observed in simulations and experiments. In the experiments the particles line up along the rigid walls of the container which produces a strong distortion of the symmetry of the system so that regular triangular structures are mainly observed in the middle of the container.

At high concentrations in BDMs typically binary lattice structures of a high packing fraction can be obtained, however, concentrations too close to the highest coverage ($\phi \approx 0.9$) are disadvantageous because they prevent particle motion and result in freezing into local energy minima. Hence, the best square lattice structures can be achieved at $\phi \approx 0.65 - 0.75$. This type of lattice which builds up from BCIII, contains the same amount of both types of particles so that $\phi_r = 1$ and $\mu_r = 1$ follows, see Fig. 7.4. The parameter regime providing square lattices where each particle has 2-2 neighbors of both types, agrees well with the experimental observation of Ref. [68]. The values of the parameters characterizing the emergence of different crystalline structures are summarized in Table 7.1.

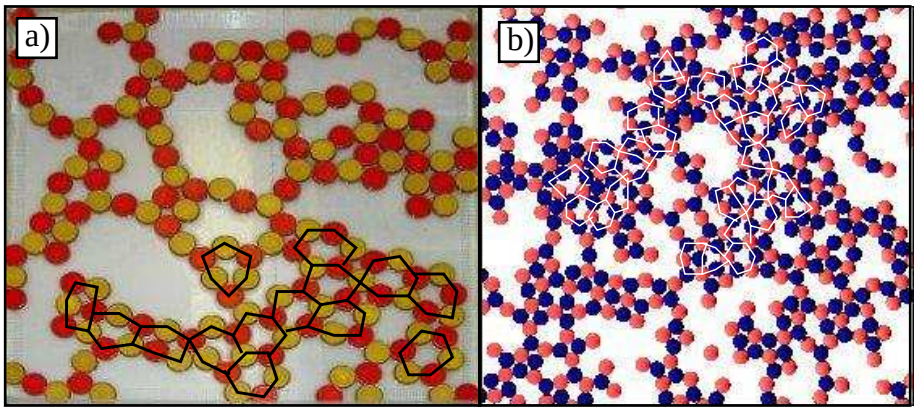


7.6. Figure: Honeycomb I lattice obtained by experiments ($a$) and computer simulations ($b$). For clarity, a few plaquettes of the crystalline structures are highlighted.

In order to quantify the degree of crystalline order in BDMs, we consider the $n$-fold local bond orientational order parameter with the definition

$$\widetilde{\phi}_n = \frac{1}{2N} \sum_j \frac{1}{N_j} \left| \sum_k \Theta(d - r_{j,k}) e^{in\alpha_{j,k}} \right| . \tag{7.2}$$

Here $\Theta(.)$ denotes the usual step function ($\Theta(x) = 1$ for $x > 0$, and zero otherwise) so that $N_j = \sum_k \Theta(r_{max} - r_{j,k})$ is the number of neighbors of particle $j$ (particles with distance smaller than the diameter $d$). Note that in the simulations the touching particles slightly overlap each other, hence, for them $r_{i,j} < d$ holds. In the exponent $\alpha_{j,k} = \angle(\vec{r}_{j,k}, \vec{e}_0)$ is the bond angle between the pair vector $\vec{r}_{j,k}$ and an arbitrary but fixed direction $\vec{e}_0$. Since the bond angle in a perfect crystal with $n$-fold symmetry is always an integer multiple of $\pi/n$, the value of the order parameter is $\widetilde{\phi}_n = 1$ in this case. In the opposite limit $\widetilde{\phi} = 0$ reflects a completely disordered state of the system. This way the actual value of $\widetilde{\phi}_n$ in a given configuration can characterize how close the structure is to the desired crystalline lattice. Since the absolute value in Eq. (7.2) is taken before averaging over all particles, $\widetilde{\phi}_n$ is sensitive to the $n$-fold arrangements of nearest neighbors around any particles and is

| *Structure* | $\phi$ | $\phi_r$ | $\mu_r$ |
|---|---|---|---|
| triangular latt. | $0-0.9$ | – | – |
| square lattice | $0.65-0.75$ | 1 | 1 |
| Honeycomb I | $0.45-0.50$ | 1 | $\approx 2.5$ |
| Honeycomb II | $0.80-0.82$ | 2 | 2.5– |
| quasi-crystal | $0.65-0.75$ | 2 | $1.5-2.0$ |
| super lattice | $0.45-0.50$ | $\approx 2-2.5$ | $2.5-4.5$ |

7.1. Table: The parameter regimes determining the final structure of the system. For explanation see the text. (In the first row missing values of $\phi_r$, and $\mu_r$ indicate that the system consists exclusively of one component.)

insensitive to the spatial variation of the bond orientation over the system.

We also determined the density-density correlation function $C(r)$ with the definition

$$C(r) = \frac{1}{N 2r\pi\delta r} \sum_{r-\delta r/2<|\vec{r}_i-\vec{r}_j|<r+\delta r/2} \rho(\vec{r}_i)\rho(\vec{r}_j), \tag{7.3}$$

where $\rho(\vec{r})$ is 1 if there is a particle at $\vec{r}$ and 0 otherwise. The correlation function is normalized so that for homogeneous disordered particle arrangements $C(r)$ takes a constant value close to 1, while for crystalline structures it has well-defined peaks at distances $r$ with a high probability of particle pair locations. The density-density correlation function $C(r)$ and the bond orientational order parameter $\widetilde{\phi}_4$ are presented in Fig. 7.5 for the square lattice, which were determined by computer simulations of a system with $N = 1000$ particles. It can be observed that $C(r)$ has relatively sharp peaks whose position correspond to $r = d, \sqrt{2}d, \ldots$ which are characteristic for the square lattice structure. For large inter-particle separation $C(r)$ converges to 1 as it can be expected. The bond orientational order parameter $\widetilde{\phi}_4$ in Fig. 7.5($b$) rapidly converges to a value close to 1 which indicates the high degree of square packed order in the system.

The first type of Honeycomb lattice (Honeycomb I) builds up from BCII where each particle has 3 neighbors of the other type, has not been observed

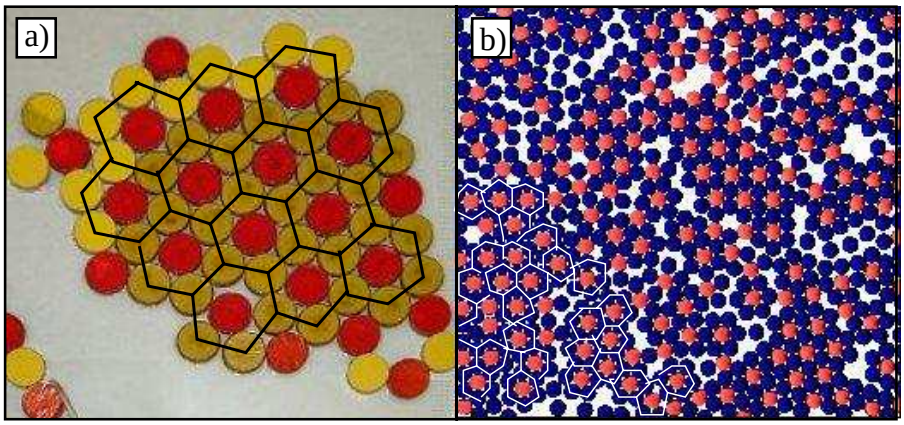


7.7. Figure: At large enough relative concentrations and relative dipole moments the system rapidly orders into the Honeycomb II lattice. Experiments ($a$) and computer simulations ($b$) are in a good agreement.

experimentally earlier. However, our analytic calculations showed that energetically it can be favorable for the system in a certain parameter range. Examples are presented in Fig. 7.6 which were obtained at $\phi = 0.5$ and $\phi_r = 1$ by experiments and computer simulations. For clarity, some plaquettes of the lattice are highlighted in the figure. Since the two types of particles have the same amount in the lattice, the relative concentration $\phi_r$ is set to unity $\phi_r = 1$. The basis of this structure is $BCII$ which is always stable for $\mu_r < 1$, *i.e.* when a larger dipole is surrounded by 3 smaller ones. However, to make the opposite configuration (one small plus three large dipoles) more favorable, $\mu_r$ has to be increased above the stability limit of $BCIII$ (above $\mu_r^{max}(5) \approx 2.4$), otherwise, the system ends up in a square packed structure. $\mu_r \approx 2.5$ proved to be an excellent choice numerically to make the Honeycomb $I$ lattice energetically more favorable than the square lattice structure. Since the Honeycomb $I$ lattice has a relatively low packing fraction, the initial concentration $\phi$ has to be set in the range $\phi = 0.45 - 0.5$.

In the experiments we could also obtain Honeycomb $I$ structure at lower values of $\mu_r$, even at $\mu_r = 1$ setting the other two parameters as $\phi_r = 1$ and

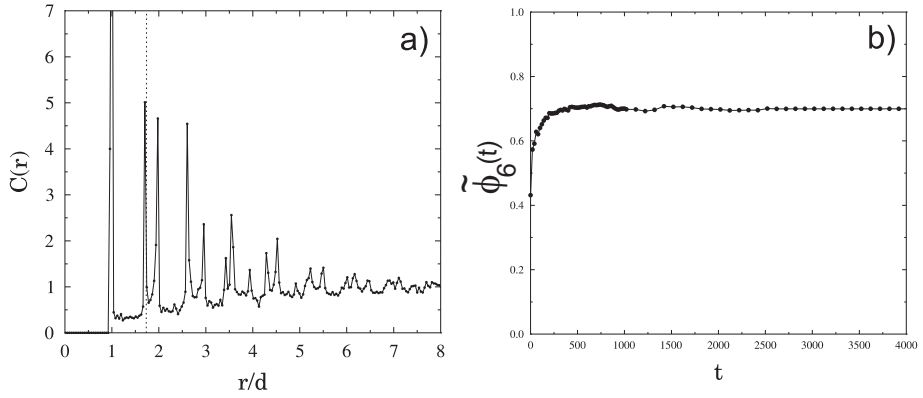


7.8. Figure: The density-density correlation function $C(r)$ $(a)$ and the bond orientation order parameter $\widetilde{\phi}_6(t)$ $(b)$ were determined by computer simulations with $N = 1000$ particles. Both quantities indicate a high degree of HCP order in the monolayer.

$\phi \approx 0.5$. However, in computer simulations, a relatively small irregularity of the Honeycomb $I$ structure at $\mu_r = 1$ initiates a collapse into a square lattice achieving a deeper energy. This discrepancy between the experimental and theoretical results can be attributed to the static friction in the experiment at the contact surface of the particles, which stabilizes the structures like in the packing of granular materials. Static friction was also found to have an important stabilizing effect in experiments on magnetic monolayers with in-plane dipole moments [100]. In the computer simulations, no static friction was implemented [92], so the central inter-particle forces allowed a rearrangement of the whole system. In the experiments of Ref. [68], the Honeycomb $I$ lattice was not observed. However, it was argued that the electrohydrodynamic flow of the embedding liquid plays an important role in the structure formation, namely, it brings the particles in the vicinity of each other. Our experiments showed that such a flow can also generate strong enough perturbation to destroy the lose structure of the Honeycomb $I$ lattice.

If the magnitude of the two dipole moments are different ($\mu_r \neq 1$) con-

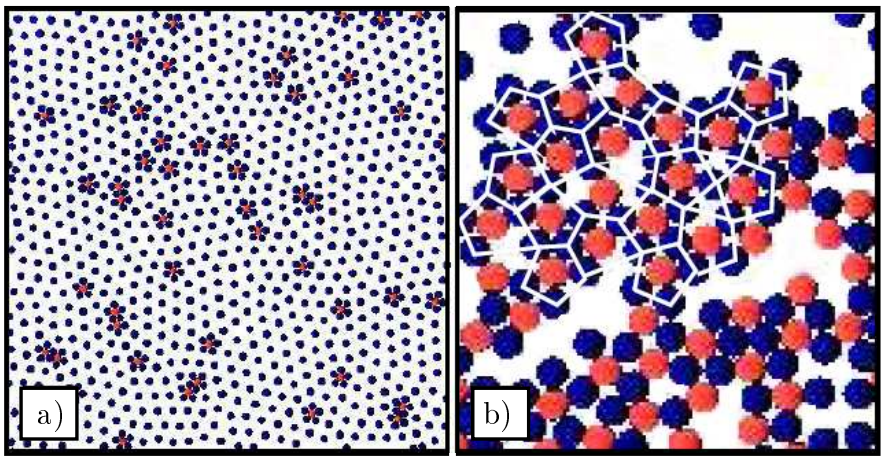


7.9. Figure: $(a)$ Flower-like islands in a triangular lattice obtained by computer simulations at the parameter values $\phi = 0.5, \phi_r = 5, \mu_r = 2.0$. $(b)$ Quasi crystalline structure with local five fold symmetry ($\phi = 0.66, \phi_r = 2, \mu_r = 1.8$).

centration fluctuations easily lead to the formation of the second type of Honeycomb lattice (Honeycomb $II$), which has a hexagonal-closed-packed (HCP) structure, where particles of the larger dipole moment have 6 neighbors of the other type, and the ones with smaller dipole moment have 3 neighbors of both types. The highest portion of the system was found to crystallize into Honeycomb $II$ at $\phi \approx 0.80 - 0.82$ with the ratio of $\phi_r = 2$ of the components and with high enough asymmetry of the magnitude of dipole moments $\mu_r \approx 2.5$, which is needed to prevent the system to crystallize locally into the square packed structure. The corresponding simulation results can be seen in Fig. 7.7$(b)$, which are in a nice agreement also with the experiments of Ref. [68]. In the experiments (Fig. 7.7$(a)$) the concentration $\phi$ had to be lowered compared to the simulations to the range $\phi \geq 0.7$, since at higher concentrations the static friction of the particles stabilizes the system almost in the initial configuration preventing crystallization.

The density-density correlation function $C(r)$ and the bond orientational order parameter $\widetilde{\phi}_6$ were also determined for the Honeycomb $II$

lattice by computer simulations with $N = 1000$ particles. It can be observed in Fig. 7.8($a$) that $C(r)$ exhibits sharp peaks with the locations $r = d, 2\cos(\pi/6)d, \ldots$ corresponding to the HCP structure of the lattice. The bond orientation order parameter rapidly converges to a constant value close to 1, which indicates a high degree of crystalline order with 6-fold symmetry.

Besides the crystalline lattices under certain conditions some peculiar structures can also emerge in BDMs. If the relative dipole moment $\mu_r$ favors the formation of $BCIV$, quasi-crystalline ordering can be obtained with local five-fold symmetry, since the plane cannot be covered by regular pentagons. Figure 7.9 presents an example of such quasi-crystallites which can even span a large fraction of the monolayer. In a slightly different context quasi-crystals of dipole have recently been studied in Ref. [73]. At low concentration when $\phi_r$ is high and $\mu_r \approx 2.0$ flower-like islands can be observed in a triangular lattice. When the relative dipole moment $\mu_r$ is even higher ( $\mu_r > 2.5$) but the concentration and the relative concentration do not favor the emergence of Honeycomb $II$, so-called super structures can be observed in the colloid. These structures do not have ordered crystalline morphology, instead they are characterized by long straight binary chains which connect disordered or small crystalline islands as we illustrated in Ref. [90].

# 8 Chapter

# Molecular crystals

In Section 2.3.2 we have presented that novel crystalline states have been reported for colloids interacting with two-dimensional periodic substrates [66, 4, 46, 67, 72, 1]. In this Chapter we show that in binary dipolar monolayers (BDM) crystalline states analogous to colloidal molecular crystals can emerge without the application of an underlying periodic substrate. The $n$-mers of BDMs are the basic particle configurations presented in Sec. 7.1, which are bounded configurations of particles with oppositely oriented permanent dipoles. The formation of such dipolar $n$-mers requires some initial external assistance but then they behave as rigid bodies against external perturbations up to the level of the binding energy without any additional confining potential (substrate). We show that a large variety of molecular crystalline states obtained in colloids by integer filling of periodic substrates can be recovered in BDMs, furthermore, the translational degrees of freedom give rise to additional structures not observed with traps. However, the absence of confining substrates has the consequence that at any nonzero temperature binary dipolar molecular crystals (BDMCs) have a finite lifetime $t_c$ which is a decreasing function of both the temperature and system size. An advantageous feature of binary dipolar $n$-mers, increasing their potential applications, is that their mutual interaction can be modulated by varying the relative dipole moment and the dispersity (particle size) of the

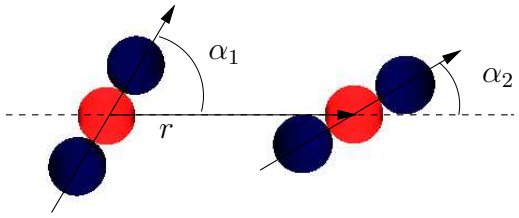


8.1. Figure: The relative position and orientation of trimers (BCI) characterized by the center-to-center distance $r$ and the two angles $\alpha_1$ and $\alpha_2$.

two components which also addresses the possibility of targeted assembly of structures [65, 63, 64]. At high enough temperature, trimers aggregate and form clusters of square lattice structure, analogously to the "freezing-by-heating" transition observed in various types of systems [22]. The details of this work can be found in Ref. [91].

## 8.1 Interaction of trimers

Basic particle configurations have been introduced in Section 7.1 in order to analyze the formation of crystalline lattices in BDMs. Setting appropriate values for the relative dipole moment $\mu_r < \mu_r^{max}(N)$, BCs remain stable and behave as $n$-mers of colloidal molecular crystals without the application of an underlying confining substrate. Note that such a system of identical BCs does not emerge spontaneously in a BDM starting from a random initial mixture of the two components with a relative concentration $\phi_r$ and relative dipole moment $\mu_r$. The formation of a large number of BCs of the same type needs external assistance, *e.g.* they can be fabricated by micro-manipulation techniques.

In order to understand the formation of molecular crystalline structures in BDMs, the interaction of identical BCs has to be analyzed. This analyzes can be performed similarly to $n$-mers of CMCs as in Ref. [1] with the additional degree of freedom of varying $\mu_r$ in the range $0 < \mu_r < \mu_r^{max}(N)$.

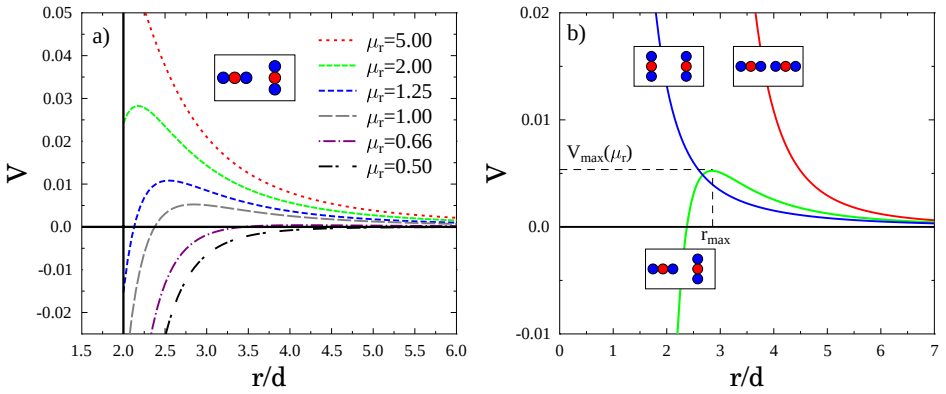


8.2. Figure: $(a)$ Interaction of trimers with a fixed relative orientation $\alpha_1 = 0$, $\alpha_2 = \pi/2$ as a function of $r$ for several values of $\mu_r$. $(b)$ $V(r)$ for different relative orientations at $\mu_r = 1.0$. For the case of perpendicular orientation a potential barrier exists with height $V_{max}$ and location $r_{max}$.

Since the basic configurations have a discrete rotational symmetry, the interaction of the same type of BCs depends not only on their center-to-center distance $r$ but also on their relative orientation. In the following the detailed presentation is restricted to the simplest case of BCIs, *i.e.* trimers, whose relative orientation can be characterized by the angles $\alpha_1, \alpha_2 \in \left[-\frac{\pi}{2}, +\frac{\pi}{2}\right]$ of their symmetry axis with the line connecting the center of their middle particle, see Fig. 8.1 for the definition of variables. Following the arguments of Ref. [1], in the interaction potential $U(r, \alpha_1, \alpha_2)$ of trimers the radial and angular dependence can be factorized into a product as

$$U(r, \alpha_1, \alpha_2) \sim V(r) \cosh(\xi \cos\alpha_1) \cosh(\xi \cos\alpha_2), \tag{8.1}$$

where the multiplication factor $\xi$ depends both on the distance $r$ and the particle diameter $d$. Figure 8.2$(a)$ demonstrates the radial part of the interaction $V(r)$ of two trimers at a fixed relative orientation $\alpha_1 = 0$, $\alpha_2 = \pi/2$ for several values of the relative dipole moment $\mu_r$. It can be observed that varying the value of $\mu_r$ in the range $\mu_r \geq 0.5$ the interaction can change from purely attractive $\mu_r = 0.5$ to purely repulsive $1.4769 < \mu_r < \mu_r^{max}(3) \approx 16.0$

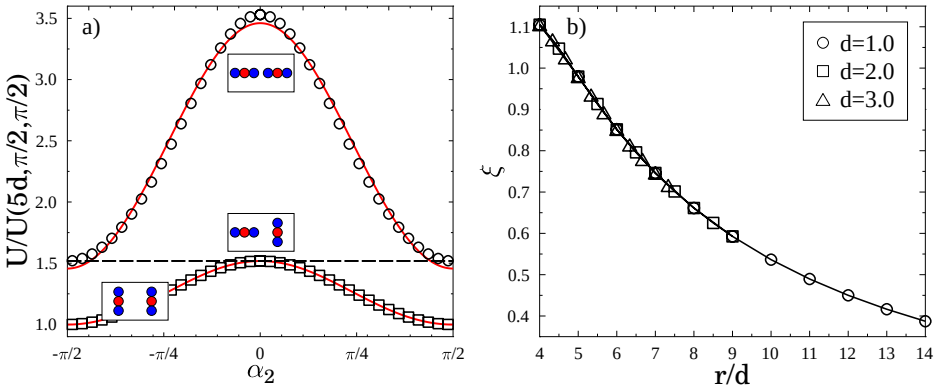


8.3. Figure: ($a$) Angular dependence of the interaction of trimers placed at a distance $r = 5d$ with $\mu_r = 1.0$. The value of $\alpha_1$ was fixed to 0 and $\pi/2$ for the upper and lower curves, respectively, while $\alpha_2$ was varied. The symbols show the numerical results, while the continuous lines were obtained by fitting with Eq. (8.1). ($b$) The parameter $\xi$ of the angular component of the interaction potential as a function of $r/d$.

with a transient regime where short range attraction and long range repulsion exist $0.5 < \mu_r < 1.4769$. The attractive and repulsive regimes are separated by an energy barrier $V_{max}$ at the position $r_{max}$, which both depend on the value of $\mu_r$. The energy barrier is also illustrated in Fig. 8.2($b$) for the case of perpendicular orientation. The functional form of the long range dependence of the interaction potential is $V(r) \sim 1/r^3$ in all cases. Note that for $\mu_r < 0.5$ the middle particles of trimers dominate the radial part of the interaction $V(r)$ which can again be purely repulsive or attractive-repulsive. Figure 8.2($b$) shows that contrary to the perpendicular orientation ($\alpha_1 = 0, \pm\pi/2$ and $\alpha_2 = \pm\pi/2, 0$), for head-to-head ($\alpha_1 = 0$ and $\alpha_2 = 0$) and parallel orientation ($\alpha_1 = \pm\pi/2$ and $\alpha_2 = \pm\pi/2$) of trimers the interaction is purely repulsive at any $\mu_r$. The dependence of the interaction of the trimers on their relative orientation is illustrated in Fig. 8.3($a$), where an excellent agreement of the numerical results and analytic predictions can be observed. The multiplication factor $\xi$ of $V(r)$ in Eq. (8.1) is a decreasing

function of $r/d$ which indicates the weakening of the anisotropy of the interaction at larger distances (see Fig. 8.3($b$)). It follows from Eq. (8.1) that for fixed positions of two trimers the lowest angular contribution is provided by the parallel orientation, while the head-to-head orientation is energetically the most disadvantageous. The perpendicular orientation is also favored by trimers with a local energy minimum. Note that in the calculation of the interaction potential the trimers were treated as a rigid linear objects, no deformation was allowed.

## 8.2 Crystalline lattices of trimers

We explore the possible crystal structures of trimers by means of computer simulations of the monolayer setting the initial particle positions based on the above analyzes of the trimer potential Eq. (8.1). It has to be emphasized that starting from a perfectly random configuration of the two-component mixture, the particles do not form $n$-mers, instead, an aggregation process occurs resulting in growing dipolar clusters as it has been presented in Chapter 6 and in Refs. [90, 94, 92, 106]. Hence, in the simulations we created the trimers by hand in such a way that in the initial state trimers were placed into an ordered structure based on the potential Eq. (8.1). Then the particles were randomly displaced independently of each other within a circle of diameter $d_r = d$. The placement of trimers and randomization of the particles' position practically substitute the substrate in the initial state of the simulations. Lattice structures of a high degree of positional and orientational order were obtained by computer simulations relaxing the system by solving the equation of motion of the particles Eq. (4.5) without thermal noise [2] as it has been discussed in Section 4.3.

In the range of $\mu_r$ where trimers of perpendicular orientation can attract each other $0.5 \leq \mu_r < 1.4769$, a regular square lattice structure emerges if trimers of perpendicular orientation are placed close enough in the initial configuration $r_0 < r_{max}$. Here $r_0$ denotes the initial distance of the center of adjacent trimers. In Fig. 8.4($a$) the two different types of particles (up and

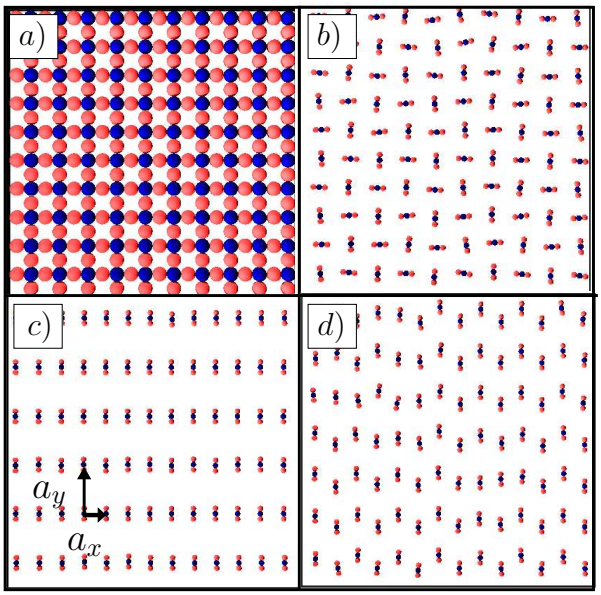


8.4. Figure: A bounded crystal of trimers with $\mu_r = 1$. $(a)$ Molecular crystalline states of trimers obtained with $\mu_r = 1$ at different values of the lattice spacings in the horizontal $a_x$ and vertical direction $a_y$: $(b)$ $a_x = a_y = 5d$, $(c)$ $a_x = 5d, a_y = 10d$, and $(d)$ $a_x = 4d, a_y = 8d$.

down dipoles) have two and four neighbors of the other type, respectively. Such a binary crystal is a bounded state of the system with a negative total energy. For the calculations $\mu_r = 1$ was used which gives rise to $r_{max} \approx 2.6d$ so that the initial distance $r_0$ was set to $r_0 = 2.4d$.

Colloidal molecular crystals with positional and orientational order emerge in the parameter regime $0.5 < \mu_r < \mu_r^{max}(3)$, when the trimers are initially placed in the repulsive range of the interaction $r_0 > r_{max}$ with appropriate orientation. Several types of lattice structures can be obtained which minimize the overall repulsion of trimers provided that the system is confined by an external potential since no substrate is used. First, we consider trimers with perpendicular relative orientation of the neighboring ones in a square box of side length $L$ ensuring the confinement by periodic boundary conditions. For stability reasons, in the simulations an even num-

ber $n$ of trimers has to be placed in each row and column of the lattice, *i.e.* the first and last trimers in rows and columns have perpendicular relative orientation (see Fig. 8.4($b$)). The value of $n$ has to be chosen such that for the lattice spacing $a = L/n$ it holds that $a > r_{max}$, see also Fig. 8.2($a$). After the initial positioning of trimers we again randomly displaced all the single particles in a circle of diameter $d_r = d$ around their original position. The molecular crystalline lattice in Fig. 8.4($b$) was obtained by computer simulations starting from the randomized initial state at the parameter values $\mu_r = 1.0$, $n = 10$, $a = 5d$. Simulations revealed a rapid convergence of the system to the highly ordered configuration of Fig. 8.4($b$). Increasing the diameter of randomization $d_r$ over $\sim 1.5d$, however, no trimers are formed, instead the particles of different trimers mix up with each other and the system undergoes an aggregation process forming clusters of dipoles similar to Chapter 6. The limit value of the diameter of randomization $d_r$ can be considered as the "capture distance" of trimer creation, which of course depends on $r_0$. Note that the only difference between the initial states of computer simulations in Fig. 8.4($a$) and Fig. 8.4($b$) was the value of $r_0$, *i.e.* the initial location of the center of trimers before randomization.

Varying the number of trimers in the horizontal $n_x$ and vertical directions $n_y$ at a fixed system size $L$, *i.e.* tuning the corresponding lattice spacings $a_x$ and $a_y$ (both in the range $a_x, a_y > r_{max}$) at a fixed $\mu_r$, further structures can be obtained which have been predicted for periodic arrays of traps [66, 1]. Contrary to $n$-mers of repulsive colloid particles on periodic substrates, in BDMs not the ratio $\beta = a_x/a_y$ of the two lattice spacings $a_x$ and $a_y$ but their actual values determine the optimal lattice structure due to the form of $V(r)$. For the two cases Figs. 8.4($c$), ($d$) the computer simulations started from the same initial state, namely, trimers were first put into the ordered structure of Fig. 8.4($c$) with parallel orientation, then the particles were randomized inside a circle of diameter $d_r = d$. In Figs. 8.4($c$) and 8.4($d$) the same ratio $\beta = 2$ and $\mu_r = 1$ are used but the different values of the lattice spacings $a_x = 5d$, $a_y = 10d$ and $a_x = 4d$, $a_y = 8d$ give rise to different structures. Since no

positional confinement is applied, the translational degrees of freedom can result in molecular crystals not observed with substrates as in Fig. 8.4($d$), where in the stable state of the system consecutive columns are shifted with respect to each other by the distance $\approx 2d$. Simulations revealed that for high aspect ratio $\beta \gg 1$ the deepest energy conformation is provided by the lattice structure of Fig. 8.4($c$).

## 8.3 Brownian dynamics simulations

Molecular dynamics simulation solving first or second order differential equation systems described in Chapter 4, provide trajectories of particles $\vec{r}_i(t)$, $i = 1, ..., N$ undergoing deterministic motion. The equation of motion Eq. (4.5) does not contain any stochastic force, randomness is introduced only by the random initial particle positions and velocities. This approach provides a satisfactory description of the system when the thermal motion of particles is hindered, for instance, by the large particle size and low temperature. However, in certain parameter regimes of BDMs thermal noise can have a substantial roll in the time evolution of the system which cannot be captured by the simulation techniques presented in Chapter 4.

In order to study the effect of thermal noise on the structure formation of binary dipolar monolayers (BDM) we carried out Brownian dynamics simulations by solving the Langevin equation

$$m_i \ddot{\vec{r}}_i = \vec{F}_i + \vec{\zeta}, \tag{8.2}$$

where $\vec{F}_i$ denotes the systematic force on particle $i$ exerted by the other dipoles and by the contacting particles, and $\vec{\zeta}$ is the stochastic force arising due to the finite temperature of the carrier liquid. Particle positions $\vec{r}_i$ are obtained using the Euler scheme

$$\vec{r}_i(t + \Delta t) = \vec{r}_i(t) + \frac{D}{k_B T}\vec{F}_i(t)\Delta t + \Delta\vec{r}_i^G, \tag{8.3}$$

where each component $\Delta r_{i\alpha}^G$ of $\Delta\vec{r}_i^G$ is sampled from a Gaussian distribution,

with the density function

$$p(x) = \frac{1}{\sqrt{2\pi}\sigma} e^{-\frac{(x-m)^2}{2\sigma^2}}. \tag{8.4}$$

The mean of the components $\Delta r_{i\alpha}^G$ is zero (m=0), while for their variance $\left\langle (\Delta r_{i\alpha}^G)^2 \right\rangle = 2D\Delta t$ holds. In Eq. (8.3) $\Delta t$ denotes the time step used in the integration of the equation of motion. $D$ is the diffusion coefficient of a particle, which is calculated from the solvent viscosity $\eta$ and the size $R$ of the particles according to the Stokes-Einstein relation

$$D = \frac{k_B T}{6\pi\eta R}. \tag{8.5}$$

Here $k_B$ and $T$ denote the Boltzmann constant and temperature, respectively. The unit of length in the system is the particle diameter $d$ and the unit of time $\tau$ is defined as $\tau = d^2/D$. We measure the temperature in units of the binding energy $E_3(\mu_r)$ of trimers at the given $\mu_r$ used, *i.e.* $T^* = k_B T/E_3(\mu_r)$ is the dimensionless temperature. In the simulations the time step $\Delta t$ should be at least two orders of magnitude smaller than the characteristic time scale $\tau$. We set $\Delta t = 0.01\tau$ from which the temperature range accessible at a given parameter set of the model can be determined. (For further details of the simulation technique see [2].)

## 8.4 The effect of thermal noise

Since no periodic substrate is applied, the colloidal molecular states of binary dipolar monolayers are purely based on the minimization of the repulsive interaction of $BCs$. It follows that BDMCs can be very sensitive to perturbations. In order to study the stability of the colloidal molecular crystal with respect to thermal excitations, we carried out Brownian dynamics simulations of trimer systems as described above. Simulations were carried out starting from the completely ordered lattice of trimers of Fig. 8.4($b$) varying the temperature in a broad range. Brownian dynamics simulations revealed that the binary dipolar molecular crystals are instable states of the

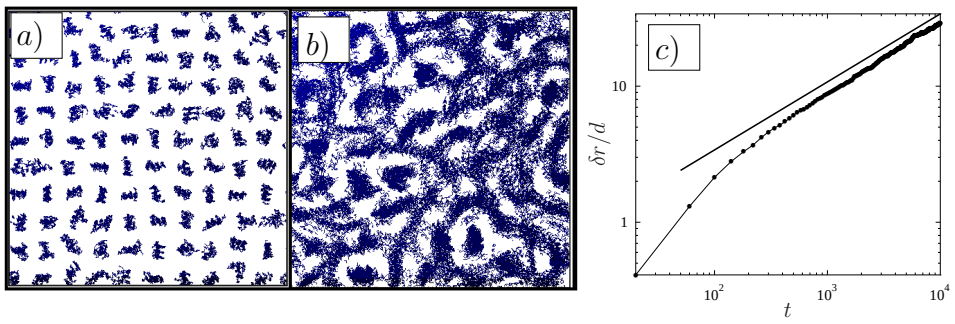


8.5. Figure: Trajectory of particles obtained by Brownian dynamics simulations at two different temperatures $T^*$ starting from the trimer lattice of Fig. 8.4($b$). The trajectories are followed up to the same time $t$ in ($a$) and ($b$). At the lower temperature $T^* = 0.03$ the crystalline order can be recognized because $t$ is smaller than the corresponding lifetime $t < t_c$ of the lattice ($a$), while at the higher temperature $T^* = 0.15$ the crystalline order is already lost $t > t_c$. ($c$) The average displacement $\delta r$ of particles from their original position as a function of time for the temperature of ($b$). The straight line has slope 1/2.

monolayer, *i.e.* at any non-zero temperature $T^*$ the crystalline order has a finite lifetime. To demonstrate the degradation of positional and orientational order of BDMCs at finite temperatures, we present the trajectory of particles in Figs. 8.5($a$), ($b$) accumulated up to the same time $t$ at two different temperatures $T_1^* = 0.03$ (Fig. 8.5($a$)) and $T_2^* = 0.15$ (Fig. 8.5($b$)). These contour plots clearly show that at the lower temperature the crystalline order prevails, while at the same time $t$ at the higher temperature the crystal structure is already lost, *i.e.* some trimers exchange particles or merge to form clusters which diffuse over the entire system. To characterize the mobility of particles in the system we calculated the average displacement of particles

$$\delta r(t) = \left\langle (\vec{r}(t) - \vec{r}_0)^2 \right\rangle^{1/2}, \tag{8.6}$$

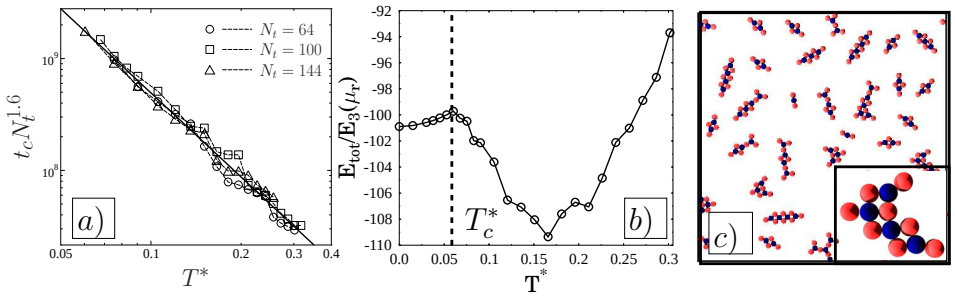


8.6. Figure: $(a)$ Lifetime $t_c$ of the crystalline state presented in Fig. 8.4$(b)$ as a function of temperature $T^*$ for different system sizes $N_t$ at $\mu_r = 1$. Data collapse is obtained by rescaling $t_c$ by the number of trimers $N_t$. The slope of the straight line is 2.5. (Note the log-log scale of the figure.) $(b)$ Energy $E_{tot}$ of the system of $N_t = 100$ trimers of Fig. 8.4$(b)$ as a function of $T^*$. $(c)$ Thermal noise driven aggregation of trimers. At high enough temperatures $T^* > T_c^*$, large clusters are formed with square packed structure. The inset shows a magnified view of a single cluster where the internal structure can be observed.

measured from their original positions $\vec{r}_0$ as a function of time. Here $\langle \cdots \rangle$ denotes the averaging over all the particles $i = 1, \ldots, N$. Figure 8.5$(c)$ presents $\delta r$ as a function of time for the setup of Fig. 8.5$(b)$. A power law relation is revealed $\delta r \sim t^{1/2}$ asymptotically with an exponent $1/2$, which shows that after the order is lost in the system the particles undergo diffusive motion.

Since BDMCs are purely based on repulsive interactions, the collapse of the lattice occurs as a relatively sudden event which results in a well-defined lifetime $t_c$ of the crystalline structure. We measured the lifetime of the BDMC presented in Fig. 8.4$(b)$ at $\mu_r = 1$ for three different system sizes $N_t$ varying the temperature $T^*$. The number of trimers $N_t$ was changed together with the side length $L$ of the simulation box keeping the lattice spacing $a_x = a_y = 5d$ fixed. It can be observed in Fig. 8.6$(a)$ that in the limiting case $T^* \to 0$ the lifetime diverges $t_c \to \infty$ since the crystalline structure is stable

at $T^* = 0$ temperature, while increasing $T^*$ gives rise to a rapid decrease of $t_c$. The temperature range in Fig. 8.6($a$) is determined by computational reasons, namely, at high temperature the lifetime becomes very short, only a few time-steps of the simulations, while at low temperature $t_c$ diverges which implies very long simulation times. Computer simulations showed that increasing the system size $N_t$ at a fixed temperature, the lifetime of the lattice decreases. Figure 8.6($a$) presents that rescaling $t_c$ by an appropriate power of $N_t$, the curves obtained at different system sizes can be collapsed on the top of each other. The good quality data collapse in Fig. 8.6($a$) obtained with the scaling transformation reveals the power law functional form

$$t_c \sim N_t^{-\beta} T^{*-\alpha}, \tag{8.7}$$

where $\alpha = 2.5 \pm 0.2$ and $\beta = 1.6 \pm 0.15$ were measured numerically. The temperature range on the double logarithmic plot is rather limited, however, the good quality of the fitted straight line supports the power law form Eq. (8.7). We also checked the numerical results on semi-logarithmic plot, which clearly showed that $t_c$ is not an exponential function of the temperature so that the observed behavior of the lifetime of the crystalline state cannot be described by an Arrhenius type law. It follows that at a fixed temperature $T^*$ starting from an ordered structure, the system is in a molecular crystalline state up to time $t_c$, while for $t > t_c$ a gas-like state is obtained where trimers or small dipole clusters slowly diffuse due to their repulsive interaction.

For the parameter regime where the trimer interaction has a short range attraction and the temperature is high enough so that the trimers can exceed the energy barrier $V_{max}$ but still remain stable $V_{max} < k_B T < E_3(\mu_r)$, in the diffusive regime of the system a very interesting transition occurs. When the trimers overcome the energy barrier $V_{max}$, they aggregate due to the short range attraction and form clusters reducing the overall energy of the system, see Fig. 8.6($c$). Figure 8.6($c$) presents a snapshot of the aggregating system at the temperature $T^* = 0.2$, where it can be observed that the particles inside the clusters rearrange and tend to organize into a square lattice structure, which provides the lowest energy configuration at $\mu_r = 1$

[92, 93, 106]. This aggregation and ordering is driven by the thermal noise analogously to the *freezing-by-heating* transition observed recently [22]. We measured the total energy $E_{tot}$ of the ensemble of trimers starting from the lattice structure of Fig. 8.4($b$) at $\mu_r = 1$ in the steady state attained after long time relaxation $t > t_c(T^*)$ when the crystalline state is lost, as a function of the temperature $T^*$. In Fig. 8.6($b$) the critical temperature $T_c^* \approx 0.06$ of thermal noise driven aggregation can be identified by the sudden decrease of $E_{tot}$. For $T^* < T_c^*$ the trimers do not aggregate just diffuse in the system after the crystalline order is lost $t > t_c(T^*)$. Since the relative concentration of oppositely oriented dipoles for trimers is $2:1$, the interaction of growing clusters becomes purely repulsive and the aggregation stops so that the size of clusters is limited. The minimum of $E_{tot}$ in Fig. 8.6($b$) at $T^* \approx 0.17$ corresponds to the temperature where the largest clusters could be achieved whose surface is covered by the dipoles of the higher concentration.

Colloidal molecular crystals interacting with periodic substrates show a two-step melting mechanism: when increasing the temperature first the orientational order gets lost while the colloids are still confined, then the positional order disappears at a higher temperature when the particles get delocalized over the substrate. In BDMCs the absence of confining substrate has the consequence that such two-step melting cannot occur, orientational and positional orders are strongly coupled and get lost at the same time.

A very interesting property of dipolar $n$-mers is that their interaction potential can be tuned up to some extent by varying the relative dipole moment $\mu_r$ and the dispersity $\sigma$ (i.e. relative size of particles) of the two components. Changing also the composition of $n$-mers (trimers, quadromers, ...) one can design composite particles with a desired interaction potential for the purpose of directed self-assembly [65, 63, 64].

# 9 Chapter

# Summary

Binary dipolar monolayers are two-component colloids in which the motion of particles is constrained to the two-dimensional plane. The particles have an induced or permanent dipole moment whose direction is fixed to be perpendicular to the plane of motion with opposite orientation for the two components. In the framework of my Ph.D. I carried out a detailed experimental and theoretical investigation of the structure formation processes in binary dipolar monolayers.

I worked out an experimental technique which provides a straightforward and controllable realization of binary dipolar monolayers with particles of oppositely oriented dipole moments constrained to be perpendicular to the plane of motion. In the experimental setup macroscopic particles are constructed by attaching metal particles of cylinder shape to swimmers. The metal particles are magnetized so that they have a permanent magnetic moment parallel to their axis. The swimmers are cork discs which have two major roles in the setup: (*i*) they ensure the confinement of the composite particles to the air-water interface (floating) reducing also the friction force, (*ii*) they prevent flipping constraining the dipole moments to be perpendicular to the plane of motion. The two components of the system are realized by the two opposite orientation of the dipole moments of the particles which are set by hand when preparing the initial configuration. My

experimental method overcomes several difficulties of the techniques used in the literature, *i.e.*, there is no need for an external driving field, hence, electro-hydrodynamic effects are completely eliminated, there is no sliding friction with the substrate, the initial condition is well-controllable. Due to the large particle size the thermal motion is hindered so that the particles move along deterministic trajectories. The time evolution of the system is easily accessible by direct optical observations making possible a quantitative analysis of structure formation processes.

I introduced a model of binary dipolar monolayers which takes into account all the relevant interactions in the particle system. In the model spherical particles are considered which have a point-like dipole moment in the middle. The particles move in two dimensions under the action of the dipole-dipole force with dipole moments fixed to be perpendicular to the plane of motion. The carrier liquid only exerts a Stokes drag on the particles. The finite size of the particles is captured by introducing a repulsive contact force between the touching particles in the form of the Hertz contact law. Since thermal motion does not play a crucial role, the time evolution of the model system is obtained by computer simulations solving numerically the equation of motion of particles (molecular dynamics) without considering thermal noise. In order to study the stability of molecular crystals with respect to thermal fluctuations, I also developed a computer simulation program to solve the Langevin equation of the particles (Brownian dynamics) which explicitly captures the effect of thermal noise. Besides the computer simulation programs, I also worked out a computer program package for the evaluation of the experimental and simulation results.

I pointed out that at low concentrations $\phi \leq 25\%$ BDMs undergo kinetic aggregation, which also represents an interesting special case of heteroaggregation phenomena of colloids. Experiments revealed that the dipolar clusters are fractals which show a crossover from the universality class of self-avoiding random walks to the more compact branching morphologies of reaction limited cluster-cluster aggregation. The dynamic exponents of the

average cluster size and cluster number are increasing functions of the concentration with an increasing difference so that Vicsek-Family scaling only holds in the dilute limit. Computer simulations are in a good quantitative agreement with the experimental findings. Additionally, I showed that in the absence of contact friction of the particles, the growing clusters are less compact characterized by a lower value of the fractal dimension.

I showed experimentally and by means of computer simulations that in aggregation processes of BDMs cluster discrimination occurs, *i.e.*, clusters of an even and odd number of particles have a different time dependent behavior. Even clusters have a higher reaction rate than the odd ones leading to even-odd oscillations of the concentration of clusters. I explained the phenomenon in terms of the morphology of clusters and their long-range anisotropic interaction. I showed that discrimination can be observed up to the crossover cluster size, and the higher relative dipole moment of the components leads to a more pronounced discrimination effect.

My experiments and computer simulations revealed that at higher concentrations $\phi > 25\%$ crystallization occurs, *i.e.*, particles of the two components form various types of planar crystal lattices. I showed analytically that in a mono-disperse particle system the outcome of structure formation is determined by three parameters: depending on the value of the total concentration $\phi$ of the particles, and on the relative concentration $\phi_r$ and relative dipole moment $\mu_r$ of the two components triangular lattice, square lattice, and two-types of honeycomb lattices can be obtained. I determined analytically the parameter regimes of different lattice types and concluded that electro-hydrodynamic flow discussed in the literature does not play a crucial role in crystallization. The experiments and computer simulations are in a good agreement with my analytic predictions.

I showed that in binary dipolar monolayers crystalline states analogous to colloidal molecular crystals observed in colloids interacting with a periodic array of traps, can emerge without the application of an underlying substrate. The $n$-mers of BDMs are bounded configurations of particles

with oppositely oriented permanent dipoles whose interaction depends both on their distance and relative orientation. I carried out a detailed analysis of trimer lattices and pointed out that the translational degrees of freedom leads to novel structures not observed with substrates. Brownian dynamics simulations revealed that at finite temperatures the molecular crystalline structures are instable states of BDMs whose lifetime is a decreasing function of both the temperature and the system size. For trimers there exists a critical temperature $T_c$ above which thermal noise driven aggregation occurs resulting in clusters of square lattice structure, analogously to the "freezing-by-heating" transition.

# 10 Chapter

# Összefoglalás

A bináris dipoláris vékonyrétegek olyan kétkomponensű kolloidok, amelyekben a részecskék mozgása egy síkra korlátozódik. A részecskék indukált, vagy permanens dipólmomentummal rendelkeznek, amelynek iránya a mozgás síkjára merőlegesen rögzített s a két komponens esetén egymással ellentétes. Doktori dolgozatom keretében a bináris dipoláris vékonyrétegekben lejátszódó struktúraképződéssel járó folyamatok kísérleti és elméleti vizsgálatát végeztem.

Kidolgoztam egy kísérleti eljárást, amely lehetővé teszi a bináris dipoláris vékonyrétegek kontrollált előállítását és részletes kvantitatív vizsgálatát. A kísérletek során makroszkopikus méretű részecskéket állítottam elő úgy, hogy henger alakú felmágnesezett fém részecskéket parafa korongokhoz rögzítettem. A parafa korongoknak két fontos szerepe van a kísérletek során: (*i*) egyrészt biztosítják a kompozit részecskék vízfelszinen történő úszását, azaz a részecskék súrlódásmentes kétdimenziós mozgását, (*ii*) másrészt megakadályozzák a részecskék átbillenését, így rögzítve a dipólusok irányát a vízfelszínre merőlegesen. A rendszer két komponenséhez tartozó részecskék dipólmomentuma ellentétes irányítottságú, amelyet a kezdőfeltétel létrehozásakor kell beállítani. Ezzel az egyszerű kísérleti eljárással sikerült kiküszöbölni az irodalomban használt mérési módszerek problémáinak jelentős részét: módszeremmel nincs szükség külső gerjesztő térre, így sikerült teljesen kikü-

szöbölni a hordozó folyadék elektro-hidrodinamikai áramlását; a részecskék gyakorlatilag súrlódásmentesen mozognak; a kezdőállapot előállítása minden részletében kontrollálható. A rendszerben a viszonylag nagytömegű részecskék determinisztikus mozgást végeznek, a hőmozgás elhanyagolható. A rendszer időfejlődése optikai módszerekkel jól követhető, ami lehetővé teszi a bináris dipoláris vékonyréteg struktúraképződéssel járó folyamatainak részletes kvantitatív vizsgálatát.

Bináris dipoláris vékonyrétegek elméleti vizsgálatára bevezettem egy realisztikus modellt, amely figyelembe veszi a rendszer releváns kölcsönhatásait. A kétdimenziós modellben a részecskéket gömbök reprezentálják, amelyek közepébe pontszerű dipólust helyezek a mozgás síkjára merőlegesen rögzített iránnyal. A beágyazó folyadék hatását a Stokes fékezési erővel, a részecskék véges méretét pedig a Hertz féle kontaktus törvénnyel veszem figyelembe. Mivel a hőmozgás nem játszik fontos szerepet, a rendszer időfejlődését a determinisztikus mozgásegyenletek numerikus megoldásával, azaz molekuláris dinamikai szimulációval állítom elő. A dipoláris vékonyrétegben lehetséges molekuláris krisztályok előállítása, amelyek nagyon érzékenyek a perturbációkra. Molekuláris kristályok termikus gerjesztésekkel szembeni stabilitásának vizsgálatára kifejlesztettem egy Brown dinamikai szimulációs programot, amely már a sztochasztikus erőket is figyelembe veszi. A szimulációs programok mellett kidolgoztam egy adatfeldolgozó programcsomagot is a szimulációs és kísérleti eredmények kiértékelésére.

Kimutattam, hogy a bináris dipoláris vékonyrétegben alacsony koncentráció esetén aggregációs folyamatok játszódnak le, amelyek egyben érdekes megvalósítását adják az úgynevezett hetero-aggregációs folyamatoknak. Kísérleti eszközökkel feltártam, hogy az aggregációval létrejött dipoláris klaszterek fraktálok, amelyek struktúrája átmenetet mutat az önelkerülő bolyongás univerzalitási osztályából a reakciólimitált klaszter-klaszter aggregáció osztályába. Azt találtam, hogy az átlagos klaszterméret és klaszter darabszám dinamikus exponensei a koncentráció növekvő függvényei, és aVicsek-Family skálázás csak a híg kolloid határesetben teljesül. A számítógépes

szimulációk jó egyezést mutatnak a kísérleti eredményekkel. Az összevetés egyik eredményeként kiderült, hogy az érintkező részecskék súrlódása kompaktabb klasztereket eredményez, amit alacsonyabb fraktáldimenzió jellemez.

Kísérleti és elméleti eszközökkel megmutattam, hogy bináris dipoláris vékonyrétegek aggregációs folyamatai során úgynevezett klaszter-diszkrimináció lép fel, azaz a páros és páratlan számú részecskét tartalmazó klaszterek időfejlődése különböző. Páros számú részecskét tartalmazó klaszterek reakció képessége nagyobb a páratlanokénál, ami a klaszterkoncentráció páros-páratlan oszcillációira vezet. A klaszterek morphológiája és hosszúhatótávolságú, anizotróp kölcsönhatása alapján magyarázatát adtam a jelenségnek. Sikerült megmutatni, hogy diszkrimináció csak a láncszerű klaszterekre, azaz csak az univerzalitási osztályok közötti átmeneti klaszterméretig figyelhető meg, továbbá a komponensek növekvő relatív dipólmomentuma erősebb effektust eredményez.

Kellően nagy koncentráció esetén a dipoláris vékonyrétegben kristályosodási folyamat figyelhető meg: véletlenszerű kezdőfeltételből kiindulva a két komponens részecskéi nagyon gyorsan változatos szerkezetű síkbeli kristályrácsokba rendeződnek. Analitikus számolásokkal megmutattam, hogy a struktúra-kialakulás végállapotát a rendszer három paraméterének értéke határozza meg: a részecskék teljes koncentrációjától, továbbá a két komponens relatív koncentrációjától és relatív dipólmomentumától függően a részecskék háromszögrácsba, négyzetrácsba és kétfajta méh-sejt rácsszerkezetbe rendeződhetnek. Analitikusan megadtam az egyes rácstípusokhoz tartozó paraméter tartományokat, továbbá arra a következtetésre jutottam, hogy az irodalomban használt kísérleti technikák az elektro-hidrodinamikai áramlás miatt nem teszik lehetővé az alacsony sűrűségű méh-sejt rács megfigyelését. Kísérleti és szimulációs eredményeim jó egyezést mutatnak az analitikus számolásom eredményeivel.

Kimutattam, hogy bináris dipoláris vékonyrétegben létrejöhet olyan molekuláris kristályszerkezet, amelyet korábban kolloidokban optikai csapdák

periódikus rácsán sikerült csak létrehozni. A dipoláris vékonyréteg $n$-merjei (építőkövei) ellentétes irányítású dipólusok kötött konfigurációi, amelyek távolság és irányfüggő kölcsönhatást mutatnak. Részletesen elemeztem trimerek kölcsönhatását és feltártam, hogy a transzlációs szabadsági fokok miatt bináris dipoláris vékonyrétegekben olyan molekula-kristályos szerkezetek is létrejöhetnek, amelyeket optikai csapdákkal nem lehet megfigyelni. Brown-dinamikai szimulációkkal kimutattam, hogy ezek a molekula kristályok véges hőmérsékleten instabilak, nem nulla hőmérsékleten véges életidővel rendelkeznek. A kristályos állapot életideje a hőmérsékletnek és a rendszer méretének hatványfüggvényeként csökken, ami egyszerű Arrhenius típusú viselkedéssel nem magyarázható. Olyan paraméterek mellett, amikor a trimer-trimer kölcsönhatás vonzó és taszító tartománnyal is rendelkezik, egy kritikus hőmérséklet fölött termikus zaj hajtotta aggregáció lép fel négyzetrácsos szerkezetű klasztereket eredményezve, az úgynevezett "melegítéssel kiváltott fagyás"-hoz hasonlóan.

## Acknowledgment

It is my pleasure to express my gratitude to all the people who helped me during my Ph.D. studies. Without their skills, knowledge and friendship this work would have never been completed.

I would like to thank my supervisor Ferenc Kun, who made possible this work creating the necessary conditions for performing it. His support and guidance are fully acknowledged. I am very grateful to him for his continuous help and encouragement.

I would like to thank Károly F. Pál, Hideki Yamada, Hans-Georg Matuttis, Nobuyasu Ito, Naoki Yoshioka, Satoshi Yukawa, Irén Hoczka, Ottó Zséder, the members of the Department of Theoretical Physics of the University of Debrecen and of the Hajdúböszörmény College Faculty of Education of University of Debrecen for their help in my work.

Finally, I wish to thank my wife, Mariann Kovács and my son Milán Varga, for their patience.

# Bibliography


[1] R. Agra, F. van Wijland, E. Trizac, Phys. Rev. Lett. **93** (2004) 18304.

[2] M. P. Allen and D. J. Tildesley, *Computer Simulation of Liquids*. Oxford University Press (1984).

[3] P. Bandini, C. A. Prestidge and J. Ralston, Miner. Eng. **14** (2001) 487.

[4] C. Bechinger, M. Brunner and P. Leiderer, Phys. Rev. Lett. **86** (2001) 930.

[5] M. Berka and J. A. Rice, Langmuir **20** (2004) 6152-6157.

[6] B. M. Berkovsky, V. F. Medvedev and M. S. Krakov, *Magnetic Fluids-Engineering Applications*. Cambridge University Press, Oxford (1993).

[7] D. L. Blair and A Kudrolli, Phys. Rev. E **67** (2003) 021302.

[8] R. Botet, R. Jullien and M. Kolb, J. Phys. A **17** (1984) L75.

[9] M. Brunner and C. Bechinger, Phys. Rev. Lett. **88** (2002) 248302.

[10] J. Buffle, K. J. Wilkinson, S. Stoll, M. Filella and J. Zhang, Environ. Sci. Technol. **32** (1998) 2887-2899.

[11] J. Cernak, G. Helgesen, A. Skjeltorp, Phys. Rev. E **70** (2004) 031504.

[12] A. Chakrabarti, D. Fry, C. M. Sorensen, Phys. Rev. E **69** (2004) 031408.

[13] Y. Choi, K. Kim and H. K. Pak, Physica A **281** (2000) 99.

[14] P. G. de Gennes, P. A. Pincus, Phys. Kondens. Mater. **11** (1970) 189.

[15] S. R. Deshiikan and K. D. Papadopoulos, Colloid Polym. Sci. **275** (1997) 440-448.

[16] A. DiFeo, J. A. Finch, Z. Xu, Int. J. Miner. Process. **61** (2001) 57.

[17] A. Fernández-Barbero and B. Vincent, Phys. Rev. E **63** (2000) 11509.

[18] A. D. Findlay, D. W. Thompson and E. Tipping, Colloids Surf. A **118** (1996) 97-105.

[19] V. A. Froltsov, R. Blaak, C. N. Likos and H Löwen, Phys. Rev. E **68** (2003) 061406.

[20] C. Galindo-González, J. de Vicente, M. M. Ramos-Tejada, M. T. López-López, F. González-Caballero and J. D. G. Durán, Langmuir **21** (2005) 4410-4419.

[21] P. Galletto, W. Lin and M. Borkovec, Phys. Chem. Chem. Phys. **7** (2005) 1464-1471.

[22] D. Helbing, I. J. Farkas, T. Vicsek, Phys. Rev. Lett. **84** (2000) 1240.

[23] G. Helgesen, A. T. Skjeltorp, P. M. Mors, R. Botet and R. Jullien, Phys. Rev. Lett. **61** (1988) 1736.

[24] L. E. Helseth and T. M. Fischer, Phys. Rev. E **68** (2003) 051403.

[25] R. Hidalgo-Álvarez, A Martin, A. Fernández, D. Bastos, F. Martinez and F. J. de las Nieves, Adv. Colloid Interface Sci. **67** (1996) 1-118.

[26] R.M. Ion, I. Yilmaz, O. Bekaroglu, J. Serb. Chem. Soc. **64** (1999) 453.

[27] A. M. Islam, B. Z. Chowdhry and M. J. Snowden, Adv. Colloid Interface Sci. **62** (1995) 109-136.

[28] S. Jadhav, B. S. Bochner and K. Konstantopoulos, J. Immunol. **167** (2001) 5986-5993.

[29] H. Jaeger, S. Nagel, R. P. Behringer, Rev. Mod. Phys. **68** (1996) 1259.

[30] J. T. Jenkins and S. B. Savage, J. Fluid Mech. **130** (1983) 187.

[31] R. A. L. Jones, *Soft Condensed Matter*. Oxford University Press (2002).

[32] P. Jund, S. G. Kim, D. Tománek and J. Hethernington, Phys. Rev. Lett. **74** (1995) 3049.

[33] A. Y. Kim and J. C. Berg, J. Colloid Interface Sci. **229** (2000) 607-614.

[34] A. Y. Kim and J. C. Berg, Langmuir **18** (2002) 3418-3422.

[35] A. Y. Kim, K. D. Hauch, J. C. Berg, J. E. Martin, R. A Anderson, J. Colloid Interface Sci. **260** (2003) 149-159.

[36] M. Kolb, Phys. Rev. Lett. **53** (1984) 1653.

[37] M. Kolb, R. Botet and R. Jullien, Phys. Rev. Lett. **51** (1983) 1123.

[38] A. Kudrolli and J. Henry, Phys. Rev. E **62** (2000) 1489R.

[39] F. Kun, K. F. Pál, W. Wen, K. N. Tu, Phys. Lett. A **277** (2000) 287.

[40] R. G. Larson, *The structure and theology of complex fluids*. Oxford University Press (1999).

[41] W. Lin, M. Kobayashi, M. Skarba, C. Mu, P. Galletto and M. Borkovec, Langmuir **22** (2006) 1038-1047.

[42] J. F. Lipskier and T. H. Tran-Thi, Inorg. Chem. **32** (1993) 722-731.

[43] Y. Liu, K. Shah, F. Yang, L. Witucki, K. M. Shokat, H. Deng and Z. Lu, Supramol. Sci. **5** (1998) 669-674.

[44] H. M. López-López, A. Schmitt, A. Moncho-Jordá and R. Hidalgo-Álvarez, Rev. Mod. Phys. **68** (1996) 1259.

[45] W. Losert, D. Copper, J. Deolur, A. Kudrolli and J. P. Gollub, Chaos **9** (1999) 682.

[46] K. Mangold, P. Leiderer, C. Bechinger, Phys. Rev. Lett. **90** (2003) 158302.

[47] J. A. Maroto and F. J. de las Nieves, Colloids Surf. A **96** (1995) 121.

[48] J. A. Maroto and F. J. de las Nieves, Colloids Surf. A **132** (1998) 153.

[49] O. J. T. McCarty, S. Jadhav, M. M. Burdick, W. R. Bell and K. Konstantopoulos, Biophys. J. **83** (2002) 836-848.

[50] P. Meakin, Phys. Rev. Lett. **51** (1983) 1119.

[51] P. Meakin, T. Vicsek and F. Family, Phys. Rev. B **31** (1985) 564.

[52] M.C. Miguel and R. Pastor-Sattoras, Phys. Rev. E **59** (1999) 826.

[53] M. Mikulis, C. J. Olson Reichhardt, C. Reichhardt, R. T. Scalettar and G. T. Zimányi, J. Phys.: Condens Matter 16 (2004) 7909.

[54] G. E. Morris, W. A. Skinner, P. G. Self and R. St. C. Smart, Colloids Surf. A **155** (1999) 27-41.

[55] S. Mukherjee, S. Basak, S. Khowala, Biotechnol. Prog. **18** (2002) 404.

[56] D. R. Nelson, *Phase Transitions and Critical Phenomena*. Academic (1983) London.

[57] K. N. Plunkett, A. Mohraz, R. T. Haasch, J. A. Lewis and J. S. Moore, J. Am. Chem. Soc. **172** (2005) 14574-14575.

[58] W. H. Press, S. A. Teukolsky, W. T. Vetterling and B. P. Flannery, *Numerical recipes in Fortran*. Cambridge University Press (1992).

[59] J. H. E. Promislow, A. P. Gast and M. Fermigier, J. Chem. Phys. **102** (1995) 5492.

[60] A. M. Puertas, A. Fernández Barbero and F. J. de las Nieves, Eur. Phys. J. E **18** (2005) 335-341.

[61] A. M. Puertas, A. Fernández-Barbero and F. J. de las Nieves, Physica A **304** (2002) 340.

[62] A. M. Puertas, J. A. Maroto, A. Fernández Barbero and F. J. de las Nieves, Phys. Rev. E **59** (1999) 1943.

[63] M. Rechtsman, F. Stillinger, S. Torquato, Phys. Rev. E **73** (2006) 011406.

[64] M. Rechtsman, F. Stillinger, S. Torquato, Phys. Rev. E **75** (2007) 031403.

[65] M. C. Rechtsman, F. H. Stillinger and S. Torquato, Phys. Rev. Lett. **95** (2005) 228301.

[66] C. Reichardt and C. J. Olson, Phys. Rev. Lett. **88** (2002) 248301.

[67] C. Reichardt and C. J. Olson, Phys. Rev. E **71** (2005) 062403.

[68] W. D. Ristenpart, I. A. Aksay and D. A. Saville, Phys. Rev. Lett. **90** (2003) 128303.

[69] W. D. Ristenpart, I. A. Aksay and D. A. Saville, Phys. Rev. E **69** (2004) 21405.

[70] N. Ryde, E. Matijevic, J. Chem. Soc. Faraday Trans. **90** (1994) 6641.

[71] M. V. Sapozhnikov, Y. V. Tolmachev, I. S. Aranson and W.-K. Kwok, Phys. Rev. Lett. **90** (2003) 114301.

[72] A. Sarlah, T. Franosch and E. Frey, Phys. Rev. Lett. **95** (2005) 088302.

[73] F. Scheffler, P. Maass, J. Roth, H. Stark, Eur. Phys. J. B **42** (2004) 85.

[74] H. See and M. Doi, J. Phys. Soc. Jpn. **60** (1991) 2778.

[75] M. Seed, G. S. Hobson, R. C. Tozer and A. J. Simmonds, *Voltage-controlled Electrorheological brake*. Proc. IASTED Int. Symp. Measurement, Sig. Proc. and Control (1986) p. 105-092-1.

[76] A. Senzhko, I. S. Aranson, W.-K. Kwok, Phys. Rev. Lett. **94** (2005) 108002.

[77] A. T. Skjeltorp, Phys. Rev. Lett. **51** (1983) 2306.

[78] D. R. E. Snoswell, Th. J. Rogers, A. M. Howe and B. Vicent, Langmuir **21** (2005) 11439-11445.

[79] J. Stambaugh, D. Lathrop, E. Ott and W. Losert, Phys. Rev. E **68** (2003) 026207.

[80] J. Stambaugh, Z. Smith, E. Ott, W. Losert, Phys. Rev. E **69** (2004) 031304.

[81] R. Stanway, J. L. Sproston and A. K. El-Wahed, Smart Mater. Struct **5** (1996) 464-482.

[82] T. Stirner and J. Sun, Langmuir **21** (2005) 6636.

[83] P. Tangboriboonrat and U. Buranabunya, Colloid Polym. Sci. **279** (2001) 615-620.

[84] J. M. Tavares, J. J. Weis and M. M. Telo da Gama, Phys. Rev. E **65** (2002) 061201.

[85] M. L. Taylor, G. E. Morris and R. St. C. Smart, J. Colloid Interface Sci. **262** (2003) 81.

[86] P. I. C. Teixeira, J. M. Tavares and M. M. T. de Gamma, J. Phys.: Condens Matter **12** (2000) 411.

[87] Y. Terada and M. Tokuyama, Physica A **334** (2004) 327.

[88] M. Trau, D. A. Saville and I. A. Aksay, Langmuir **13** (1997) 6375.

[89] T. G. M. van de Ven, B. Alince, J. Colloid Interface Sci. **181** (1996) 73.

[90] I. Varga and F. Kun, Philosophical Magazine **86** (2006) 2011-2031.

[91] I. Varga, F. Kun, N. Ito and W. Wen, Journal of Statistical Mechanics: Theory and Experiments, accepted (2007).

[92] I. Varga, F. Kun and K. F. Pál, Phys. Rev. E **69** (2004) 030501(R).

[93] I. Varga, H. Yamada, F. Kun, H.-G. Matuttis and N. Ito, Phys. Rev. E **71** (2005) 051405.

[94] I. Varga, N. Yoshioka, F. Kun, S. Gang and N. Ito, Journal of Statistical Mechanics: Theory and Experiment (2007) P09015.

[95] T. Vicsek, *Fractal Growth Phenomena.* World Scientific, Singapore (1999).

[96] T. Vicsek and F. Family, Phys. Rev. Lett. **52** (1984) 1669.

[97] T. P. C. von Noije and M. H. Ernst, Granular Media **1** (1998) 57.

[98] M. von Smoluchowski, Z. Phys. Chem **17** (1916) 557.

[99] W. Wen, X. Huang, S. Yang, K. Lu and P. Sheng, Nature Materials **2** (2003) 727.

[100] W. Wen, F. Kun, K. F. Pál, D. W. Zheng and K. N. Tu, Phys. Rev. E **51** (1995) 4325.

[101] W. Wen, L Zhang and P. Sheng, Phys. Rev. Lett. **85** (2000) 5464.

[102] T. A. Witten, P. Pincus, *Structured fluids.* Oxford University Press (2004).

[103] T. A. Witten and L. M. Sander, Phys. Rev. Lett. **47** (1981) 1400.

[104] S. Yeh, M. Seul and B. L. Shraiman, Nature **386** (1997) 57.

[105] Q. Ying, J. Zhang, D. Liang, W. Nakanishi, H. Isobe, E. Nakamura and B. Chu, Langmuir **21** (2005) 9824-9831.

[106] N. Yoshioka, I. Varga, F. Kun, S. Yukawa and N. Ito, Phys. Rev. E **72** (2005) 061403.

[107] W. L. Yu and M. Borkovec, J. Phys. Chem. B **106** (2002) 13106-13110.

[108] K. Zahn, A. Wille, G. Maret, S. Sengupta and P. Nielaba, Phys. Rev. Lett. **90** (2003) 155506.

# 11 Chapter

# Publications

**Refereed journals**

1. I. Varga, F. Kun, and K. F. Pál, *Structure formation in binary colloids*, Physical Review E **69**, 030501(R) (2004).

2. I. Varga, H. Yamada, F. Kun, H.-G. Matuttis, and N. Ito, *Structure formation in a binary monolayer of dipolar particles*, Physical Review E **71**, 051405 (2005).

3. N. Yoshioka, I. Varga, F. Kun, S. Yukawa, and N. Ito, *Attraction-limited cluster-cluster aggregation of Ising dipolar particles*, Physical Review E **72**, 061403 (2005).

4. I. Varga and F. Kun, *Pattern formation in binary colloids*, Philosophical Magazine **86**, 2011 (2006).

5. I. Varga, N. Yoshioka, F. Kun, S. Gang, and N. Ito, *Structure and kinetics of heteroaggregation in binary dipolar monolayers*, Journal of Statistical Mechanics: Theory and Experiments, P09015 (2007).

6. I. Varga, F. Kun, N. Ito, and W. Wen, *Molecular Crystalline States in Binary Dipolar Monolayers*, Journal of Statistical Mechanics: Theory and Experiments, accepted (2007).

**Conference proceedings**

1. I. Varga and F. Kun, *Aggregation of particles in a binary dipolar monolayer*, in the Proceedings of microCAD 2005 International Scientific Conference, Miskolc, Hungary, March 10.-11. 2005, pp. 43-48.

**Posters**

1. I. Varga, F. Kun and K. F. Pál, *Ordered structures in a binary monolayer of dipolar particles*, 1st Szeged International Workshop on Advances in Nanoscience, Szeged, Hungary, October 26.-28. 2003.
2. I. Varga, F. Kun and K. F. Pál, *Structure formation in binary colloids*, 29th Conference of the Middle European Cooperation in Statistical Physics, Bratislava, Slovakia, March 28.-April 1. 2004.
3. I. Varga and F. Kun, *Aggregation and crystallization in binary colloids*, 3rd Graduate School on Condensed Matter Physics, Debrecen, Hungary, September 6.-11. 2004.
4. I. Varga and F. Kun, *Cluster discrimination in binary dipolar monolayers*, 30th Conference of the Middle European Cooperation in Statistical Physics, Cortona, Italy, April 3.-6. 2005.
5. I. Varga and F. Kun, *Colloidal molecular crystals in dipolar monolayers*, 31th Conference of the Middle European Cooperation in Statistical Physics, Primosten, Croatia, April 23.-26. 2006.

**Talks**

1. I. Varga and F. Kun, *Aggregation of particles in a binary dipolar monolayer*, microCAD 2005 International Scientific Conference, Miskolc, Hungary, March 10.-11. 2005.
2. I. Varga, *Mágneses részecskék síkbeli rendeződése*, Tudomány napja 2004, Hajdúböszörmény, Hungary, November 3. 2004.